

1 **FLUXNET-CH4: A global, multi-ecosystem dataset and analysis**
2 **of methane seasonality from freshwater wetlands**

3
4 Kyle B. Delwiche¹, Sara Helen Knox², Avni Malhotra¹, Etienne Fluet-Chouinard¹, Gavin
5 McNicol¹, Sarah Feron^{1,3}, Zutao Ouyang¹, Dario Papale^{4,5}, Carlo Trotta⁵, Eleonora Canfora⁵,
6 You-Wei Cheah⁶, Danielle Christianson⁶, Ma. Carmelita R. Alberto⁷, Pavel Alekseychik⁸, Mika
7 Aurela⁹, Dennis Baldocchi¹⁰, Sheel Bansal¹¹, David P. Billesbach¹², Gil Bohrer¹³, Rosvel
8 Bracho¹⁴, Nina Buchmann¹⁵, David I. Campbell¹⁶, Gerardo Celis¹⁷, Jiquan Chen¹⁸, Weinan
9 Chen¹⁹, Housen Chu²⁰, Higo J Dalmagro²¹, Sigrid Dengel⁶, Ankur R Desai²², Matteo Dettò²³,
10 Han Dolman²⁴, Elke Eichelmann²⁵, Eugenie Euskirchen²⁶, Daniela Famulari²⁷, Kathrin Fuchs²⁸,
11 Mathias Goeckede²⁹, Sébastien Gogo³⁰, Mangaliso J. Gondwe³¹, Jordan P Goodrich¹⁶, Pia
12 Gottschalk³², Scott L. Graham³³, Martin Heimann²⁹, Manuel Helbig^{34,35}, Carole Helfter³⁶, Kyle
13 S. Hemes^{1,37}, Takashi Hirano³⁸, David Hollinger³⁹, Lukas Hörtnagl¹⁵, Hiroki Iwata⁴⁰, Adrien
14 Jacotot³⁰, Gerald Jurasiczki⁴¹, Minseok Kang⁴², Kuno Kasak⁴³, John King⁴⁴, Janina Klatt⁴⁵,
15 Franziska Koebsch⁴¹, Ken W Krauss⁴⁶, Derrick Y.F. Lai⁴⁷, Annalea Lohila^{9,48}, Ivan
16 Mammarella⁴⁸, Giovanni Manca⁴⁹, Luca Belelli Marchesini⁵⁰, Jaclyn Hatala Matthes⁵¹, Trofim
17 Maximon⁵², Lutz Merbold⁵³, Bhaskar Mitra⁵⁴, Timothy H. Morin⁵⁵, Eiko Nemitz³⁶, Mats B.
18 Nilsson⁵⁶, Shuli Niu¹⁹, Walter C Oechel⁵⁷, Patricia Y. Oikawa⁵⁸, Keisuke Ono⁵⁹, Matthias
19 Peichl⁵⁶, Olli Peltola⁹, Michele L. Reba⁶⁰, Andrew D. Richardson^{61,62}, William Riley⁶, Benjamin
20 R. K. Runkle⁶³, Youngryel Ryu⁶⁴, Torsten Sachs³², Ayaka Sakabe⁶⁵, Camilo Rey Sanchez¹⁰,
21 Edward A Schuur⁶⁶, Karina VR Schäfer⁶⁷, Oliver Sonnentag⁶⁸, Jed P. Sparks⁶⁹, Ellen Stuart-
22 Häntjens⁷⁰, Cove Sturtevant⁷¹, Ryan C. Sullivan⁷², Daphne J. Szutu¹⁰, Jonathan E Thom⁷³,
23 Margaret S. Torn⁶, Eeva-Stiina Tuittila⁷⁴, Jessica Turner⁷⁵, Masahito Ueyama⁷⁶, Alex C.
24 Valach¹⁰, Rodrigo Vargas⁷⁷, Andrej Varlagin⁷⁸, Alma Vazquez-Lule⁷⁷, Joseph G. Verfaillie¹⁰,
25 Timo Vesala^{48,79}, George L Vourlitis⁸⁰, Eric J. Ward⁴⁶, Christian Wille³², Georg Wohlfahrt⁸¹,
26 Guan Xuan Wong⁸², Zhen Zhang⁸³, Donatella Zona^{57,84}, Lisamarie Windham-Myers⁸⁵,
27 Benjamin Poulter⁸⁶, Robert B. Jackson^{1,37,87}

28

29

30

31 ¹ Department of Earth System Science, Stanford University, Stanford, California

32 ² Department of Geography, The University of British Columbia, Vancouver, British Columbia, Canada

33 ³ Department of Physics, University of Santiago de Chile, Santiago, Chile

34 ⁴ Dipartimento per la Innovazione nei Sistemi Biologici, Agroalimentari e Forestali, Università degli Studi della
35 Tuscia, Largo dell'Università, Viterbo, Italy e Forestali, Università

36 ⁵ euroMediterranean Center on Climate Change CMCC, Lecce, Italy

37 ⁶ Earth and Environmental Sciences Area, Lawrence Berkeley National Lab, Berkeley, California

38 ⁷ International Rice Research Institute, Los Banos, Laguna, Philippines

39 ⁸ Natural Resources Institute Finland (LUKE), Helsinki, Finland

40 ⁹ Finnish Meteorological Institute, PO Box 501, 00101 Helsinki, Finland

41 ¹⁰ Department of Environmental Science, Policy and Management, University of California, Berkeley, CA, USA

42 ¹¹ U.S. Geological Survey, Northern Prairie Wildlife Research Center, 8711 37th St Southeast, Jamestown, ND
43 58401 USA

44 ¹² University of Nebraska-Lincoln, Department of Biological Systems Engineering, Lincoln, NE 68583, USA

45 ¹³ Department of Civil, Environmental & Geodetic Engineering, Ohio State University

46 ¹⁴ School of Forest Resources and Conservation, University of Florida, Gainesville FL, 32611

- 47 ¹⁵ Department of Environmental Systems Science, Institute of Agricultural Sciences, ETH Zurich, 8092 Zurich,
48 Switzerland
49 ¹⁶ School of Science, University of Waikato, Hamilton, New Zealand
50 ¹⁷ Agronomy Department, University of Florida, Gainesville FL, 32601
51 ¹⁸ Department of Geography, Environment, and Spatial Sciences, Michigan State University, East Lansing, MI
52 48823, USA
53 ¹⁹ Institute of Geographic Sciences and Natural Resources Research, Chinese Academy of Sciences, Beijing 100101,
54 PR China.
55 ²⁰ Climate and Ecosystem Sciences Division, Lawrence Berkeley National Lab, Berkeley, CA 94702, USA
56 ²¹ Universidade de Cuiaba, Cuiaba, Mato Grosso, Brazil
57 ²² Dept of Atmospheric and Oceanic Sciences, University of Wisconsin-Madison, Madison, WI 53706 USA
58 ²³ Department of Ecology and Evolutionary Biology, Princeton University, Princeton NJ, USA
59 ²⁴ Department of Earth Sciences, Vrije Universiteit, Amsterdam, Netherlands
60 ²⁵ School of Biology and Environmental Science, University College Dublin, Ireland
61 ²⁶ University of Alaska Fairbanks, Institute of Arctic Biology, Fairbanks, AK, USA
62 ²⁷ C NR - institute for Mediterranean Agricultural and Forest Systems, Piazzale Enrico Fermi, 1 Portici (Napoli)
63 Italy
64 ²⁸ Institute of Meteorology and Climate Research - Atmospheric Environmental Research, Karlsruhe Institute of
65 Technology (KIT Campus Alpin), 82467 Garmisch-Partenkirchen, Germany
66 ²⁹ Max Planck Institute for Biogeochemistry, Jena, Germany
67 ³⁰ ISTO, Université d'Orléans, CNRS, BRGM, UMR 7327, 45071, Orléans, France
68 ³¹ Okavango Research Institute, University of Botswana, Maun, Botswana.
69 ³² GFZ German Research Centre for Geosciences, Telegrafenberg, 14473 Potsdam, Germany
70 ³³ Manaaki Whenua - Landcare Research, Lincoln, NZ
71 ³⁴ Université de Montréal, Département de géographie, Université de Montréal, Montréal, QC H2V 0B3,
72 ³⁵ Canada & Dalhousie University, Department of Physics and Atmospheric Science, Halifax, NS B2Y 1P3, Canada
73 ³⁶ UK Centre for Ecology and Hydrology, Edinburgh, UK
74 ³⁷ Woods Institute for the Environment, Stanford University, Stanford, California
75 ³⁸ Research Faculty of Agriculture, Hokkaido University, Sapporo, Japan
76 ³⁹ Northern Research Station, USDA Forest Service, Durham, NH 03824, USA
77 ⁴⁰ Department of Environmental Science, Faculty of Science, Shinshu University
78 ⁴¹ University of Rostock, Rostock, Germany
79 ⁴² National Center for Agro Meteorology, Seoul, South Korea
80 ⁴³ Department of Geography, University of Tartu, Vanemuise st 46, Tartu, 51410, Estonia
81 ⁴⁴ Department of Forestry and Environmental Resources, North Carolina State University, Raleigh, NC, USA
82 ⁴⁵ Vegetation Ecology, Institute of Ecology and Landscape, Department Landscape Architecture, Weihenstephan-
83 Triesdorf University of Applied Sciences, Am Hofgarten 1, 85354 Freising, Germany
84 ⁴⁶ U.S. Geological Survey, Wetland and Aquatic Research Center, Lafayette LA
85 ⁴⁷ Department of Geography and Resource Management, The Chinese University of Hong Kong, Shatin, New
86 Territories, Hong Kong SAR, China
87 ⁴⁸ Institute for Atmospheric and Earth System Research/Physics, Faculty of Science, University of Helsinki,
88 Helsinki, Finland
89 ⁴⁹ European Commission, Joint Research Centre (JRC), Ispra, Italy.
90 ⁵⁰ Dept. of Sustainable Agro-Ecosystems and Bioresources, Research and Innovation Centre, Fondazione Edmund
91 Mach, San Michele all'Adige , Italy
92 ⁵¹ Department of Biological Sciences, Wellesley College, Wellesley, MA 02481, USA
93 ⁵² Institute for Biological Problems of the Cryolithozone, RAS, Yakutsk, REp. Yakutia.
94 ⁵³ Mazingira Centre, International Livestock Research Institute (ILRI), Old Naivasha Road, PO Box 30709, 00100
95 Nairobi, Kenya
96 ⁵⁴ Northern Arizona University, School of Informatics, Computing and Cyber Systems
97 ⁵⁵ Environmental Resources Engineering, SUNY College of Environmental Science and Forestry
98 ⁵⁶ Dept. of Forest Ecology and Management, Swedish University of Agricultural Sciences, 901 83 Umeå, Sweden
99 ⁵⁷ Dept. Biology, San Diego State University, San Diego, CA 92182, USA
100 ⁵⁸ Department of Earth and Environmental Sciences, Cal State East Bay, Hayward CA 94542 USA
101 ⁵⁹ National Agriculture and Food Research Organization, Tsukuba, Japan
102 ⁶⁰ USDA-ARS Delta Water Management Research Unit, Jonesboro, Arkansas 72401, United States

103 ⁶¹ School of Informatics, Computing & Cyber Systems, Northern Arizona University, Flagstaff, AZ 86011, USA
104 ⁶² Center for Ecosystem Science and Society, Northern Arizona University, Flagstaff, AZ 86011, USA
105 ⁶³ Department of Biological & Agricultural Engineering, University of Arkansas, Fayetteville, Arkansas 72701,
106 United States
107 ⁶⁴ Department of Landscape Architecture and Rural Systems Engineering, Seoul National University, South Korea
108 ⁶⁵ Hakubi center, Kyoto University, Kyoto, Japan
109 ⁶⁶ Department of Biological Sciences, Northern Arizona University, Flagstaff, AZ, USA
110 ⁶⁷ Dept of Earth and Environmental Science, Rutgers University Newark, NJ
111 ⁶⁸ Université de Montréal, Département de géographie, Université de Montréal, Montréal, QC H2V 0B3, Canada
112 ⁶⁹ Department of Ecology and Evolution, Cornell
113 ⁷⁰ U.S. Geological Survey, California Water Science Center, 6000 J Street, Placer Hall, Sacramento, CA, 95819
114 ⁷¹ National Ecological Observatory Network, Battelle, 1685 38th St Ste 100, Boulder, Colorado, 80301, USA
115 ⁷² Environmental Science Division, Argonne National Laboratory, Lemont, IL, USA
116 ⁷³ Space Sciences and Engineering Center, University of Wisconsin-Madison, Madison, WI 53706 USA
117 ⁷⁴ School of Forest Sciences, University of Eastern Finland, Joesnuu, Finland
118 ⁷⁵ Freshwater and Marine Science, University of Wisconsin-Madison
119 ⁷⁶ Graduate School of Life and Environmental Sciences, Osaka Prefecture University
120 ⁷⁷ Department of Plant and Soil Sciences, University of Delaware, Newark, DE, USA
121 ⁷⁸ A.N. Severtsov Institute of Ecology and Evolution, Russian Academy of Sciences
122 ⁷⁹ Yugra State University, 628012, Khanty-Mansiysk, Russia
123 ⁸⁰ California State University San Marcos, San Marcos, CA, USA
124 ⁸¹University of Innsbruck, Department of Ecology, Sternwartestr. 15, 6020 Innsbruck, AUSTRIA
125 ⁸² Sarawak Tropical Peat Research Institute, Sarawak, Malaysia
126 ⁸³ Department of Geographical Sciences, University of Maryland, College Park, MD 20740, USA
127 ⁸⁴ Department of Animal and Plant Sciences, University of Sheffield, Western Bank, Sheffield, S10 2TN, United
128 Kingdom
129 ⁸⁵ U.S. Geological Survey, Water Mission Area, 345 Middlefield Road, Menlo Park, CA, 94025
130 ⁸⁶ Biospheric Sciences Laboratory, NASA Goddard Space Flight Center, Greenbelt, Maryland
131 ⁸⁷ Precourt Institute for Energy, Stanford University, Stanford, California
132
133
134

135 *Correspondence to:* Kyle B. Delwiche (delwiche@stanford.edu)

136
137 **Abstract.** Methane (CH_4) emissions from natural landscapes constitute roughly half of global CH_4 contributions to
138 the atmosphere, yet large uncertainties remain in the absolute magnitude and the seasonality of emission quantities
139 and drivers. Eddy covariance (EC) measurements of CH_4 flux are ideal for constraining ecosystem-scale CH_4
140 emissions due to quasi-continuous and high temporal resolution of CH_4 flux measurements, coincident carbon dioxide,
141 water, and energy flux measurements, lack of ecosystem disturbance, and increased availability of datasets over the
142 last decade. Here, we 1) describe the newly published dataset, FLUXNET-CH4 Version 1.0, the first, open source
143 global dataset of CH_4 EC measurements (available at <https://fluxnet.org/data/fluxnet-ch4-community-product/>).
144 FLUXNET-CH4 includes half-hourly and daily gap-filled and non gap-filled aggregated CH_4 fluxes and
145 meteorological data from 79 sites globally: 42 freshwater wetlands, 6 brackish and saline wetlands, 7 formerly drained
146 ecosystems, 7 rice paddy sites, 2 lakes, and 15 uplands. Then, we 2) evaluate FLUXNET-CH4 representativeness for
147 freshwater wetland coverage globally, because the majority of sites in FLUXNET-CH4 Version 1.0 are freshwater
148 wetlands which are a substantial source of total atmospheric CH_4 emissions; and 3) provide the first global estimates
149 of the seasonal variability and seasonality predictors of freshwater wetland CH_4 fluxes. Our representativeness analysis
150 suggests that the freshwater wetland sites in the dataset cover global wetland bioclimatic attributes (encompassing
151 energy, moisture, and vegetation-related parameters) in arctic, boreal, and temperate regions, but only sparsely cover
152 humid tropical regions. Seasonality metrics of wetland CH_4 emissions vary considerably across latitudinal bands. In
153 freshwater wetlands (except those between 20° S to 20° N) the spring onset of elevated CH_4 emissions starts three

154 days earlier, and the CH₄ emission season lasts 4 days longer, for each degree C increase in mean annual air
155 temperature. On average, the spring onset of increasing CH₄ emissions lags soil warming by one month, with very
156 few sites experiencing increased CH₄ emissions prior to the onset of soil warming. In contrast, roughly half of these
157 sites experience the spring onset of rising CH₄ emissions prior to the spring increase in gross primary productivity
158 (GPP). The timing of peak summer CH₄ emissions does not correlate with the timing for either peak summer
159 temperature or peak GPP. Our results provide seasonality parameters for CH₄ modeling, and highlight seasonality
160 metrics that cannot be predicted by temperature or GPP (i.e., seasonality of CH₄ peak). FLUXNET-CH₄ is a powerful
161 new resource for diagnosing and understanding the role of terrestrial ecosystems and climate drivers in the global CH₄
162 cycle; and future additions of sites in tropical ecosystems and site-years of data collection will provide added value to
163 this database. All seasonality parameters are available at <https://doi.org/10.5281/zenodo.4672601>. Additionally, raw
164 FLUXNET-CH₄ data used to extract seasonality parameters can be downloaded from <https://fluxnet.org/data/fluxnet-ch4-community-product/>, and a complete list of the 79 individual site data DOIs is provided in Table 2 in the Data
165 Availability section of this document.
166

167
168
169
170
171

172 1 Introduction

173 Methane (CH₄) has a global warming potential that is 28 times larger than carbon dioxide (CO₂) on a 100-
174 year time scale (Myhre et al., 2013), and its atmospheric concentration has increased by >1000 ppb since 1800
175 (Etheridge et al., 1998). While atmospheric CH₄ concentrations are substantially lower than those of CO₂, CH₄ has
176 contributed 20-25% as much radiative forcing as CO₂ since 1750 (Etminan et al., 2016). Despite its importance to
177 global climate change, natural CH₄ sources and sinks remain poorly constrained, and with uncertain attribution to the
178 various biogenic and anthropogenic sources (Saunois et al., 2016, 2020). Bottom-up and top-down estimates differ
179 by 154 Tg/yr (745 versus 591 Tg/yr, respectively); much of this difference arises from natural sources (Saunois et al.,
180 2020). Vegetated wetlands and inland water bodies account for most natural CH₄ emissions, as well as the majority
181 of uncertainty in bottom-up emissions estimates (Saunois et al., 2016). Better diagnosis and prediction of terrestrial
182 CH₄ sources to the atmosphere requires high frequency and continuous measurements of CH₄ exchange across a
183 continuum of time (hours to years) and space (meters to kilometers) scales.

184 Tower-based eddy covariance (EC) measurements provide ecosystem-scale CH₄ fluxes at high temporal
185 resolution across years, are coupled with measurements of key CH₄ drivers such as temperature, water and recent
186 substrate input (inferred from CO₂ flux), and thus help constrain bottom-up CH₄ budgets and improve CH₄ predictions.
187 Although EC towers began measuring CO₂ fluxes in the late 1970s (Desjardins 1974; Anderson et al., 1984), and
188 some towers began measuring CH₄ in the 1990s (Verma et al., 1992), most CH₄ flux EC measurements began within
189 the last decade (2010s). Given that many EC CH₄ sites are relatively new, the flux community has only recently
190 compiled them for global synthesis efforts (e.g., Chang et al., 2021) and is still working to standardize CH₄ flux
191 measurements and establish gap-filling protocols (Nemitz et al., 2018; Knox et al., 2019). Furthermore, the growth of
192 EC networks for CH₄ fluxes has sometimes taken place in a relatively *ad hoc* fashion, often at sites that were already
193 measuring CO₂ fluxes or where higher CH₄ fluxes were expected, potentially introducing bias. The representativeness
194 and spatial distribution of CO₂ flux tower networks have been assessed to evaluate its ability to upscale fluxes
195 regionally (Hargrove et al., 2003; Hoffman et al., 2013; Papale et al., 2015; Villarreal et al., 2018, 2019) and globally
196 (Jung et al., 2009; 2020). However, a relatively sparse coverage of CH₄ flux towers prompts the question of how well
197 the current observation network provides a sufficient sampling of global or ecosystem-specific bioclimatic conditions.

198 Broad-scale wetland CH₄ seasonality estimates, such as when fluxes increase, peak, and decrease and the
199 predictors of seasonality, remain relatively unconstrained across wetlands globally. These key seasonality metrics
200 vary considerably across high-emitting systems such as wetlands and other aquatic systems (Desjardins, 1974; Dise,
201 1992; Melloh and Crill 1996; Wik et al., 2013; Zona et al., 2016; Treat et al., 2018). Few continuous CH₄ flux datasets
202 across representative site-years make it difficult to establish trends in seasonal dynamics, though monthly or annually
203 aggregated estimates of CH₄ fluxes from different seasons do exist for high latitudes (Zona et al., 2016; Treat et al.,
204 2018). Seasonal variability in freshwater wetland CH₄ fluxes is expected to be driven by changes in air and soil
205 temperature, soil moisture (including water table dynamics), and recent carbon substrate availability, which influence
206 the rates of CH₄ production and consumption (Lai, 2009; Bridgman et al., 2013; Dean et al., 2018). Temperature has
207 widely been found to strongly affect CH₄ flux (Chu et al., 2014; Yvon-Durocher et al., 2014; Sturtevant et al., 2016),
208 but the relationship is complex (Chang et al., 2020) and varies seasonally (Koebusch et al., 2015; Helbig et al., 2017).
209 CH₄ flux is also driven by inundation depth since anoxic conditions are typically necessary for methanogenesis (Lai,
210 2009; Bridgman et al., 2013), though CH₄ production under bulk-oxic conditions has been observed (Angle et al.,
211 2017). Substrate availability influences CH₄ production potential and is linked with gross primary productivity (GPP)
212 because recent photosynthate fuels methanogenesis though this relationship can vary by ecosystem type, plant
213 functional type and biome (Megonigal et al., 1999; Chanton et al., 2008; Hatala et al., 2012; Lai et al., 2014; Malhotra
214 and Roulet, 2015; Sturtevant et al., 2016). In process models, the seasonality of CH₄ emissions from wetlands globally
215 is primarily constrained by inundation (Poulter et al., 2017), with secondary within-wetland influences from
216 temperature and availability of carbon (C) substrates (Melton et al., 2013; Castro-Morales et al., 2018). Bottom-up
217 and top-down global CH₄ estimates continue to disagree on total CH₄ flux magnitudes and seasonality, including the
218 timing of annual peak emissions (Spahni et al., 2011; Saunois et al., 2020). Thus, the variability and predictors of
219 wetland CH₄ seasonality globally remain a knowledge gap that high-frequency and long-term EC data can help fill.

220 Here, we first describe Version 1.0 of the FLUXNET-CH₄ dataset (available at
221 <https://fluxnet.org/data/fluxnet-ch4-community-product/>). Version 1.0 of the dataset expands and formalizes the
222 publication of data scattered among regional flux networks as described previously in Knox et al. (2019). FLUXNET-
223 CH₄ includes half-hourly and daily gap-filled and non gap-filled aggregated CH₄ fluxes and meteorological data from
224 79 sites globally: 42 freshwater wetlands, 6 brackish and saline wetlands, 7 formerly drained ecosystems, 7 rice paddy
225 sites, 2 lakes, and 15 upland ecosystems. FLUXNET-CH₄ includes an additional 2 wetland sites (RU-Vrk and SE-
226 St1), but they are not available under the CC BY 4.0 data policy and thus are excluded from this analysis. Since the
227 majority of sites in FLUXNET-CH₄ Version 1.0 (hereafter referred to solely as “FLUXNET-CH₄”) are freshwater
228 wetlands, which are a substantial source of total atmospheric CH₄ emissions, we use the subset of data from freshwater
229 wetlands to evaluate the representativeness of freshwater wetland coverage in the FLUXNET-CH₄ dataset relative to
230 wetlands globally, and provide the first assessment of global variability and predictors of freshwater wetland CH₄ flux
231 seasonality. We quantify a suite of CH₄ seasonality metrics and evaluate temperature and GPP (a proxy for recent
232 substrate input) as predictors of seasonality across four latitudinal bands (northern, temperate, subtropical, and
233 tropical). Due to a lack of high-temporal resolution water table data at all sites, our analyses are unable to evaluate the
234 critical role of water table on CH₄ seasonality. Here we provide parameters for better understanding and modeling
235 seasonal variability in freshwater wetland CH₄ fluxes and generate new hypotheses and data resources for future
236 syntheses.

237 **2. Methods**

238 **2.1 FLUXNET-CH₄ dataset**

239 **2.1.1 History and data description**

240 The FLUXNET-CH₄ dataset was initiated by the Global Carbon Project (GCP) in 2017 to better constrain
241 the global CH₄ budget (<https://www.globalcarbonproject.org/methanebudget/index.htm>). Beginning with a kick off

242 meeting in May 2018 in Washington DC, hosted by Stanford University, we coordinated with the AmeriFlux
243 Management Project, the European Ecosystem Fluxes Database, and the ICOS Ecosystem Thematic Centre (ICOS-
244 ETC) to avoid duplication of efforts, as most sites are part of different regional networks (albeit with different data
245 products). We collected and standardized data for FLUXNET-CH4 with assistance from the regional flux networks,
246 AmeriFlux's "Year of Methane", FLUXNET, the EU's Readiness of ICOS for Necessities of Integrated Global
247 Observations (RINGO) project, and a U.S. Geological Survey Powell Center working group. FLUXNET-CH4 is a
248 community-led project, so while we developed it with assistance from FLUXNET, we do not necessarily use standard
249 FLUXNET data variables, formats, or methods.

250 FLUXNET-CH4 includes gap-filled half-hourly CH₄ fluxes and meteorological variables. Gaps in
251 meteorological variables (TA - air temperature, SW_IN - incoming shortwave radiation, LW_IN - incoming longwave
252 radiation, VPD - vapor pressure deficit, PA - pressure, P - precipitation, WS - wind speed) were filled with the
253 ERA-Interim (ERA-I) reanalysis product (Vuichard and Papale, 2015). We used the REddyProc package (Wutzler et
254 al., 2018) to filter flux values with low friction velocity (u_*) based on relating nighttime u_* , to fill gaps in CO₂, latent
255 heat, and sensible heat fluxes, and to partition net CO₂ fluxes into gross primary production (GPP) and ecosystem
256 respiration (RECO) using both the daytime (Lasslop et al., 2010) and nighttime (Reichstein et al., 2005) approaches.
257 Data gaps of CH₄ flux were filled using artificial neural network (ANN) methods first described in Knox et al. (2015)
258 and in Knox et al. (2019), and summarized here in Sect. 2.1.2. Gap-filled data for gaps exceeding two months are
259 provided and flagged for quality. Please see Table B1 for variable description and units, as well as quality flag
260 information. For the seasonality analysis in this paper we excluded data from gaps exceeding two months, and we
261 encourage future users of FLUXNET-CH4 to critically evaluate gap-filled values from long data gaps before including
262 them in analyses (Dengel et al., 2013; Kim et al., 2020).

263 In addition to half-hourly data, the FLUXNET-CH4 Version 1.0 release also contains a full set of daily mean
264 values for all parameters except wind direction and precipitation. Daily precipitation is included as the daily sum of
265 the half-hourly data, and daily average wind direction is not included.

266 2.1.2 Gap-filling methods and uncertainty estimates

267 As described in Knox et al. (2015) and in Knox et al. (2019), the ANN routine used to gap-fill the CH₄ data
268 was optimized for generalizability and representativeness. To avoid biasing the ANN toward environmental conditions
269 with typically better data coverage (e.g., summer-time and daytime measurements), the explanatory data were divided
270 into a maximum of 15 clusters using a k-means clustering algorithm. Data used to train, test, and validate the ANN
271 were proportionally sampled from these clusters. For generalizability, the simplest ANN architecture with good
272 performance (<5% gain in model accuracy for additional increases in architecture complexity) was selected for 20
273 extractions of the training, test, and validation data. Within each extraction, each tested ANN architecture was
274 reinitialized 10 times, and the initialization with the lowest root-mean-square-error was selected to avoid local minima.
275 The median of the 20 predictions was used to fill each gap. A standard set of variables available across all sites was
276 used to gap-fill CH₄ fluxes (Dengel et al., 2013), which included the previously mentioned meteorological variables
277 TA, SW_IN, WS, PA, and sine and cosine functions to represent seasonality. These meteorological variables were
278 selected for their relevance to CH₄ exchange and were gap-filled using the ERA-I reanalysis data. Other variables
279 related to CH₄ flux (e.g., water table depth [WTD] and soil temperature [TS]) were not included as explanatory
280 variables as they were not available across all sites or had large gaps that could not be filled using the ERA-I reanalysis
281 data (Knox et al., 2019). The ANN gap-filling was performed using MATLAB (MathWorks 2018, version 9.4.0).

282 While the median of the 20 predictions was used to fill each gap, the spread of the predictions was used to
283 provide a measure of uncertainty resulting from the ANN gap-filling procedure. Specifically, the combined annual
284 gap-filling and random uncertainty was calculated from the variance of the cumulative sums of the 20 ANN predictions
285 (Knox et al., 2015; Anderson et al., 2016; Oikawa et al., 2017). The (non-cumulative) variance of the 20 ANN

286 predictions was also used to provide gap-filling uncertainty for each half-hourly gap-filled value. While this output is
287 useful for data-model comparisons, it cannot be used to estimate cumulative annual gap-filling error because gap-
288 filling error is not random, which is why the cumulative sums of the 20 ANN predictions are used to estimate annual
289 gap-filling error.

290 Random errors in EC fluxes follow a double exponential (Laplace) distribution with the standard deviation
291 varying with flux magnitude (Richardson et al., 2006; Richardson et al., 2012). For half-hourly CH₄ flux
292 measurements, random error was estimated using the residuals of the median ANN predictions, providing a
293 conservative “upper limit” estimate of the random flux uncertainty (Moffat et al., 2007; Richardson et al., 2008). The
294 annual cumulative uncertainty at 95% confidence was estimated by adding the cumulative gap-filling and random
295 measurement uncertainties in quadrature (Richardson and Hollinger, 2007; Anderson et al., 2016). Annual
296 uncertainties in CH₄ flux for individual site-years are provided in Table B2. Throughout this paper, we include
297 uncertainties on individual site years when discussing single years of data. In sites with multiple years of data, we
298 report the standard deviation of the multiple years.

299 **2.1.3 Dataset structure and site metadata**

300 FLUXNET-CH4 contains two comma-separated data files per site at half-hourly and daily resolutions which
301 are available for download at <https://fluxnet.org/data/fluxnet-ch4-community-product/>, along with a file containing
302 select site metadata. Each site has a unique FLUXNET-CH4 DOI. All data from the 79 sites used in this analysis are
303 available under CC BY 4.0 (<https://creativecommons.org/licenses/by/4.0/>) copyright license (FLUXNET-CH4 has an
304 additional 2 sites available under the FLUXNET Tier 2 license (<https://fluxnet.org/data/data-policy/>), though these
305 sites are not included in our analysis).

306 Metadata (Table B3) include site coordinates, ecosystem classification based on site literature,
307 presence/absence and dominance for specific vegetation types, and DOI link, as well as calculated data such as annual
308 and quarterly CH₄ flux values. FLUXNET-CH4 Version 1.0 sites were classified based on site-specific literature as
309 fen, bog, swamp, marsh, salt marsh, lake, mangrove, rice paddy/field, wet tundra, upland, or drained ecosystems that
310 previously could have been wetlands, seasonally flooded pastures, or agricultural areas. To the extent possible, we
311 followed classification systems of previous wetland CH₄ syntheses (Olefeldt et al., 2013; Turetsky et al., 2014; Treat
312 et al., 2018). Drained systems are former wetlands that have subsequently been drained but may maintain a relatively
313 shallow water table, which can contribute to occasional methane emissions, although we do not have specific water
314 table depth information at all drained sites. Upland ecosystems are further divided into alpine meadows, grasslands,
315 needleleaf forests, mixed forest, crops, tundra, and urban. Freshwater wetland classifications follow hydrological
316 definitions of bog (ombrotrophic), fen (minerotrophic), wet tundra, marshes and swamps, and were designated as per
317 primary literature on the site. For all sites, vegetation was classified for presence or absence of brown mosses (all
318 species from the division Bryophyta except those in the class Sphagnopsida), *Sphagnum* mosses (any species from
319 class Sphagnopsida), ericaceous shrubs, trees (of any height) and aerenchymatous species (mostly Order Poales but
320 includes exceptions). These categories closely follow Treat et al., (2018), except that aerenchymatous species had to
321 be expanded beyond Cyperaceae to incorporate wetlands globally. Presence/absence of vegetation groups was
322 designated based on species lists in primary literature from the site. Out of the vegetation groups present, the dominant
323 (most abundant) group is also reported and is based on information provided by lead site investigators.

324 In addition to the variable description table (Table B1) and the site metadata (Table B3), we provide several
325 more tables to complement our analysis. Table B4 includes the climatic data used in the representativeness analysis.
326 Table 5 provides seasonality parameters for CH₄ flux, air temperature, soil temperature (from the probe closest to the
327 ground surface), and GPP. For sites with multiple soil temperature probes, the full set of soil temperature parameters
328 are in Table B6. Table B7 contains the soil temperature probe depths. Table B2 contains the annual CH₄ flux and
329 uncertainty. All Appendix B tables are also available at <https://doi.org/10.5281/zenodo.4672601>.

330

331 **2.1.4 Annual CH₄ fluxes**

332 Annual CH₄ fluxes were calculated from gap-filled data for site-years with data gaps shorter than two
333 consecutive months, or for sites above 20° N where >2 month data gaps occurred outside of the highest CH₄-emission
334 months of May 1 through October 31. Since we did not sum gap-filled values for >2 month gaps during the winter,
335 annual sums from these years will be an underestimate since winter fluxes can be important (Zona et al., 2016; Treat
336 et al., 2018). Several sites had less than one year of data, and we report gap-filled CH₄ flux annual sums for sites with
337 between six months and one year of data (BW-Gum = 228 days, CH-Oe2 = 200 days, JP-Swl = 210 days, US-EDN =
338 182 days). While these sums will be an underestimate of annual CH₄ flux since they do not span a full year (and we
339 therefore do not use them in the seasonality analysis), their relative magnitude can still be informative. For example,
340 site JP-SWL is a lake site, and even with less than a year of data the summed CH₄ flux of 66 g C m⁻² is relatively high
341 (Taoka et al., 2020). In addition to sites with short time series, the annual CH₄ sum for site ID-Pag represents 365 days
342 spanning June 2016 to June 2017.

343 **2.1.5 Subset analysis on freshwater wetland CH₄ flux**

344 In addition to the FLUXNET-CH₄-wide description of site class distributions and annual CH₄ fluxes, we
345 also include a subset analysis on freshwater wetlands, given that it is the dominant ecosystem type in our dataset and
346 an important global CH₄ source (Saunois et al., 2016). First, we analyze freshwater wetland representativeness, and
347 subsequently the seasonality of their CH₄ emissions. Freshwater wetlands included in the seasonality and
348 representativeness analysis are indicated in Table B3, column “IN_SEASONALITY_ANALYSIS”.

349

350 **2.2 Wetland representativeness**

351 **2.2.1 Principal Component Analysis**

352 To compare the FLUXNET-CH₄ site distribution to the global wetland distribution, we evaluated their
353 representativeness in the entire global wetland cover along four bioclimatic gradients. Only freshwater wetland sites
354 were included in this analysis. Coastal sites were excluded because salinity, an important control on CH₄ production,
355 could not be evaluated across the tower network due to a lack of global gridded salinity data (Bartlett et al., 1987;
356 Poffenbarger et al., 2011). The four bioclimatic variables used were: mean annual air temperature (MAT), latent heat
357 flux (LE), enhanced vegetation index (EVI), and simple ratio water index (SRWI; data sources in Table B4). We use
358 EVI because it is a more direct measurement than GPP from global gridded products and is considered a reasonable
359 proxy for GPP (Sims et al., 2006). Together, these environmental variables account for, or are, proxies for key controls
360 of CH₄ production, oxidation at the surface, and transport (Bridgman et al., 2013). We use a principal components
361 analysis (PCA) to visualize the site distribution across the four environmental drivers at once. For this analysis, we
362 consider the annual average bioclimatic conditions over 2003-2015. In the PCA output, we evaluate the coverage of
363 the 42 freshwater sites over 0.25° grid cells containing >5% wetland mean cover in Wetland Area and Dynamics for
364 Methane Modeling (WAD2M; Zhang et al., 2020; Zhang et al., 2021) for the same time period.

365 **2.2.2 Global Dissimilarity and Constituency Analysis**

366 To further identify geographical gaps in the coverage of the FLUXNET-CH₄ Version 1.0 network, we
367 quantified the dissimilarity of global wetlands from the tower network, using a similar approach to that taken for CO₂
368 flux towers (Meyer and Pebesma 2020). We calculated the 4-dimensional Euclidean distance from the four bioclimatic
369 variables between every point at the land surface to every tower location at the FLUXNET-CH₄ network. We then
370 divided these distances by the average distance between towers to produce a dissimilarity index. Dissimilarity scores

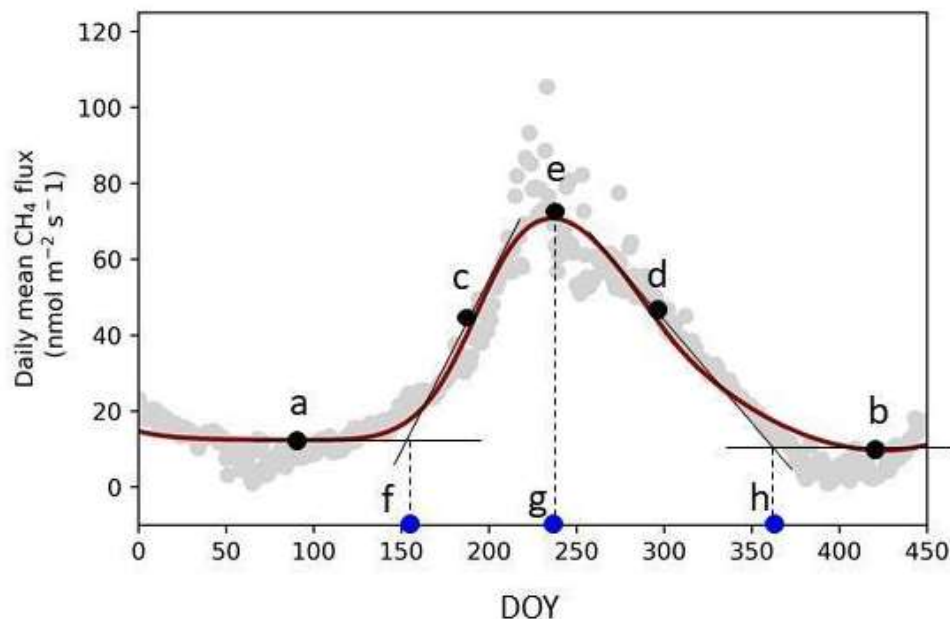
371 <1 represent areas whose nearest tower is closer than the average distance among towers, while areas with scores >1
372 are more distant. Lastly, we identified the importance of an individual tower in the network by estimating the
373 geographical area to which it is most analogous in bioclimate space. We divided the world's land surface according
374 to closest towers in bioclimatic space. The area to which each tower is nearest is defined as the tower's constituency.

375 **2.3 Wetland CH₄ seasonality**

376 To examine freshwater wetland CH₄ seasonality across the global range of sites in FLUXNET-CH4, we
377 extracted seasonality parameters for CH₄, temperature, and GPP using Timesat, a software package designed to
378 analyze seasonality of environmental systems (Jönsson and Eklundh, 2002; Jönsson and Eklundh, 2004; Eklundh
379 and Jönsson, 2015). Timesat calculates several seasonality parameters, including baseline flux, peak flux, and the
380 slope of spring flux increase and fall decrease (Fig. 1). We also calculate parameters such as amplitude (peak flux -
381 baseline, which is the average of spring and fall baselines; ("e" - ((a" + "b")/2) in Fig. 1), and relative peak timing (
382 ("g" - "f") / ("h" - "f") in Fig. 1). Timesat uses a double-logistic fitting function to create a series of localized fits
383 centered on data minima and maxima. Localized fits are determined by minimizing a merit function with the
384 Levenberg-Marquardt method (Madsen et al., 2004; Nielsen, 1999). These localized fits are then merged using a
385 global function to create a smooth fit over the full time interval. To fit CH₄ time-series in Timesat, we used gap-
386 filled data after removing gaps exceeding two months. We do not report Timesat parameters when large gaps occur
387 during CH₄ emissions spring increase, peak, or fall decrease.

388 We estimate 'start of elevated emissions season' when CH₄ emissions begin to increase in the spring ("f"
389 in Fig. 1), and 'end of elevated emissions season' when the period of elevated CH₄ flux ends in the fall ("h" in Fig.
390 1), as the intercept between the Timesat fitted baseline parameter and shoulder-season slope (similar to Gu et al.,
391 2009). To extract seasonality parameters with Timesat, sites need a sufficiently pronounced seasonality, a
392 sufficiently long time period, and minimal data gaps (we note that while Timesat is capable of fitting two peaks per
393 year, all the freshwater wetland sites have a single annual peak). We excluded site-years in restored wetlands when
394 wetlands were still under construction. Of the 42 freshwater wetland sites in FLUXNET-CH4 Version 1.0, 36 had
395 sufficient data series to extract seasonality parameters. These 36 wetlands had 141 site-years of data total, which we
396 fit with the double-logistic fitting method which followed site data well (representative examples in Fig. 2). For
397 extratropical sites in the Southern Hemisphere, we shifted all data by 182 days so that maximum solar insolation
398 seasonality would be congruent across the globe.

399 We also used Timesat to extract seasonality metrics for GPP, partitioned using the daytime-based approach
400 (Lasslop et al., 2010) (GPP_DT), air temperature (TA), and soil temperature (TS_1, TS_2, etc). For sites where
401 winter soil temperatures fall significantly below 0 °C, Timesat fits a soil temperature "start of elevated season" date
402 to periods when the soil is still frozen. In order for Timesat to define the soil temperature seasonality within the
403 thawed season, we converted all negative soil temperatures to zero (simply removing these values results in too
404 many missing values for Timesat to fit). Many sites have more than one soil temperature probe, so we extracted
405 separate seasonality metrics from each individual probe (although we used the metrics from the shallowest
406 temperature probe in our analysis). Tables B4 contain the Timesat seasonality parameters used in the seasonality
407 analysis. We did not include water table depth in the seasonality analysis because many sites either lack water table
408 depth measurements or have sparse data.

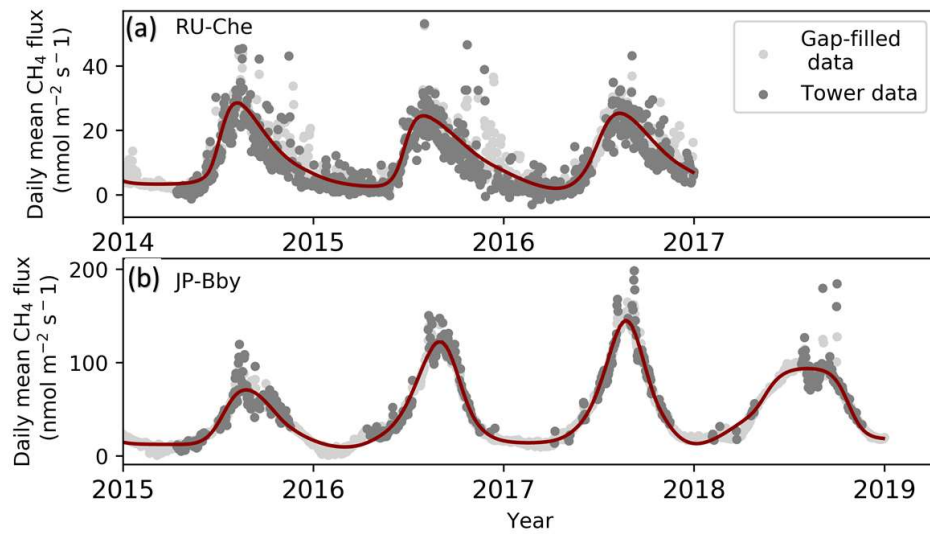


409

410 Figure 1: TIMESAT parameter description. (a) and (b) base values (Timesat reports the average of these two values), (c)
 411 and (d) slopes of seasonal curves (lines drawn between 20% and 80% of the amplitude), (e) peak value, and day of year
 412 (DOY) for the start (f), peak (g), and end (h) of the elevated methane (CH_4) emissions season. Data points are the mean
 413 daily gap-filled CH_4 fluxes from site JP-Bby in 2015.

414

415



416

417 Figure 2: Examples of Timesat fits for two FLUXNET- CH_4 sites, (a) RU-Che and (b) JP-Bby. Methane (CH_4) flux data
 418 showing daily average flux tower data, with several high outliers excluded to improve the plot (dark gray), gap-filled

419 values (light gray), and Timesat-fitted curve (dark red line) for sites JP-Bby and RU-Che. Timesat captures the size and
420 shape of peaks (note different scale on y-axes). CH₄ = methane.

421

422 We regressed the CH₄ seasonality parameters from Timesat against annual temperature, annual water table
423 depth, and Timesat seasonality parameters for air temperature, soil temperature, and GPP (proxy for recent carbon
424 input available as substrate) using linear mixed-effect modeling with the *lmer* command (with site as a random
425 effect) from the R (R Core Team 2018, version 3.6.2) package lmerTest (Kuznetsova et al., 2017). For these
426 regressions we present the marginal R² outputs from *lmer*, which represent the variance explained only by the fixed
427 effects. Mixed-effect modeling was necessary to account for the non-independence between measurements taken at
428 the same site during different years (Zona et al., 2016; Treat et al., 2018). We also compared how seasonality
429 metrics varied across latitudinal bands by dividing sites into northern (> 60° N), temperate (between 40° N and 60°
430 N), subtropical (absolute value between 20° and 40° latitude, with site NZ-KOP being the only Southern hemisphere
431 site), and tropical (absolute value below 20°). Site-year totals for the northern, temperate, subtropical, and tropical
432 bands were $n = 57, 36, 39$, and 9, respectively. We used the Kruskal-Wallis test to establish whether groups (either
433 across quarters or across latitudes) were from similar distributions, and the post hoc multiple comparison “Dwass,
434 Steel, Critchlow, and Fligner” procedure for inter-group comparisons. Kruskal-Wallis and post-hoc tests were
435 implemented in Python Version 3.7.4, using stats from scipy for Kruskal-Wallis and posthoc_dscf from
436 scikit_posthocs.

437 We also compared quarterly CH₄ flux sums by dividing data into quarterly periods:
438 January/February/March (JFM), April/May/June (AMJ), July/August/September (JAS), and
439 October/November/December (OND). For the sake of simplicity, we chose to compare quarterly periods rather than
440 site-specific growing/non-growing season periods so that all time periods would be the same length. Quarterly sums
441 were computed from the gap-filled CH₄ fluxes when the longest continuous data gap within the quarter did not
442 exceed 30 days, leading to site-year counts of 67, 92, 95, 72 for JFM, AMJ, JAS, and OND, respectively. We
443 compared quarterly CH₄ fluxes across latitudinal bands both for the total CH₄ flux, and for the quarterly percentage
444 of the annual CH₄ flux. Quarterly statistics were also conducted with the Kruskal-Wallis test and the post hoc
445 multiple comparison “Dwass, Steel, Critchlow, and Fligner” procedure implemented in Python. Quarterly values
446 are provided in Table B3, and the sum of mean quarterly CH₄ flux does not always equal mean annual CH₄ flux
447 because some quarters either do not have data, or have data gaps that exceed 30 days.
448

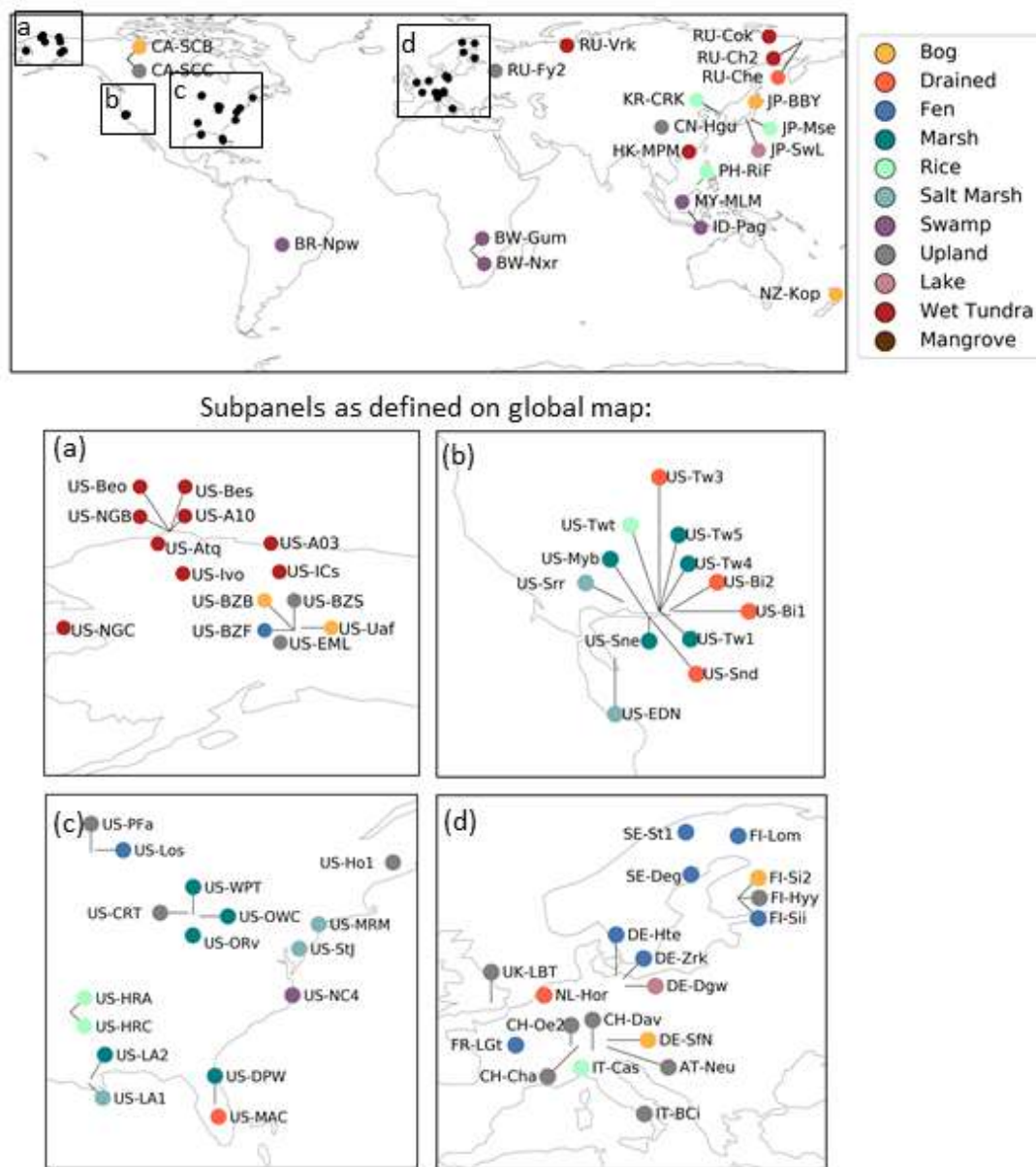
449 3. Results and Discussion

450 3.1 FLUXNET-CH4 dataset

451 3.1.1 Dataset description

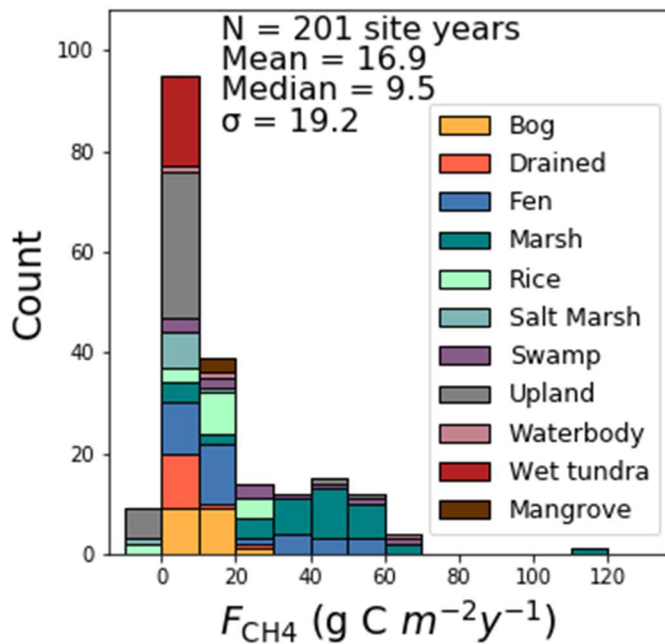
452 Version 1.0 of the FLUXNET-CH4 dataset contains 79 unique sites, 293 total site-years of data, and 201
453 site-years with sufficient data to estimate annual CH₄ emissions. A synthesis paper, published prior to the public data
454 release of FLUXNET-CH4 Version 1.0, had 60 unique sites and 139 site-years with annual CH₄ emissions estimates
455 (Knox et al., 2019). Freshwater wetlands make up the majority of sites ($n = 42$), and the dataset also includes five salt
456 marshes and one mangrove wetland. Notable additions to FLUXNET-CH4 from the previous unpublished dataset
457 used in Knox et al., (2019) include six tropical sites (between 20° S and 20° N), including one site in South America,
458 two sites in southern Africa, and three sites in Southeast Asia. The 15 upland sites include six needleleaf forests, three
459 crop sites (excluding rice), two alpine meadows, one grassland, one mixed forest, one tundra, and one urban site. The
460 drained sites represent former wetlands that have been artificially drained for use as grasslands ($n = 3$) or croplands

461 (n = 3). FLUXNET-CH4 sites span the globe, though are concentrated in North America and Europe (Fig. 3). Table
462 B3 includes characteristics of all sites in the dataset.



463

464 Figure 3. Global map of FLUXNET-CH4 Version 1.0 site locations colored by site type. Insets (a)-(d) show sites that were
465 too closely located to distinguish in the global map.



466

467 **Figure 4.** Histogram of annual methane fluxes (F_{CH_4} , $\text{g C m}^{-2} \text{yr}^{-1}$) grouped by site type.

468 Sites represent a range of ecosystem types, latitudes, median fluxes, and seasonality patterns (Table 1).
 469 Across all FLUXNET-CH4 sites (including non-wetland sites), mean average annual CH₄ flux is positively skewed
 470 with a median flux of $9.5 \text{ g C m}^{-2} \text{yr}^{-1}$, a mean flux of $16.9 \text{ g C m}^{-2} \text{yr}^{-1}$, and numerous annual CH₄ fluxes exceeding
 471 $60 \text{ g C m}^{-2} \text{yr}^{-1}$. Marshes and swamps have the highest median flux, and upland, salt marsh, and tundra sites have
 472 the lowest (Fig. 4). Lake emissions are highly variable due to one high-flux lake site (JP-SWL). Flux data at many
 473 sites show strong seasonality in CH₄ emissions, but data coverage is also lower outside the growing season (Table
 474 1). Data coverage is lowest during the JFM quarter (on average 20% of half-hourly time periods contain flux data)
 475 reflecting the predominance of Northern hemisphere sites and the practical difficulties in maintaining EC tower sites
 476 during colder winter months (Table 1). Bogs, fens, and marshes have pronounced seasonality, with fluxes being
 477 highest in the AMJ and JAS quarters. In contrast, CH₄ fluxes from uplands, drained sites, and salt marshes are more
 478 uniform and low year-round.

479 **Table 1:** Summary table of sites grouped by ecosystem class reporting annual mean flux (Ann_Flux) and standard
 480 deviation from inter-annual variability (Ann_Flux_SD), site-years of data, % data cover per quarter, and median (med.)
 481 flux across site class. JFM= January, February, March; AMJ = April, May, June; JAS = July, August, September; OND
 482 = October, November, December.

	# of Sites	# of Site- Year s	Ann_Fl ux g C year ⁻¹	Ann_Flu x_SD g C m ⁻² year ⁻¹	JFM cover- age (%)	AMJ cover- age (%)	JAS cover- age (%)	OND cover- age (%)	JFM flux (med.)	AMJ flux (med.)	JAS flux (med.)	OND flux (med.)
Salt marsh	5	10	2.9	4.7	7	42	50	37	1.5	1.7	2.1	1.6
Wet tundra	11	39	3.8	1.8	8	28	40	18	0.4	2.6	8.1	3.2

Upland	15	47	4.0	10.5	23	35	39	28	1.2	0.5	1.4	0.8
Drained	7	20	6.3	7.1	22	39	39	29	4.6	3.6	5.1	3.6
Bog	7	32	10.5	6.4	8	27	37	18	7.2	11.0	24.8	9.5
Mangrove	1	3	11.1	0.5	46	28	30	41	3.2	7.2	22.5	14.1
Rice	7	20	14.4	8.8	16	37	45	27	3.2	11.9	43.1	4.2
Fen	8	40	20.5	16.0	29	43	40	30	2.8	14.2	26.0	6.4
Swamp	6	15	26.4	19.9	24	34	29	19	14.7	24.9	31.0	24.4
Lake	2	4	28.2	33.4	15	13	27	36	0.2	47.6	90.2	40.3
Marsh	10	42	40.8	20.7	22	43	53	30	13.5	55.0	85.8	36.1

483

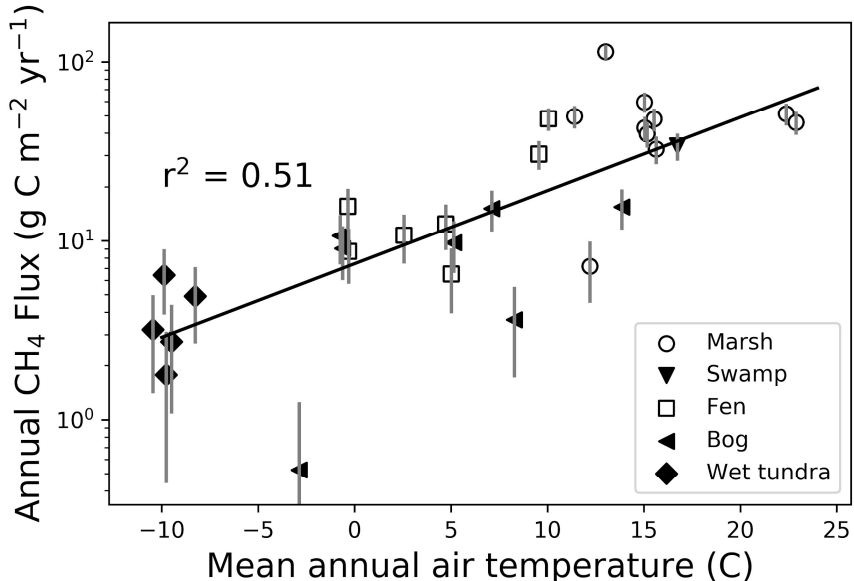
484

485 **3.1.2 Freshwater wetland CH₄ characteristics**

486 The FLUXNET-CH4 Version 1.0 dataset contains 42 freshwater wetlands that span 37°S to 69°N, including
 487 bogs, fens, wet tundra, marshes, and swamps, and a range of annual CH₄ emission rates (Fig. 4). The majority of
 488 freshwater wetlands in our dataset emit 0–20 g C m⁻² yr⁻¹, with 10 emitting 20–60 g C m⁻² yr⁻¹, and one more than 60 g
 489 C m⁻² yr⁻¹. Differences in annual CH₄ flux among wetland types is partially driven by temperature (which is often
 490 linked to site type), with mean annual air temperature explaining 51% of the variance between sites (Fig. 5, exponential
 491 relationship). The global relationship between annual methane emissions and temperature can be described using a
 492 Q₁₀ relationship where $Q_{10} = R_2/R_1^{((T_2-T_1)/10)}$, with R₂ and R₁ being the CH₄ emission rates at temperatures T₂ and T₁,
 493 respectively (temperature in degrees C). The Q₁₀ based on Fig. 5 data is 2.57. We also note that annual CH₄ flux from
 494 individual biomes may have different relationships with temperature, as previous work has shown biome-specific
 495 trends in CH₄ flux with environmental drivers (Abdalla et al., 2016). However, there currently are not enough data
 496 points in each biome category to compare relationships between mean annual CH₄ flux and temperature. Annual CH₄
 497 flux is not correlated with mean annual water table depth in FLUXNET-CH4, unlike in Knox et al., (2019), which
 498 used a subset of the FLUXNET-CH4 sites where CH₄ flux was correlated with water table depth only for sites with
 499 water table below ground for 90% of measured days ($r^2 = 0.31$, $p < 0.05$, $n = 27$ site years). Freshwater wetland
 500 seasonality is further described in Sect. 3.3.

501

502



503
504 **Figure 5:** Relationship between mean annual wetland methane (CH₄) flux (g C m⁻² yr⁻¹, logarithmic scale) and mean
505 annual air temperature (°C) for each freshwater wetland site, with wetland type indicated by symbol. Markers represent
506 individual site means, with vertical error bars representing the standard deviation of interannual variability.

507

508

509 3.1.3 Upland, rice and urban CH₄ characteristics

510 Upland agricultural sites are characterized by a lack of seasonal pattern in CH₄ emissions, relatively low flux,
511 and sometimes negative daily flux (i.e., CH₄ uptake) averages. All of the upland non-agricultural sites in FLUXNET-
512 CH₄ Version 1.0 are net (albeit weak) CH₄ sources except for the needleleaf forest site US-Ho1, which has mean
513 annual CH₄ flux of -0.1 ± 0.1 g C m⁻² yr⁻¹ (see Table B3 for site acronyms and metadata). The average agricultural site
514 emissions are 1.3 ± 0.8 g C m⁻² yr⁻¹ and non-agricultural site emissions are 1.6 ± 1.2 g C m⁻² yr⁻¹ across sites.

515 Rice sites ($n = 7$) have average annual emissions across all sites of 16.7 ± 7.7 g C m⁻² yr⁻¹ and are characterized
516 by strong seasonal patterns, with either one or more CH₄ emission peaks per year depending on the number of rice
517 seasons and field water management. One peak is typically observed during the reproductive period for the
518 continuously flooded sites with one rice season (i.e., US-HRC, JP-MSE) (Iwata et al., 2018; Runkle et al., 2019;
519 Hwang et al., 2020). For sites with only one rice season but with single or multiple drainage and re-flooding periods,
520 a secondary peak may appear before the reproductive peak (i.e., KR-CRK, IT-Cas, and US-HRA; Meijide et al., 2011;
521 Runkle et al., 2019; Hwang et al., 2020). Two reproductive peaks appear for sites with two rice seasons (i.e., PH-RiF),
522 and each reproductive peak may be accompanied by a secondary peak due to drainage events (Alberto et al., 2015).
523 Even sites with one, continuously flooded rice season may experience a second peak if the field is flooded during the
524 fallow season to provide habitat for migrating birds (e.g., US-Twt; Knox et al., 2016).

525 The dataset has one year of urban data from site UK-LBT in London, England. UK-LBT observes CH₄ fluxes
526 from a 190 m tall communications tower in the center of London, and has a mean annual CH₄ flux of 46.5 ± 5.6 g C
527 m⁻² yr⁻¹. This flux is more than twice as high as the mean annual CH₄ flux across all FLUXNET-CH₄ sites, 16.9 g C
528 m⁻² yr⁻¹. The London site has higher CH₄ emissions in the winter compared to summer, which is attributed to a seasonal
529 increase in natural gas usage (Helfter et al., 2016.)

530 **3.1.4 Saltwater and mangrove wetland CH₄ characteristics**

531 Three of the five saltwater wetlands in FLUXNET-CH₄ (US-Edn, US-MRM, and US-Srr) have a very low
532 mean annual CH₄ flux (see Table B2 for individual site-year CH₄ flux sums and associated uncertainty) and minimal
533 seasonality. Two other FLUXNET-CH₄ saltwater sites (US-La1 and US-StJ) have significantly higher fluxes, with
534 annual sums of 12.6 ± 0.6 and 9.6 ± 1.0 g C m⁻² yr⁻¹, respectively, while the mangrove site HK-MPM has annual mean
535 fluxes of 11.1 ± 0.5 g C m⁻² yr⁻¹. This range of CH₄ fluxes across different saltwater ecosystems could be valuable for
536 exploring the effect of salinity and different biogeochemical pathways of CH₄ production, oxidation, and transport of
537 CH₄ (Bartlett et al., 1987; Poffenbarger et al., 2011). Saltwater wetlands along the coast have unique CH₄ dynamics
538 attributable to the presence of abundant electron acceptors, most importantly sulphates, which inhibit methanogenesis
539 (Pattnaik et al., 2000; Mishra et al., 2003; Weston et al., 2006), but at low concentrations can have no effect (Chambers
540 et al., 2011) or even increase methanogenesis (Weston et al., 2011). In fact, estuarine wetlands with moderate salinity
541 can still be significant sources of CH₄ (Liu et al., 2020). Even under sulfate-rich conditions, high CH₄ production can
542 be found via methylotrophic methanogenesis (Dalcin Martins et al. 2017; Seyfferth et al., 2020,) or because the
543 processes of sulfate reduction and methanogenesis are spatially separated (Koebisch et al., 2019). Consequently,
544 representing the biophysical drivers of ecosystem-scale CH₄ fluxes in non-freshwater wetlands is challenging and may
545 represent a combination of competing or confounding effects (Vazquez-Lule and Vargas 2021).

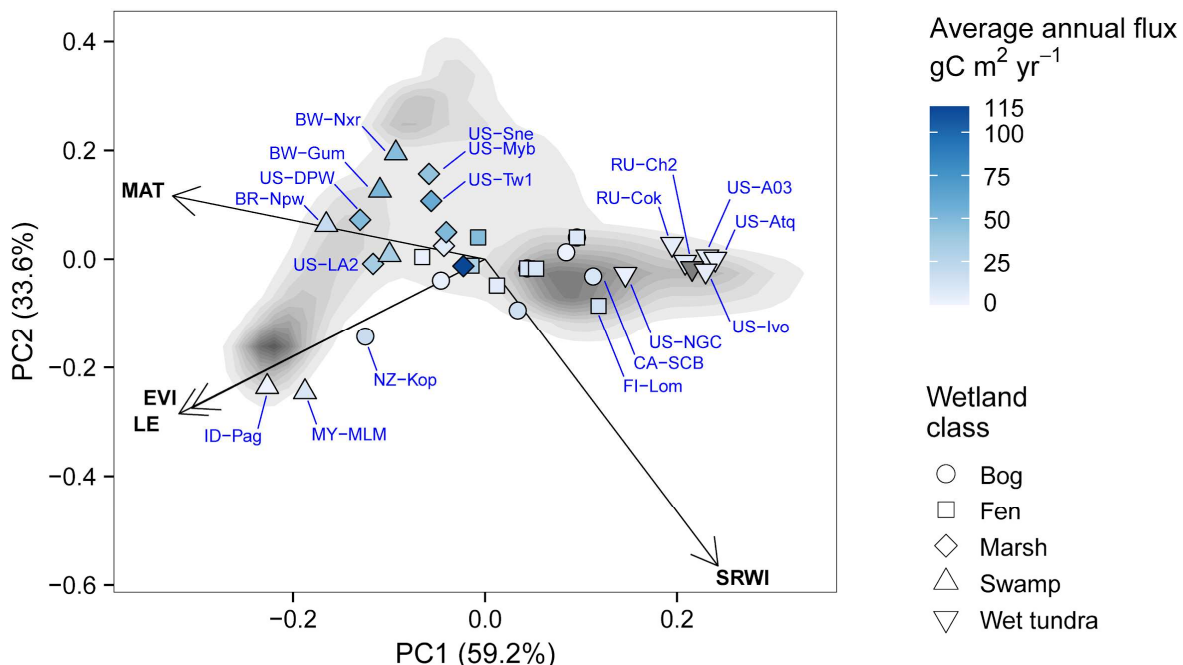
546

547 **3.2 Freshwater wetland representativeness**

548 We evaluated the representativeness of freshwater wetland sites in the FLUXNET-CH₄ Version 1.0 dataset
549 against wetlands globally, based on bioclimatic conditions of our sites. When evaluating bioclimatic variables
550 individually, the distribution of freshwater wetlands across the network was significantly different from the global
551 distribution ($\alpha > 0.05$; two-tailed Kolmogorov-Smirnov tests; see Table B4). We exclude wetlands classified as
552 “Salt Marsh” in this representativeness analysis and the seasonality analysis below because of the unique CH₄ flux
553 dynamics in saltwater ecosystems (as discussed in section 3.1.4), though we note that some of the coastal wetlands
554 included in the freshwater analysis periodically experience brackish water (i.e.: US-Myb, US-Sne).

555 When considering the four bioclimatic variables, MAT, LE, EVI and SRWI in a PCA, we found that our
556 tower network generally samples the bioclimatic conditions of global wetland cover, but some noticeable gaps remain
557 (Fig. 6). Three clusters of the world’s wetland-dense regions are identified, but are not equally sampled by the network.
558 A cluster of low temperature wetlands is sampled by a large number of high-latitude sites. The other two wetland
559 clusters are not as well sampled: a high temperature and LE cluster is represented only by two towers (ID-Pag and
560 MY-MLM), while drier and temperate and subtropical wetlands including large swathes of the Sahel in Africa only
561 have a site in Botswana (BW-Npw) as their closest-analog tower.

562



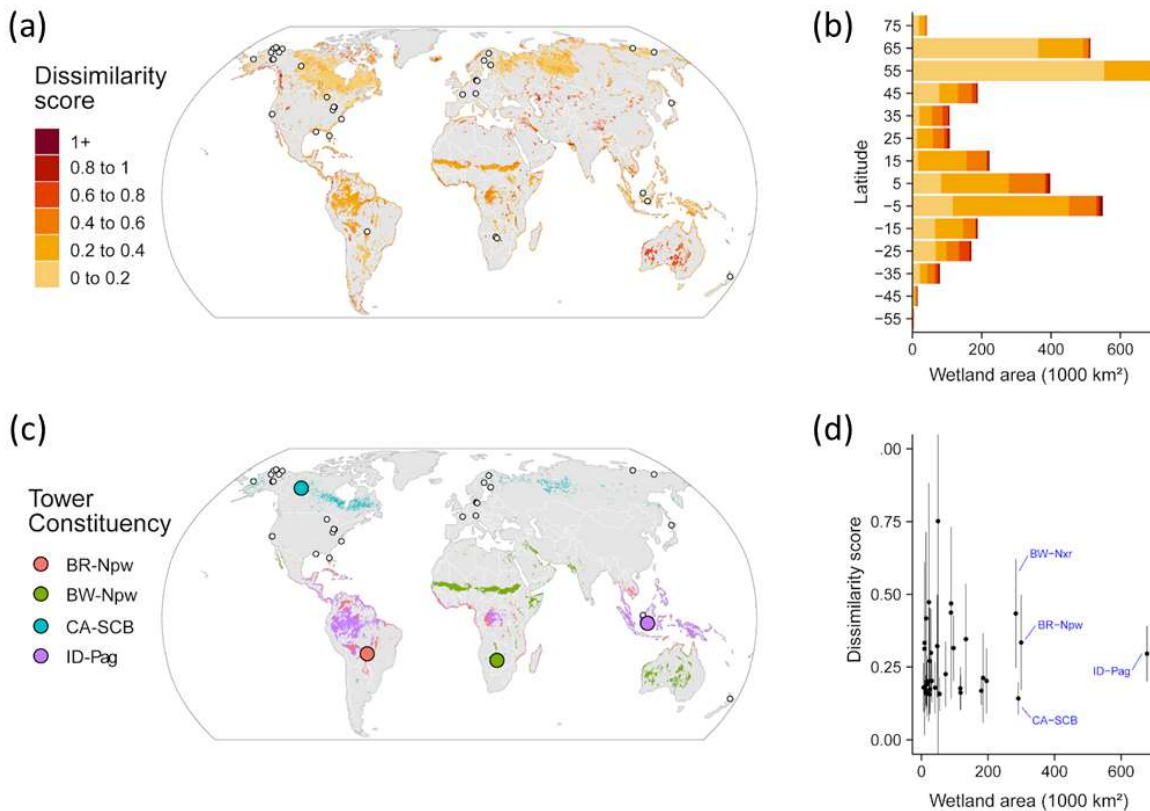
563

564 **Figure 6:** Principal Component Analysis displaying the distribution of freshwater wetland sites (points) along the two main
 565 principal components together accounting for 91.9% of variance. Tower sites are represented as points with shapes
 566 indicating their wetland type and color shade representing the annual methane (CH_4) flux (gray points represent sites for
 567 which <6 months of flux data was available to estimate annual budget). Sites codes are labeled in blue text for selected sites
 568 deviating from average conditions. Loading variables are represented by the arrows: mean annual temperature (MAT),
 569 simple ratio water index (SRWI), latent heat flux (LE) and enhanced vegetation index (EVI). The background shades of
 570 gray are a qualitative representation of the density of global wetland pixels and their distribution in the PCA climate-space,
 571 with darker color representing higher densities (excluding Greenland and Antarctica). Only grid cells with >5% average
 572 wetland fraction according to the WAD2M over 2000–2018 are included (Zhang et al., 2020). The loading variables are
 573 represented by the arrows: mean annual temperature (MAT), simple ratio water index (SRWI), latent heat flux (LE) and
 574 enhanced vegetation index (EVI).

575

576 Evaluating the bioclimatic dissimilarity of global wetlands to the FLUXNET-CH₄ network shows the least
 577 captured regions are in the tropics (Fig. 7A). Sparse coverage in the tropics also means that the few existing towers
 578 occupy a critical place in the network, particularly as tropical wetlands are the largest CH₄ emitters (Bloom et al.,
 579 2017; Poulter et al., 2017). Highly dissimilar wetlands are limited in extent and distributed across all latitudes, but the
 580 average dissimilarity is higher in north temperate (55° to 65°) and tropical (-5° to 5°) latitudes (Fig. 7B). To evaluate
 581 the importance of individual towers in the network, we estimated the geographical area to which it is most analogous
 582 in bioclimate-space (Fig. 7C). We found that some towers have disproportionately large constituencies (i.e., wetland
 583 areas that share the same closest bioclimatic analog tower). Towers in Indonesia (ID-Pag), Brazilian Pantanal (BR-
 584 Npw), and Botswana floodplains (BW-Nxr) represent the closest climate analog for much of the tropics (678, 300 and
 585 284 thousand km², respectively) while CA-SCB represents a vast swath (291 thousand km²) of boreal/arctic regions
 586 (Fig. 7D).

587



588

589 **Figure 7:** (a) Distance in bioclimatic space between global land surface and the FLUXNET-CH4 Version 1.0 tower network
 590 (gray areas indicate no mapped wetlands). The Euclidean distance was computed on the four bioclimatic variables and was
 591 then standardized by the average distance within-network. Most of the land surface has a dissimilarity score lower than 1,
 592 meaning these areas are closer than the average tower distance (lower dissimilarity score means a similar bioclimate to that
 593 represented by towers in the network). However, this pattern reflects more the sparsity of the tower network than a
 594 similarity of the land surface to the network. Areas with <5% coverage by wetlands were excluded to focus on wetland-
 595 dense regions. (b) Latitudinal distribution of dissimilarity score, (c) Map of the four largest tower constituencies, (d)
 596 Scatterplot of wetland area in each tower constituency plotted against the average dissimilarity score (point) and +/-
 597 standard deviation (error bar).

598 Our assessment of wetland CH₄ tower coverage determines the ability of our dataset to represent global
 599 wetland distributions and highlights some clear representation gaps in the network, particularly in tropical and humid
 600 regions. Other geographic regions such India, China, and Australia, where towers exist but are not included in the
 601 current network should be prioritized when expanding the network, even though they are not among the most distant
 602 areas to the current network. Similar representativeness assessments have been developed for CO₂ tower networks to
 603 identify gaps and priorities for expansion (Jung et al., 2009). To improve the geographic coverage of the network for
 604 representing global-scale fluxes, locations for new tower sites can be targeted to cover bio-climatically distant areas
 605 from the current network (Villarreal et al., 2019). Candidate regions for expansion that are both high CH₄ emitting
 606 (Saunois et al., 2020) as well as located in under-sampled climates are: African Sahel, Amazon basin, Congo basin,
 607 South-East Asia. Climatic conditions over boreal and arctic biomes are generally better represented (primarily at lower
 608 elevations), but there is scope to expand the network in wetland-dense regions like the Hudson Bay Lowlands and
 609 Northern Siberian Lowlands. Moreover, establishing sites in other ecosystem types, especially lakes and reservoirs
 610 (see Deemer et al. 2016, Bastviken et al. 2011, Matthews et al. 2020) in most climatic zones would help capture CH₄
 611 fluxes from these ecosystems.

612 Understanding the representativeness of the network is essential when inferring general patterns of flux
 613 magnitude, seasonality, and drivers from the tower data (Villarreal et al., 2018). We produced a first-order

614 representativeness of average bioclimatic conditions, but temporal representativeness (across seasons, climate
615 anomalies and extreme events) is particularly needed given the episodic nature of CH₄ fluxes (Chu et al., 2017;
616 Mahecha et al., 2017; Göckede et al., 2019).

617 Assessing representation of wetland CH₄ sites is complicated by the fact that wetlands occupy only a fraction
618 of most landscapes (except wetland dense regions such as Northern Siberian Lowlands, Hudson Bay Lowlands, Congo
619 basin, etc.) and that not all relevant factors affecting CH₄ production and consumption could be considered in our
620 analysis. For instance, our assessment of representation did not consider wetland types as such maps are limited by
621 the inherent difficulties in remotely sensing wetland features (Gallant, 2015). The attribution of representativeness is
622 further complicated by the fact that many EC tower locations are subject to small-scale variability within the field of
623 view, or footprint, of the sensor. Consequently, the individual time steps within EC flux time series may represent a
624 mixture of different wetland types, or different fractions of wetland contribution to the total CH₄ flux, varying with
625 wind direction, atmospheric stability, or season (Chu et al. 2021). This further complicates upscaling efforts.
626 Additionally, this representativeness analysis did not apply weights to the drivers to reflect their varying influence on
627 CH₄ flux. Such weights can be included in future versions as they are generated by a cross-validated machine learning
628 approach (Jung et al., 2020). Future efforts could include the dissimilarity index from this analysis as a metric of
629 extrapolation in a CH₄ flux upscaling effort.

630

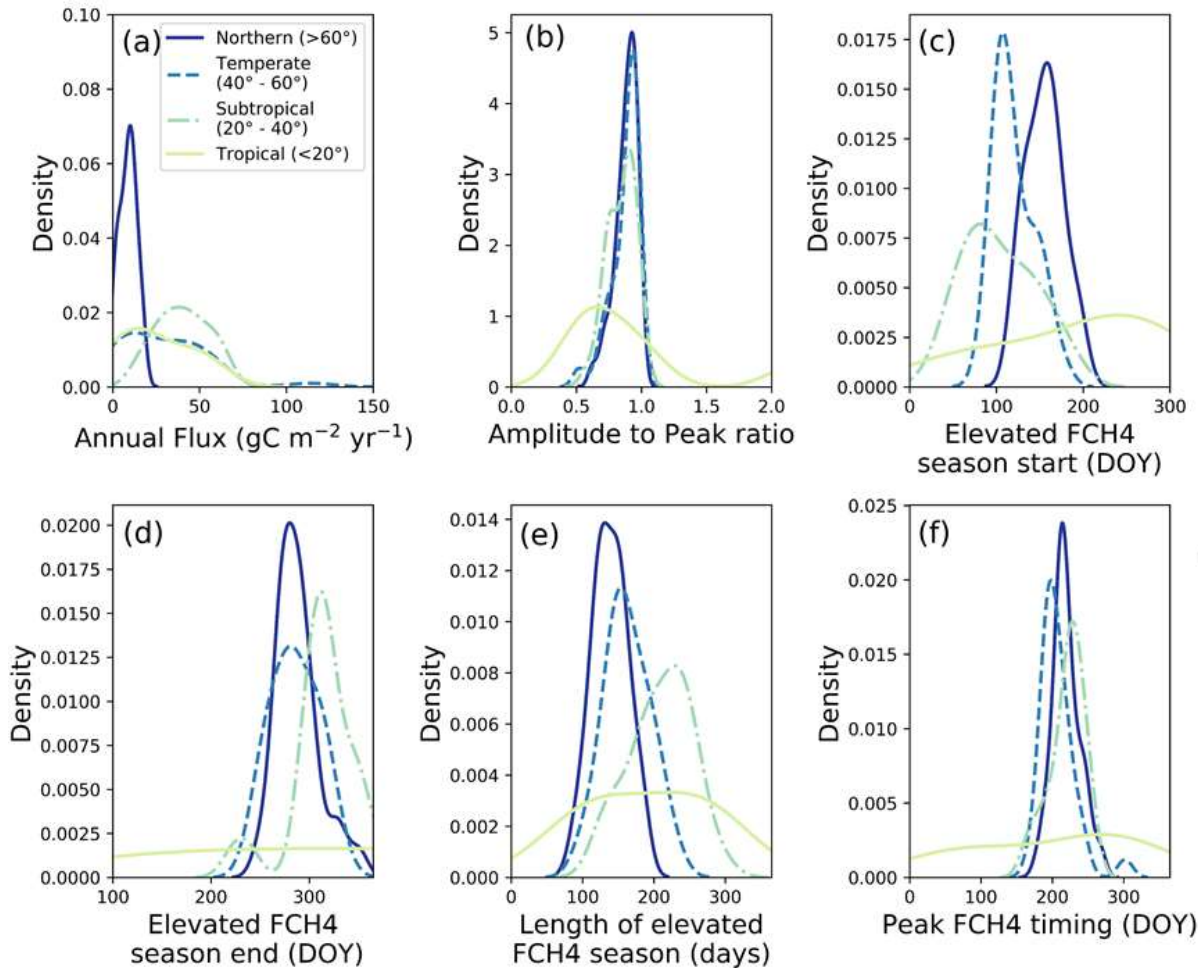
631 **3.3 Freshwater wetland flux seasonality**

632 **3.3.1 Seasonal flux comparisons by latitudinal bands**

633 CH₄ flux and seasonality varied substantially across latitudinal bands (northern, temperate, subtropical, and
634 tropical) (Fig. 8). Annual CH₄ fluxes for temperate, and subtropical sites were significantly higher than for northern
635 sites (8.7 ± 5.0 , 29.7 ± 25.2 , 40.1 ± 14.6 , and 24.5 ± 20.7 g C m⁻² yr⁻¹ for northern, temperate, subtropical, and tropical,
636 respectively, $p < 0.0001$ using Kruskal Wallis and post hoc comparisons; Fig. 8a), and tropical sites were similar to all
637 other latitudinal bands likely because of their small sample size. The ratio of seasonal amplitude to peak flux provides
638 a measure of the relative seasonal increase in emissions compared with baseline, where a ratio of zero indicates no
639 seasonal change in amplitude, a ratio of one indicates the off-season flux is zero, and values over one means the off-
640 season baseline CH₄ fluxes were negative (i.e., uptake). Average amplitude to peak flux ratios were similar across all
641 latitudinal bands (0.9 ± 0.1 , 0.9 ± 0.1 , 0.9 ± 0.1 , 1.0 ± 0.7 , for northern, temperate, subtropical, and tropical,
642 respectively; Fig. 8b). The spring increase in CH₄ emissions began later in northern sites compared with temperate
643 and subtropical sites (end of May versus April, respectively, $p = 0.001$; Fig. 8c), while tropical sites vary widely in
644 elevated emission season start date. Northern sites also had shorter elevated CH₄ flux season lengths (138 ± 24 days)
645 compared to temperate sites (162 ± 32 days), and both were shorter than subtropical sites (209 ± 43 days; $p < 0.0001$;
646 Fig. 8e). On average, CH₄ flux peaked earlier for temperate sites compared to northern ($p = 0.008$) and subtropical
647 sites ($p = 0.02$; mid to late July compared with early August; Fig. 8f), while tropical sites again vary widely. Given
648 their unique seasonality, and low number of site-years ($n = 9$), tropical systems are discussed separately in Sect. 3.3.3,
649 and not included in the comparisons in the remainder of this section. While our results on CH₄ seasonality corroborate
650 expected trends for these latitudinal bands, they provide some of the first estimates of CH₄ seasonality parameters and
651 ranges across a global distribution of sites.

652

653



654
655
656
657
658
659
660
661
662
663
664
665
666
667

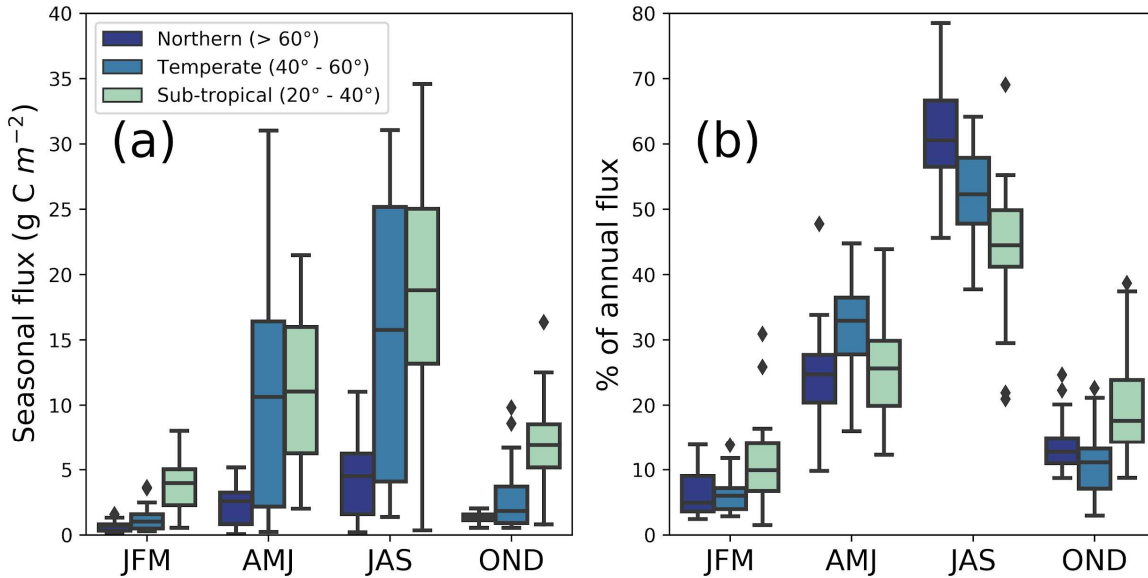
Figure 8: (a) Annual methane (CH_4) flux ($\text{g C m}^{-2} \text{ yr}^{-1}$), (b) Ratio of seasonal amplitude to seasonal peak, where values of 0 indicate uniform annual CH_4 flux, values of one indicate zero off-season fluxes, and values exceeding one indicate negative off-season fluxes, (c) CH_4 flux (FCH_4) elevated emissions season start by day of year (DOY), (d) FCH_4 elevated emissions season end by DOY, (e) Length of elevated CH_4 flux season (days), and (f) DOY of peak FCH_4 . Northern (dark blue, solid line), Temperate (blue, dashed line), Sub-tropical (green, dot-dash line) and Tropical (light green, solid line) wetlands plotted using the kernel density function. Each panel has lines that represent latitudinal bands as follows: northern (> 60°), temperate (between 40° and 60°), subtropical (between 20° and 40°), and tropical (< 20°), though the site-year totals vary between these groups ($n = 57$, $n = 36$, $n = 39$, and $n = 9$ respectively). All total CH_4 flux values and elevated season start values are positive, and the apparent continuation of the data distribution into negative values is an artifact of the kernel density function. Southern Hemisphere sites below 20° S were shifted by 182 days to make summer the middle of the year for comparability with Northern Hemisphere sites.

668
669
670
671
672
673
674
675

We found that latitudinal groups showed strong differences in absolute CH_4 flux across quarters, and narrower differences in percentage of annual CH_4 flux (Fig. 9a versus 9b). Thus, the AMJ quarter had a similar relative contribution to the annual CH_4 flux across latitudes, regardless of the absolute annual CH_4 flux. CH_4 fluxes (Fig. 9a) were highest during JAS for northern, temperate, and subtropical sites and highest in AMJ and JAS for temperate sites ($p < 0.01$). Though CH_4 fluxes in northern sites are most commonly measured during warm summer months (Sachs et al., 2010; Parmentier et al., 2011), fluxes in JFM and OND (50% of the yearly duration) on average make up $18.1 \pm 3.6\%$, $15.3 \pm 0.1\%$, and $31.2 \pm 0.1\%$ (northern, temperate, subtropical, respectively) of annual emissions. This pattern indicates that a substantial fraction of annual CH_4 fluxes occurs during cooler months. The contribution of non-

676 growing season CH₄ emissions to annual CH₄ fluxes has previously been described for arctic and boreal regions (Zona
 677 et al., 2016; Treat et al., 2018) and our analysis suggests comparable contributions in temperate and subtropical
 678 systems for the same quarterly periods.

679
680
681

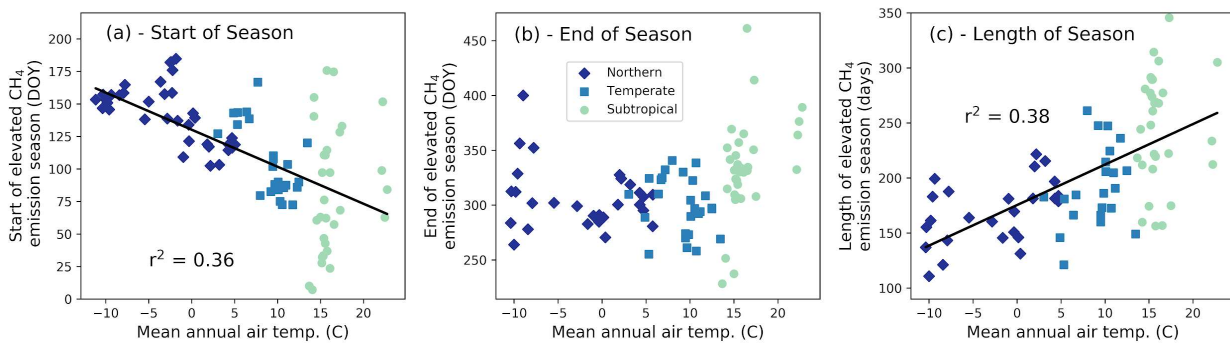


682
683
684 **Figure 9:** (a) Quarterly contribution to total annual CH₄ flux in g C m⁻², and (b) percentage of annual CH₄ flux. Sites
 685 were divided into northern (> 60° N), temperate (40° N - 60° N), and subtropical (20° N - 40° N). Quarters with
 686 continuous data gaps exceeding 30 days were excluded. We used the following quarterly periods:
 687 January/February/March (JFM), April/May/June (AMJ), July/August/September (JAS), and
 688 October/November/December (OND). Tropical sites are discussed separately in Sect. 3.3.3 because of their unique
 689 seasonality and low number of sites.
 690

691 3.3.2 Predictors of CH₄ flux phenology

692 The start of the elevated CH₄ flux season, and how long the elevated flux season lasts, correlated strongly
 693 with mean annual air temperature (Fig. 10; p<0.0001 for each). Methane flux began to increase roughly two months
 694 earlier in the warmest systems (mean annual temperature > 20 °C) compared to the coldest (mean annual
 695 temperature near -10 °C), though several of the warmer sites had high variability. Our data suggest that the CH₄
 696 season started 2.8 ± 0.5 days earlier for every degree Celsius increase in mean annual temperature (Fig. 10a). In
 697 contrast, the end of the CH₄ emission season was not correlated with mean annual temperature, but a positive trend
 698 existed despite high variability in warmest and coldest sites (Fig. 10b). The high variability seen in the end of CH₄
 699 season at northern sites is important to note and would likely be better resolved by incorporating other seasonality or
 700 phenological characteristics, such as moisture, active layer depth, and plant community composition (e.g., Kittler et
 701 al., 2017). Plants with aerenchymatous tissue, for example, influence the timing of plant-mediated CH₄ flux and are
 702 a key source of uncertainty while predicting CH₄ seasonality for northern wetlands (Xu et al., 2016, Kwon et al.,
 703 2017). Despite the relative lack of trend with season end date, the season length was still positively correlated with
 704 mean annual temperature, with the warmest sites having roughly three more months of seasonally elevated CH₄
 705 emissions than the coldest sites (Fig. 10c). CH₄ season length increased 3.6 ± 0.6 days for every degree Celsius
 706 increase in mean annual temperature (note that these relationships are correlations, and we cannot disentangle

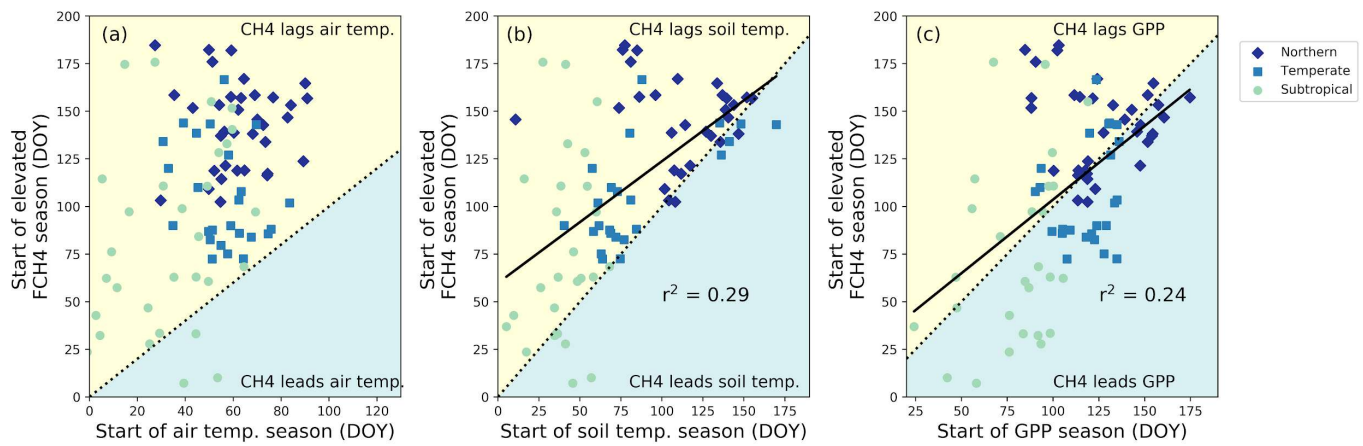
707 causality with this analysis). Temperature is highly correlated with other parameters (i.e., radiation, days of snow
 708 cover, etc.), so CH₄ flux is also likely to correlate with other environmental parameters.



709

710 **Figure 10.** The (a) start of the elevated methane (CH₄) emission season ($y = -2.8x + 130$, with 'x' in °C and 'y' in day of
 711 year (DOY)), (b) the end of the elevated emission season in DOY, and (c) the length of the emission season with mean
 712 annual site air temperature ($y = 3.6x + 176.6$, with 'x' in °C and 'y' in days). Each point represents a site-year of data and
 713 all reported r^2 are significant to $p < 0.0001$. Tropical sites are discussed separately in Sect. 3.3.3.

714 Although the spring onset of increasing CH₄ emissions correlated with mean annual air temperature, on
 715 average it lagged the spring increase in the shallowest soil temperatures by 31 ± 40 days (Fig. 11, lag is significantly
 716 different than zero, $p < 0.001$), with very few instances of CH₄ emissions beginning before seasonal soil
 717 temperatures increase (and by 20 ± 50 days for the deepest temperature probes). In contrast, for roughly half of the
 718 sites, CH₄ emission increased prior to seasonal GPP (a proxy for fresh substrate availability) increases. This
 719 suggests that the initiation of increased CH₄ fluxes at the beginning of the season was not limited by availability of
 720 substrate derived from recent photosynthate. Additionally, the onset of CH₄ fluxes tended to occur closer to the
 721 onset of soil temperature increase for cooler temperature sites (sites with later start dates tend to be cooler; Fig. 11a).
 722 This result is likely attributable to the direct influence of increased temperature on microbial processes (Chadburn et
 723 al., 2020), as well as the indirect influences of snow melt, both via release of CH₄ from the snowpack as well as a
 724 higher water table leading to more CH₄ production (Hargreaves et al., 2001; Tagesson et al., 2012; Mastepanov et
 725 al., 2013; Helbig et al., 2017). These observed trends hold for the entire temperature or GPP range of freshwater
 726 wetland sites, but are not necessarily applicable within individual latitudinal bands.

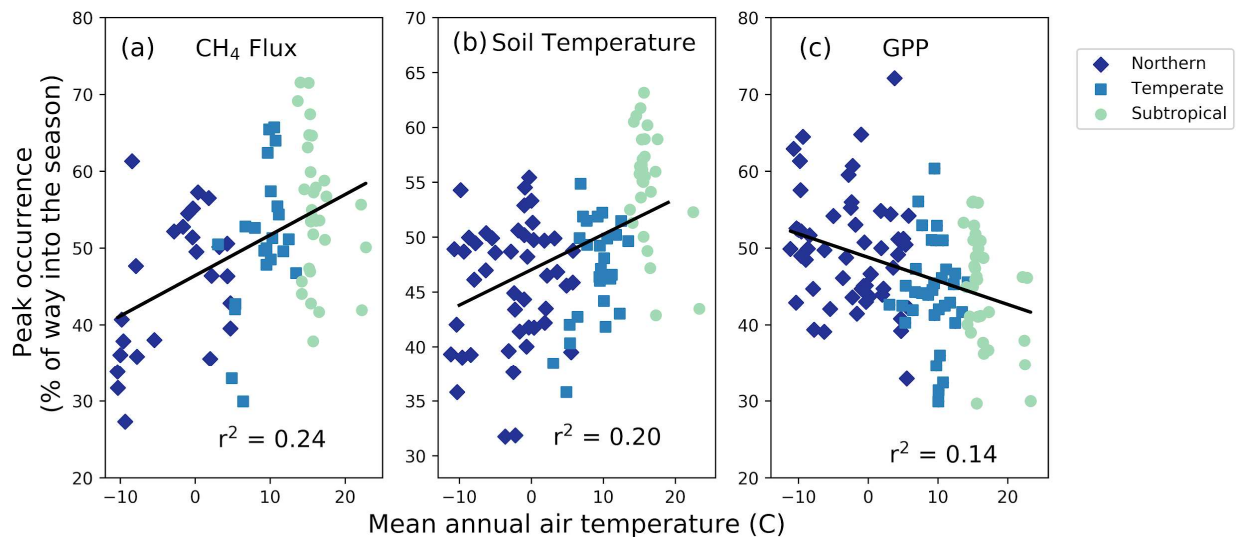


727

728

729 **Figure 11.** Relationship between the onset of the methane (CH_4) emission season to (a) the beginning of the air
 730 warming by day of year (DOY), (b) soil warming at the shallowest probe depth per site by DOY, and (c) gross primary
 731 productivity (GPP) increase for the subset of sites with soil temperature data by DOY. Each point represents a site-year
 732 of data. Dashed lines represent a 1:1 relationship, solid lines are significant ($p < 0.05$) regression fits. On average, the
 733 CH_4 emission season lags the soil temperature increase by 31 ± 40 days, and is more synchronous with GPP.

734 In contrast with the CH_4 season-start timing, the timing of the CH_4 peak did not correlate with either the
 735 timing of the soil temperature peak or the GPP peak (Fig. A1). For 63% of the sites, the average timing of peak CH_4
 736 emissions lagged the soil temperature peak, and at 83% of the sites average peak CH_4 lagged peak GPP (Fig. A1).
 737 Although there was no simple relationship between absolute CH_4 peak timing and the environmental drivers we
 738 investigated, there was a correlation ($p = 0.0005$) between the relative timing of peak CH_4 compared to season onset
 739 (calculated as described in Section 2.3) and mean annual air temperature (Fig. 12a). For cooler sites, the peak of
 740 seasonal CH_4 emissions occurred closer to the onset of the CH_4 emission season than the end of the season, resulting
 741 in an asymmetrical seasonal CH_4 flux shape that is illustrated in Fig. 2a. Soil temperature also peaked earlier in the
 742 season for cooler wetlands, though the relationship is not as pronounced ($p = 0.009$, Fig. 12b). In contrast, GPP
 743 peaked later in the season for cooler wetlands ($p = 0.009$, Fig. 12c). Previous work on Arctic sites (sites US-Ivo,
 744 US-Beo, US-Atq, US-Bes, and RU-CH2) highlighted the asymmetrical annual CH_4 peak, with higher fall emissions
 745 being attributed to the “zero curtain” period when soil below the surface remains thawed for an extended period of
 746 time due to snow insulation (Zona et al., 2016; Kittler et al., 2017). Furthermore, soils can stay above the “zero
 747 curtain” range for an extended time into the fall and winter (Helbig et al., 2017), which may also be caused by snow
 748 insulation. The rapid onset of emissions in the spring following snowmelt could be attributed to the release of
 749 accumulated CH_4 (Friborg et al., 1997), and other high latitude sites have seen similarly sharp increases in CH_4
 750 emissions at snowmelt (Dise, 1992, Windsor, 1992). However, not all studies in high latitudes have observed
 751 asymmetrical CH_4 emission peaks, pointing to the inherent complexity of these ecosystems (Rinne et al., 2007;
 752 Tagesson et al., 2012).



753

754 **Figure 12.** Site-year peak methane (CH_4) emission (a) and peak soil temperature (b) occur earlier in the season for sites
 755 with lower mean annual temperatures. (c) Gross primary productivity (GPP) tends to peak earlier in the season for
 756 warmer sites, though the trend is weak. All r^2 values are significant at $p < 0.001$. Each point represents a site-year of
 757 data.

758 **3.3.3 Uniqueness of tropical wetlands**

759 Tropical wetlands typically do not experience the large swings in temperature and GPP that contribute to
760 CH₄ flux seasonality in temperate and northern sites. Indeed, the relatively constant high temperatures and high
761 GPP in tropical ecosystems may lead to the lower ratio between seasonal amplitude and peak CH₄ flux compared
762 with temperate and northern sites (Fig. 8b). Tropical flux sites have historically been under-studied, leading to a
763 lack of synthesized information about these ecosystems. FLUXNET-CH4 has five tropical wetland sites (latitude
764 between 20° S and 20° N), and one tropical rice site, representing 13 site-years of data. These sites are especially
765 insightful as they provide the first estimates of CH₄ fluxes from tropical, large seasonal floodplain systems.
766

767 We found a broad range of annual CH₄ fluxes across tropical sites in FLUXNET-CH4 Version 1.0. Annual
768 CH₄ flux emissions from two Southeast Asian flooded peat forests were relatively low, 0.01 ± 0.1 and 9.5 ± 0.6 g C
769 m⁻² yr⁻¹ for ID-PAG and MY-MLM, respectively, which is consistent with annual CH₄ fluxes measured at another
770 peat forest in Indonesia (Deshmukh et al., 2020). In contrast, mean annual CH₄ flux for a seasonally flooded swamp
771 in the Brazilian Pantanal region (BR-NPW) was over twice as high as MY-MLM, at 19.2 ± 2.5 g C m⁻² yr⁻¹.
772 Similarly high annual CH₄ fluxes were observed at the two Botswana swamp sites in the Okavango Delta ($51.7 \pm$
773 10.6 and 47.3 ± 3.7 g C m⁻² yr⁻¹ for BW-GUM and BW-NXR, respectively), one of which is seasonally inundated
774 and surrounded by grassland (BW-NXR) and the other is a permanently flooded lagoon covered in a floating
775 papyrus mat (BW-GUM). The relatively low fluxes found at the two Southeast Asian peat forest sites indicate that
776 these ecosystems may be smaller CH₄ sources than expected, given their location in the humid tropics. Even the
777 higher-emitting tropical sites in Brazil and Botswana are still well within the range of annual CH₄ flux typical in
778 cooler latitudes (Fig. 1).

779 In addition to having highly variable CH₄ flux magnitudes, the tropical sites differ from each other in their
780 seasonality. CH₄ flux hit a minimum around July for two sites (BW-GUM, latitude 18.965 °S and MY-MLM, latitude
781 1.46 °N), while CH₄ flux increased through July and the subsequent months for the other Botswana site, BW-NXR
782 (latitude 19.548 °S). Site ID-Pag (latitude 2.32 °S) had minimal seasonality, whereas the flooded forest site in Brazil
783 (BR-NPW, latitude 16.49 °S) had near-zero fluxes from approximately July to January, and consistently high fluxes
784 for the remainder of the year. The rice site PH-RiF (latitude 14.14 °N) had two annual CH₄ flux peaks, which is
785 consistent with some other rice sites and likely reflects management practices. Baseline CH₄ flux values also differed,
786 with the two Botswana sites having the highest off-season fluxes (29 and 133 nmol m⁻² s⁻¹ for BW-NXR and BW-
787 GUM, respectively, estimated by Timesat), MY-MLM having an intermediate baseline CH₄ flux (16 nmol m⁻² s⁻¹,
788 estimated by Timesat), and the remainder of the sites having essentially zero flux at baseline. While more tropical
789 wetland data will be needed to extract broad scale conclusions about these ecosystems, the six tropical sites in
790 FLUXNET-CH4 provide an important starting point for synthesis studies and highlight tropical wetland CH₄
791 variability.

792

793 **4.0 Data Availability**

794 Half-hourly and daily aggregations are available for download at <https://fluxnet.org/data/fluxnet-ch4-community-product/>, along with a table containing site metadata compiled from Table B3. Variable descriptions and
795 units are provided in Table B1, and at <https://fluxnet.org/data/fluxnet-ch4-community-product/>. Each site has a unique
796 FLUXNET-CH4 DOI as listed in Table B3. All site data used in this analysis are available under the CC BY 4.0
797 (<https://creativecommons.org/licenses/by/4.0/>) copyright policy (2 additional sites in FLUXNET-CH4 are available
798 under the more restrictive Tier 2 data policy, <https://fluxnet.org/data/data-policy/>; these sites are not used in our
799 analysis). The individual site DOIs are provided below in Table 2. All seasonality parameters used in these analyses
800 are available at <https://doi.org/10.5281/zenodo.4672601>.

802

803 **Table 2:** Site identification (SITE_ID), data DOI, and DOI reference for each FLUXNET-CH4 site.

SITE_ID	DOI	DOI_REFERENCE
AT-Neu	10.18140/FLX/1669365	Wohlfahrt et al., 2020.
BR-Npw	10.18140/FLX/1669368	Vourlitis et al., 2020.
BW-Gum	10.18140/FLX/1669370	Helfter, 2020a.
BW-Nxr	10.18140/FLX/1669518	Helfter, 2020b.
CA-SCB	10.18140/FLX/1669613	Sonnentag and Helbig, 2020a.
CA-SCC	10.18140/FLX/1669628	Sonnentag and Helbig, 2020b.
CH-Cha	10.18140/FLX/1669629	Hörtnagl et al., 2020a.
CH-Dav	10.18140/FLX/1669630	Hörtnagl et al., 2020b.
CH-Oe2	10.18140/FLX/1669631	Hörtnagl, et al., 2020c.
CN-Hgu	10.18140/FLX/1669632	Niu and Chen, 2020.
DE-Dgw	10.18140/FLX/1669633	Sachs et al, 2020a.
DE-Hte	10.18140/FLX/1669634	Koebsch and Jurasinski, 2020.
DE-SfN	10.18140/FLX/1669635	Klatt et al., 2020.
DE-Zrk	10.18140/FLX/1669636	Sachs et al., 2020b.
FI-Hyy	10.18140/FLX/1669637	Mammarella et al. 2020.
FI-Lom	10.18140/FLX/1669638	Aurela et al., 2020.
FI-Si2	10.18140/FLX/1669639	Vesala et al., 2020a.
FI-Sii	10.18140/FLX/1669640	Vesala et al., 2020b
FR-LGt	10.18140/FLX/1669641	Jacotot et al., 2020.
HK-MPM	10.18140/FLX/1669642	Lai and Liu, 2020.
ID-Pag	10.18140/FLX/1669643	Sakabe et al., 2020.
IT-BCi	10.18140/FLX/1669644	Magliulo et al., 2020.

IT-Cas	10.18140/FLX/1669645	Manca and Goded, 2020.
JP-BBY	10.18140/FLX/1669646	Ueyama et al., 2020.
JP-Mse	10.18140/FLX/1669647	Iwata, 2020a.
JP-SwL	10.18140/FLX/1669648	Iwata, 2020b.
KR-CRK	10.18140/FLX/1669649	Ryu et al., 2020.
MY-MLM	10.18140/FLX/1669650	Wong et al., 2020.
NL-Hor	10.18140/FLX/1669651	Dolman et al., 2020a.
NZ-Kop	10.18140/FLX/1669652	Campbell and Goodrich, 2020.
PH-RiF	10.18140/FLX/1669653	Alberto and Wassmann, 2020.
RU-Ch2	10.18140/FLX/1669654	Goeckede, 2020.
RU-Che	10.18140/FLX/1669655	Merbold et al., 2020.
RU-Cok	10.18140/FLX/1669656	Dolman et al., 2020b.
RU-Fy2	10.18140/FLX/1669657	Varlagin, 2020.
SE-Deg	10.18140/FLX/1669659	Nilsson and Peichl, 2020.
UK-LBT	10.18140/FLX/1670207	Helfter, 2020c.
US-A03	10.18140/FLX/1669661	Billesbach and Sullivan, 2020a.
US-A10	10.18140/FLX/1669662	Billesbach and Sullivan, 2020b.
US-Atq	10.18140/FLX/1669663	Zona and Oechel, 2020a.
US-Beo	10.18140/FLX/1669664	Zona and Oechel, 2020b.
US-Bes	10.18140/FLX/1669665	Zona and Oechel, 2020c.
US-Bi1	10.18140/FLX/1669666	Rey-Sanchez et al., 2020a.
US-Bi2	10.18140/FLX/1669667	Rey-Sanchez et al., 2020b.
US-BZB	10.18140/FLX/1669668	Euskirchen and Edgar, 2020a.
US-BZF	10.18140/FLX/1669669	Euskirchen and Edgar, 2020b.
US-BZS	10.18140/FLX/1669670	Euskirchen and Edgar, 2020c.

US-CRT	10.18140/FLX/1669671	Chen and Chu, 2020a.
US-DPW	10.18140/FLX/1669672	Hinkle and Bracho, 2020.
US-EDN	10.18140/FLX/1669673	Oikawa, 2020.
US-EML	10.18140/FLX/1669674	Schuur, 2020.
US-Ho1	10.18140/FLX/1669675	Richardson and Hollinger, 2020.
US-HRA	10.18140/FLX/1669676	Runkle et al., 2020.
US-HRC	10.18140/FLX/1669677	Reba et al., 2020.
US-ICs	10.18140/FLX/1669678	Euskirchen et al., 2020d.
US-Ivo	10.18140/FLX/1669679	Zona and Oechel, 2020d.
US-LA1	10.18140/FLX/1669680	Holm et al., 2020a.
US-LA2	10.18140/FLX/1669681	Holm et al., 2020b.
US-Los	10.18140/FLX/1669682	Desai and Thom, 2020a.
US-MAC	10.18140/FLX/1669683	Sparks, 2020.
US-MRM	10.18140/FLX/1669684	Schafer, 2020.
US-Myb	10.18140/FLX/1669685	Matthes et al., 2020.
US-NC4	10.18140/FLX/1669686	Noormets et al., 2020.
US-NGB	10.18140/FLX/1669687	Torn and Dengel, 2020a.
US-NGC	10.18140/FLX/1669688	Torn and Dengel, 2020b.
US-ORv	10.18140/FLX/1669689	Bohrer and Morin, 2020a.
US-OWC	10.18140/FLX/1669690	Bohrer et al., 2020b.
US-PFa	10.18140/FLX/1669691	Desai and Thom, 2020b.
US-Snd	10.18140/FLX/1669692	Detto et al., 2020.
US-Sne	10.18140/FLX/1669693	Short et al., 2020.
US-Srr	10.18140/FLX/1669694	Windham-Myers et al., 2020.
US-StJ	10.18140/FLX/1669695	Vazquez-Lule and Vargas, 2020.

US-Tw1	10.18140/FLX/1669696	Valach et al., 2020a.
US-Tw3	10.18140/FLX/1669697	Chamberlain et al., 2020.
US-Tw4	10.18140/FLX/1669698	Eichelmann et al., 2020.
US-Tw5	10.18140/FLX/1669699	Valach et al., 2020b.
US-Twt	10.18140/FLX/1669700	Knox et al., 2020.
US-Uaf	10.18140/FLX/1669701	Iwata et al., 2020c.
US-WPT	10.18140/FLX/1669702	Chen and Chu, 2020b.

804

805

806

807 **5.0 Conclusions**

The breadth and scope of CH₄ flux data in the FLUXNET-CH₄ dataset make it possible to study the global patterns of CH₄ fluxes, particularly for global freshwater wetlands which release a substantial fraction of atmospheric CH₄. To help data users understand seasonal patterns within the dataset, we provide the first global estimates of CH₄ flux patterns and predictors in CH₄ seasonality using freshwater wetland data. In the seasonality analysis, we find that, on average, the seasonal increase in CH₄ emissions begins about three months earlier and lasts about four months longer at the warmest sites compared with the coolest sites. We also find that the beginning of the CH₄ emission season lags the beginning of seasonal soil warming by approximately one month, with almost no instances of CH₄ emissions increasing before temperature increases. Additionally, roughly half the sites have CH₄ emissions increasing prior to GPP increase; highlighting the importance of substrate versus temperature limitations on wetland CH₄ emissions. Furthermore, relative to warmer climates, wetland CH₄ emissions in cooler climates increase faster in the warming season and decrease slower in the cooling season. This phenomenon has previously been noted on a regional scale and we show that it persists at the global scale. Constraining the seasonality of CH₄ fluxes on a global scale can help improve the accuracy of global wetland models.

FLUXNET-CH₄ is an important new resource for the research community, but critical data gaps and opportunities remain. The current FLUXNET-CH₄ dataset is biased towards sites in boreal and temperate regions, which influence the relationships presented in our analyses. Tropical ecosystems are estimated to account for 64% of potential natural CH₄ emissions (<30° N, Saunois et al., 2020) but only account for 13% of the FLUXNET-CH₄ sites in the dataset. Unsurprisingly, tropical sites in our network do not represent the range of bioclimatic wetland conditions present in the tropics. Therefore, while maintaining flux towers in tropical ecosystems is challenging, it is necessary to further constrain the global CH₄ cycle. Coastal wetlands are also poorly represented in FLUXNET-CH₄ even though there is evidence of substantial CH₄ emissions from these ecosystems, so better representation across salinity gradients is warranted. Lastly, the average time series for FLUXNET-CH₄ Version 1.0 is relatively short, only 3.7 site-years on average compared with 7.2 for CO₂ sites in FLUXNET (Pastorello et al., 2020). Adding additional site-years of data from existing sites, as a complement to adding new sites, will increase the community's ability to explain interannual variability in CH₄ emission and seasonality. Nevertheless, FLUXNET-CH₄ is an important and unprecedented resource with which to diagnose and understand drivers of the global CH₄ cycle.

834 **Author contribution**

835 Kyle B. Delwiche oversaw the data release, performed the seasonality analysis, gathered metadata, and
836 prepared the manuscript with contributions from all co-authors. Sara Helen Knox gathered and standardized the
837 data, and gap-filled the CH₄ flux data. Avni Malhotra prepared the manuscript and gathered metadata. Etienne
838 Fluet-Chouinard did the representativeness analysis and prepared the manuscript. Gavin McNicol gathered data and
839 prepared the manuscript. Robert B. Jackson oversaw the data collection, processing, analysis, and release. Danielle
840 Christianson and You-Wei Cheah oversaw the FLUXNET-CH₄ dataset release on fluxnet.org. Dario Papale,
841 Eleonora Canfora, and Carlo Trotta did the data collection, curation, and pre-processing for all of the sites outside
842 North and South America. Remaining co-authors contributed eddy-covariance data to FLUXNET-CH₄ dataset
843 and/or participated in editing the manuscript.

844 **Competing interests**

845 The authors declare that they have no conflict of interest.

846 **Acknowledgements**

847 We acknowledge primary support from the Gordon and Betty Moore Foundation (Grant GBMF5439, “Advancing
848 Understanding of the Global Methane Cycle”; Stanford University) and from the John Wesley Powell Center for
849 Analysis and Synthesis of the U.S. Geological Survey (“Wetland FLUXNET Synthesis for Methane” working
850 group). Benjamin R. K. Runkle was supported by the U.S. National Science Foundation CBET CAREER Award
851 1752083. Ankur R. Desai acknowledges support of the DOE AmeriFlux Network Management Project. Masahito
852 Ueyama was supported by ArCS II (JPMXD1420318865) and JSPS KAKENHI (20K21849). Dario Papale and Nina
853 Buchmann acknowledge the support of the RINGO (GA 730944) H2020 EU project. Nina Buchmann and Kathrin
854 Fuchs acknowledge the SNF project M4P (40FA40_154245/1) and InnoFarm (407340_172433). Nina Buchmann
855 acknowledges support from the SNF for ICOS-CH Phases 1 and 2 (20FI21_148992, 20FI20_173691). Carlo Trotta
856 acknowledges the support of the E-SHAPE (GA 820852) H2020 EU project. William J. Riley was supported by the
857 US Department of Energy, BER, RGCM, RUBISCO project under contract no. DEAC02-05CH11231. Jessica
858 Turner acknowledges support from NSF GRFP (DGE-1747503) and NTL LTER (DEB-1440297). Minseok Kang
859 was supported by the National Research Foundation of Korea (NRF-2018 R1C1B6002917). Carole Helfter
860 acknowledges the support of the UK Natural Environment Research Council (the Global Methane Budget project,
861 grant number NE/N015746/1). Rodrigo Vargas acknowledges support from the National Science Foundation
862 (1652594). Dennis Baldocchi acknowledges the California Department of Water Resources for a funding contract
863 from the California Department of Fish and Wildlife and the United States Department of Agriculture (NIFA grant
864 #2011-67003-30371), as well as the U.S. Department of Energy’s Office of Science (AmeriFlux contract #7079856)
865 for funding the AmeriFlux core sites. US-A03 and US-A10 are operated by the Atmospheric Radiation
866 Measurement (ARM) user facility, a U.S. Department of Energy Office of Science user facility managed by the
867 Biological and Environmental Research Program (doi:10.5439/1025039, doi:10.5439/1025274,
868 doi:10.5439/1095578). Work at ANL was supported by the U.S. Department of Energy, Office of Science, Office of
869 Biological and Environmental Research, under contract DE-AC02-06CH11357. Any use of trade, firm, or product
870 names is for descriptive purposes only and does not imply endorsement by the U.S. Government. The CH-Dav, DE-
871 SfN, FI-Hyy, FI-Lom, FI-Sii, FR-LGt, IT-BCi, SE-Deg and SE-Sto sites are part of the ICOS European Research
872 Infrastructure. Oliver Sonnentag acknowledges funding by the Canada Research Chairs, Canada Foundation for
873 Innovation Leaders Opportunity Fund, and Natural Sciences and Engineering Research Council Discovery Grant
874 Programs for work at CA-SCC and CA-SCB. Benjamin Poulter acknowledges support from the NASA Carbon
875 Cycle and Ecosystems Program. Derrick Lai acknowledges the support of the Research Grants Council of the Hong
876 Kong Special Administrative Region, China (Project No. CUHK 458913). We thank Nathaniel Goenawan for his
877 help with the representativeness analysis.

878 **References**

- 879 Abdalla, M., Hastings, A., Truu, J., Espenberg, M., Mander, Ü, Smith, P. Emissions of methane from northern
 880 peatlands: a review of management impacts and implications for future management options. *Ecol. Evol.*, 6,
 881 7080–7102. <https://doi.org/10.1002/ece3.2469>.
- 882 Alberto, M. C. R., Wassmann, R., Gummert, M., Buresh, R. J., Quilty, J. R., Correa, T. Q., Centeno, C. A. R., &
 883 Oca, G. M. Straw incorporated after mechanized harvesting of irrigated rice affects net emissions of CH₄ and
 884 CO₂ based on eddy covariance measurements. *Field Crop. Res.*, 184, 162–175.
 885 <https://doi.org/10.1016/j.fcr.2015.10.004>. 2015.
- 886 Alberto, M., & Wassmann, R. FLUXNET-CH4 PH-RiF Philippines Rice Institute flooded. Philippines.
 887 <https://doi:10.18140/FLX/1669653>. 2020.
- 888 Anderson, D. E., Verma, S. B., & Rosenberg, N. J. Eddy correlation measurements of CO₂, latent heat, and sensible
 889 heat fluxes over a crop surface. *Bound. Lay. Meteorol.*, 29(3), 263–272. <https://doi.org/10.1007/bf00119792>.
 890 1984.
- 891 Anderson, F. E., Bergamaschi, B., Sturtevant, C., Knox, S., Hastings, L., Windham-Myers, L., Detto, M., Hestir, E.
 892 L., Drexler, J., Miller, R. L., Matthes, J. H., Verfaillie, J., Baldocchi, D., Snyder, R. L., & Fujii R. Variation of
 893 energy and carbon fluxes from a restored temperate freshwater wetland and implications for carbon market
 894 verification protocols. *J. of Geophys. Res. – Biogeosci.*, 121(3), 777–795. <https://doi.org/10.1002/2015JG003083>.
 895 2016.
- 896 Angle, J. C., Morin, T. H., Solden, L. M., Narrowe, A. B., Smith, G. J., Borton, M. A., Rey-Sanchez, C., Daly, R.
 897 A., Mirfenderesgi, G., Hoyt, D. W., Riley, W. J., Miller, C. S., Bohrer, G., & Wrighton, K. C. Methanogenesis
 898 in oxygenated soils is a substantial fraction of wetland methane emissions. *Nat. Comm.*, 8(1), 1567.
 899 <https://doi.org/10.1038/s41467-017-01753-4>. 2017.
- 900 Aurela, M., Lohila, A., J.-P., Hatakka, J., Rainne, J., Mäkelä, T., & Lauria, T. FLUXNET-CH4 FI-Lom
 901 Lompolojankka. Finland. <https://doi:10.18140/FLX/1669638>. 2020.
- 902 Bartlett, K. B., Bartlett, D. S., Harriss, R. C., & Sebacher, D. I. Methane emissions along a salt marsh salinity
 903 gradient. *Biogeochemistry*, 4(3), 183–202. <https://doi.org/10.1007/bf02187365>. 1987.
- 904 Bastviken, D., Tranvik, L. J., Downing, J. A., Crill, P. M., & Enrich-Prast, A. Freshwater methane emissions offset
 905 the continental carbon sink. *Science*, 331(6013), 50. <https://doi.org/10.1126/science.1196808>. 2011.
- 906 Billesbach, D., & Sullivan, R. FLUXNET-CH4 US-A03 ARM-AMF3-Oliktok. United States. <https://doi:10.18140/FLX/1669661>. 2020a.
- 907 Billesbach, D., & Sullivan, R. FLUXNET-CH4 US-A10 ARM-NSA-Barrow. United States.
 908 <https://doi:10.18140/FLX/1669662>. 2020b.
- 909 Bloom, A. A., Bowman, K. W., Lee, M., Turner, A. J., Schroeder, R., Worden, J. R., Weidner, R., McDonald, K.
 910 C., & Jacob, D. J. A global wetland methane emissions and uncertainty dataset for atmospheric chemical
 911 transport models (WetCHARTs version 1.0). *Geosci. Model Dev.*, 10, 2141–2156.
 912 <https://doi.org/10.5194/gmd-10-2141-2017>. 2017.
- 913 Bridgman, S. D., Cadillo-Quiroz, H., Keller, J. K., & Zhuang, Q. Methane emissions from wetlands:
 914 biogeochemical, microbial, and modeling perspectives from local to global scales. *Glob. Change Biol.*, 19(5),
 915 1325–1346. <https://doi.org/10.1111/gcb.12131>. 2013.
- 916 Bohrer, G., & Morin, T. H. FLUXNET-CH4 US-ORv Olentangy River Wetland Research Park. United States.
 917 <https://doi:10.18140/FLX/1669689>. 2020a.
- 918 Bohrer, G., Kerns, J., Morin, T. H., Rey-Sanchez, A. C., Villa, J., & Ju, Y. FLUXNET-CH4 US-OWC Old Woman
 919 Creek. United States. <https://doi:10.18140/FLX/1669690>. 2020b.
- 920 Campbell, D., & Goodrich, J. FLUXNET-CH4 NZ-Kop Kopuatai. New Zealand.
 921 <https://doi:10.18140/FLX/1669652>. 2020.
- 922 Castro-Morales, K., Kleinen, T., Kaiser, S., Zaehle, S., Kittler, F., Kwon, M. J., Beer, C., & Göckede, M. Year-
 923 round simulated methane emissions from a permafrost ecosystem in Northeast Siberia. *Biogeosciences*, 15(9),
 924 2691–2722. <https://doi.org/10.5194/bg-15-2691-2018>. 2018.
- 925 Chadburn, S. E., Aalto, T., Aurela, M., Baldocchi, D., Biasi, C., Boike, J., Burke, E. J., Comyn-Platt, E., Dolman,
 926 A. J., Duran-Rojas, & Others. Modeled microbial dynamics explain the apparent temperature sensitivity of
 927 wetland methane emissions. *Global Biogeochemical Cycles*, 34(11). <https://doi.org/10.1029/2020gb006678>.
 928 2020.
- 929

- 930 Chamberlain, S. D., Oikawa, P., Sturtevant, C., Szutu, D., Verfaillie, J., & Baldocchi, D. FLUXNET-CH4 US-Tw3
931 Twitchell Alfalfa. United States. <https://doi:10.18140/FLX/1669697>. 2020.
- 932 Chambers, L. G., Ramesh Reddy, K., & Osborne, T. Z. Short-Term Response of Carbon Cycling to Salinity Pulses
933 in a Freshwater Wetland. *Soil Sci. Soc. Am. J.*, 75(5), 2000–2007. <https://doi.org/10.2136/sssaj2011.0026>.
934 2011.
- 935 Chang, K. Y., W. J. Riley, S. H. Knox, R. B. Jackson, G. McNicol, B. Poulter, M. Aurela, D. Baldocchi, S. Bansal,
936 G. Bohrer, D. I. Campbell, A. Cescatti, H. Chu, K. B. Delwiche, A. Desai, E. Euskirchen, T. Friberg, M.
937 Goeckede, G. Holm, M. Kang, T. Keenan, K. W. Krauss, A. Lohila, I. Mammarella, A. Miyata, M. B. Nilsson,
938 A. Noormets, D. Papale, B. R. K. Runkle, Y. Ryu, T. Sachs, K. V. R. Schäfer, H. P. Schmid, N. Shurpali, O.
939 Sonnentag, A. C. I. Tang, M. S. Torn, C. Trotta, M. Ueyama, R. Vargas, T. Vesala, L. Windham-Myers, Z.
940 Zhang, & D. Zona. Global wetland methane emissions have hysteretic responses to seasonal temperature.
941 *Nature Communications*, 12. 2266.. <https://doi.org/10.1038/s41467-021-22452-1>. 2021
- 942 Chanton, J. P., Glaser, P. H., Chasar, L. S., Burdige, D. J., Hines, M. E., Siegel, D. I., Tremblay, L. B., & Cooper,
943 W. T. Radiocarbon evidence for the importance of surface vegetation on fermentation and methanogenesis in
944 contrasting types of boreal peatlands. *Global Biogeochem. Cy.*, 22(4). <https://doi.org/10.1029/2008gb003274>.
945 2008.
- 946 Chen, J., & Chu, H. FLUXNET-CH4 US-CRT Curtice Walter-Berger cropland. United States.
947 <https://doi:10.18140/FLX/1669671>. 2020a.
- 948 Chen, J., & Chu, H. FLUXNET-CH4 US-WPT Winous Point North Marsh. United States.
949 <https://doi:10.18140/FLX/1669702>. 2020b.
- 950 Chu, H., Chen, J., Gottgens, J. F., Ouyang, Z., John, R., Czajkowski, K., & Becker, R. Net ecosystem methane and
951 carbon dioxide exchanges in a Lake Erie coastal marsh and a nearby cropland. *J. Geophys. Res.: Biogeosci.*,
952 119(5), 722–740. <https://doi.org/10.1002/2013JG002520>. 2014.
- 953 Chu, H., Baldocchi, D. D., John, R., Wolf, S., & Reichstein, M. Fluxes all of the time? A primer on the temporal
954 representativeness of FLUXNET. *Journal of Geophysical Research: Biogeosciences*, 122(2), 289–307.
955 <https://doi.org/10.1002/2016JG003576>. 2017.
- 956 Chu, H., Luo, X., Ouyang, Z., Chan, W. S., Dengel, S., Biraud, S. C., Torn, M. S., Metzger, S., Kumar, J., Arain, M.
957 A., & Others. Representativeness of Eddy-Covariance flux footprints for areas surrounding AmeriFlux sites.
958 *Agricultural and Forest Meteorology*, 301-302, 108350. <https://doi.org/10.1016/j.agrformet.2021.108350>.
959 2021.
- 960 Dalcin Martins, P., Hoyt, D. W., Bansal, S., Mills, C. T., Tfaily, M., Tangen, B. A., Finocchiaro, R. G., Johnston,
961 M. D., McAdams, B. C., Solensky, M. J., Smith, G. J., Chin, Y.-P., & Wilkins, M. J. Abundant carbon
962 substrates drive extremely high sulfate reduction rates and methane fluxes in Prairie Pothole Wetlands. *Global
963 Change Biology*, 23(8), 3107–3120. <https://doi.org/10.1111/gcb.13633>. 2017.
- 964 Dean, J. F., Middelburg, J. J., Röckmann, T., Aerts, R., Blauw, L. G., Egger, M., Jetten, M. S. M., de Jong, A. E. E.,
965 Meisel, O. H., Rasigraf, O., Slomp, C. P., in't Zandt, M. H., & Dolman, A. J. Methane Feedbacks to the Global
966 Climate System in a Warmer World. *Rev. Geophys.*, 56(1), 207–250. <https://doi.org/10.1002/2017rg000559>.
967 2018.
- 968 Deemer, B. R., Harrison, J. A., Li, S., Beaulieu, J. J., DelSontro, T., Barros, N., Bezerra-Neto, J. F., Powers, S. M.,
969 Dos Santos, M. A., & Vonk, J. A. Greenhouse Gas Emissions from Reservoir Water Surfaces: A New Global
970 Synthesis. *Bioscience*, 66(11), 949–964. <https://doi.org/10.1093/biosci/biw117>. 2016.
- 971 Dengel, S., Zona, D., Sachs, T., Aurela, M., Jammet, M., Parmentier, F.-J. W., Oechel, W., & Vesala, T. Testing the
972 applicability of neural networks as a gap-filling method using CH4 flux data from high latitude wetlands.
973 *Biogeosciences*, 10, 8185–8200. <https://doi.org/10.5194/bg-10-8185-2013>. 2013.
- 974 Deshmukh, C. S., Julius, D., Evans, C. D., Nardi, Susanto, A. P., Page, S. E., Gauci, V., Laurén, A., Sabiham, S.,
975 Agus, F., Asyhari, A., Kurnianto, S., Suardiwerianto, Y., & Desai, A. R. Impact of forest plantation on
976 methane emissions from tropical peatland. *Glob. Change Biol.*, 26, 2477-2495.
977 <https://doi.org/10.1111/gcb.15019>. 2020.
- 978 Desai, A. R., & Thom, J. FLUXNET-CH4 US-Los Lost Creek. United States. <https://doi:10.18140/FLX/1669682>.
979 2020a.
- 980 Desai, A. R., & Thom, J. FLUXNET-CH4 US-PFa Park Falls/WLEF. United States.
981 <https://doi:10.18140/FLX/1669691>. 2020b.
- 982 Desjardins, R. L. A technique to measure CO2 exchange under field conditions. *Int. J. Biometeorol.*, 18(1), 76–83.
983 <https://doi.org/10.1007/bf01450667>. 1974.
- 984 Detto, M., Sturtevant, C., Oikawa, P., Verfaillie, J., & Baldocchi, D. FLUXNET-CH4 US-Snd Sherman Island.
985 United States. <https://doi:10.18140/FLX/1669692>. 2020.

- 986 Dise, N. Winter fluxes of methane from Minnesota peatlands. *Biogeochemistry*, 17(2).
987 <https://doi.org/10.1007/bf00002641>. 1992.
- 988 Dolman, H., Hendriks, D., Parmentier, F.-J., Marchesini, L. B., Dean, J., & van Huissteden, K. FLUXNET-CH4
989 NL-Hor Horstermeer. Netherlands. <https://doi:10.18140/FLX/1669651>. 2020a.
- 990 Dolman, H., van der Molen, H., Parmentier, F.-J., Marchesini, L. B., Dean, J., van Huissteden, K., & Maximov, T.
991 FLUXNET-CH4 RU-Cok Chokurdakh. Russian Federation. <https://doi:10.18140/FLX/1669656>. 2020b.
- 992 Eichelmann, E., Knox, S., Rey Sanchez, C., Valach, A., Sturtevant, C., Szutu, D., Verfaillie, J., & Baldocchi, D.
993 FLUXNET-CH4 US-Tw4 Twitchell East End Wetland. United States. <https://doi:10.18140/FLX/1669698>.
994 2020.
- 995 Eklundh, L., & Jönsson, P. TIMESAT: A Software Package for Time-Series Processing and Assessment of
996 Vegetation Dynamics. *Remote Sensing Time Series* (pp. 141–158). https://doi.org/10.1007/978-3-319-15967-6_7. 2015.
- 997 Etheridge, D. M., Steele, L. P., Francey, R. J., & Langenfelds, R. L. Atmospheric methane between 1000 A.D. and
998 present: Evidence of anthropogenic emissions and climatic variability. *J. Geophys. Res. – Atmos.*, 103(D13),
1000 15979–15993. <https://doi.org/10.1029/98jd00923>. 1998.
- 1001 Etminan, M., Myhre, G., Highwood, E. J., & Shine, K. P. Radiative forcing of carbon dioxide, methane, and nitrous
1002 oxide: A significant revision of the methane radiative forcing. *Geophys. Res. Lett.*, 43(24), 12,614–12,623.
1003 <https://doi.org/10.1002/2016gl071930>. 2016.
- 1004 Euskirchen, E., & Edgar, C. FLUXNET-CH4 US-BZB Bonanza Creek Thermokarst Bog. United States.
1005 <https://doi:10.18140/FLX/1669668>. 2020a.
- 1006 Euskirchen, E., & Edgar, C. FLUXNET-CH4 US-BZF Bonanza Creek Rich Fen. United States.
1007 <https://doi:10.18140/FLX/1669669>. 2020b.
- 1008 Euskirchen, E., & Edgar, C. FLUXNET-CH4 US-BZS Bonanza Creek Black Spruce. United States.
1009 <https://doi:10.18140/FLX/1669670>. 2020c.
- 1010 Euskirchen, E., Bret-Harte, M., & Edgar, C Marion Bret-Harte. FLUXNET-CH4 US-ICs Innavaits Creek
1011 Watershed Wet Sedge Tundra. United States. <https://doi:10.18140/FLX/1669678>. 2020d.
- 1012 Gallant, A. The Challenges of Remote Monitoring of Wetlands. *Remote Sensing*, 7(8), 10938–10950.
1013 <https://doi.org/10.3390/rs70810938>. 2015.
- 1014 Göeckede, M., Kittler, F., & Schaller, C. Quantifying the impact of emission outbursts and non-stationary flow on
1015 eddy covariance CH4 flux measurements using wavelet techniques. *Biogeosciences*, 16(16), 3113–3131.
1016 <https://doi.org/10.5194/bg-16-3113-2019>. 2019.
- 1017 Goeckede, M. FLUXNET-CH4 RU-Ch2 Chersky reference. Russian Federation.
1018 <https://doi:10.18140/FLX/1669654>. 2020.
- 1019 Gu, L., Post, W. M., Baldocchi, D. D., Andrew Black, T., Suyker, A. E., Verma, S. B., Vesala, T., & Wofsy, S. C.
1020 Characterizing the Seasonal Dynamics of Plant Community Photosynthesis Across a Range of Vegetation
1021 Types. In: Noormets A. (eds) *Phenology of Ecosystem Processes*. Springer, New York, NY. pp. 35–58.
1022 https://doi.org/10.1007/978-1-4419-0026-5_2. 2009.
- 1023 Hargreaves, K. J., Fowler, D., Pitcairn, C. E. R., & Aurela, M. Annual methane emission from Finnish mires
1024 estimated from eddy covariance campaign measurements. *Theor. Appl. Climatol.*, 70, 203–213.
1025 <https://doi.org/10.1007/s007040170015>. 2001.
- 1026 Hargrove, W. W., Hoffman, F. M., & Law, B. E. New analysis reveals representativeness of the AmeriFlux
1027 network. *Eos, Transactions American Geophysical Union*, 84(48), 529.
1028 <https://doi.org/10.1029/2003EO480001>. 2003.
- 1029 Hatala, J. A., Detto, M., & Baldocchi, D. D. Gross ecosystem photosynthesis causes a diurnal pattern in methane
1030 emission from rice. *Geophys. Res. Lett.*, 39(6). <https://doi.org/10.1029/2012gl051303>. 2012.
- 1031 Helbig, M., Quinton, W. L., & Sonnentag, O. Warmer spring conditions increase annual methane emissions from a
1032 boreal peat landscape with sporadic permafrost. *Environ. Res. Lett.*, 12(11), 115009.
1033 <https://doi.org/10.1088/1748-9326/aa8c85>. 2017.
- 1034 Helfter, C., Tremper, A. H., Halios, C. H., Kotthaus, S., Bjorkgren, A., Grimmond, C. S. B., Barlow, J. F., &
1035 Nemitz, E. Spatial and temporal variability of urban fluxes of methane, carbon monoxide and carbon dioxide
1036 above London, UK. *Atmos. Chem. Phys.* 16, 10543–10557. <https://doi.org/10.5194/acp-2016-216-ac1>. 2016.
- 1037 Helfter, C. FLUXNET-CH4 BW-Gum Guma. Botswana. <https://doi:10.18140/FLX/1669370>. 2020a.
- 1038 Helfter, C. FLUXNET-CH4 BW-Nxr Nxaraga. Botswana. <https://doi:10.18140/FLX/1669518>. 2020b.
- 1039 Helfter, C. FLUXNET-CH4 UK-LBT London_BT. United Kingdom. <https://doi:10.18140/FLX/1670207>. 2020c.
- 1040 Hinkle, C. R., & Bracho, R. FLUXNET-CH4 US-DPW Disney Wilderness Preserve Wetland. United States.
1041 <https://doi:10.18140/FLX/1669672>. 2020.

- 1042 Hoffman, F. M., Kumar, J., Mills, R. T., & Hargrove, W. W. Representativeness-based sampling network design for
 1043 the State of Alaska. *Landscape Ecol.*, 28(8), 1567–1586. <https://doi.org/10.1007/s10980-013-9902-0>. 2013.
- 1044 Hollinger, D. Y., and A. D. Richardson. Uncertainty in Eddy Covariance Measurements and Its Application to
 1045 Physiological Models. *Tree Physiology* 25 (7): 873–85. <https://doi.org/10.1093/treephys/25.7.873>. 2005.
- 1046 Holm, G. O., Perez, B. C., McWhorter, D. E., Krauss, K. W., Raynie, R. C., & Killebrew, C. J. FLUXNET-CH4
 1047 US-LA1 Pointe-aux-Chenes Brackish Marsh. United States. <https://doi:10.18140/FLX/1669680>. 2020a.
- 1048 Holm, G. O., Perez, B. C., McWhorter, D. E., Krauss, K. W., Raynie, R. C., & Killebrew, C. J. FLUXNET-CH4
 1049 US-LA2 Salvador WMA Freshwater Marsh. United States. <https://doi:10.18140/FLX/1669681>. 2020b.
- 1050 Hörtnagl, L., Feigenwinter, I., Fuchs, K., Merbold, L., Buchmann, N., Eugster, W., Zeeman, M., Pluess, P., Käslin,
 1051 F., Meier, P., Koller, P., & Baur, T. FLUXNET-CH4 CH-Cha Chamau. Switzerland.
<https://doi:10.18140/FLX/1669629>. 2020a.
- 1052 Hörtnagl, Lukas, Werner Eugster, Lutz Merbold, Nina Buchmann, Mana Gharun, Sophia Etzold, Rudolf Haesler,
 1053 Matthias Haeni, Philip Meier, Florian Käslin, Thomas Baur, & Peter Pluess. FLUXNET-CH4 CH-Dav Davos.
 1054 Switzerland. <https://doi:10.18140/FLX/1669630>. 2020b.
- 1055 Hörtnagl, Lukas, Regine Maier, Werner Eugster, Nina Buchmann, Carmen Emmel, Patrick Koller, Thomas Baur,
 1056 Peter Pluess, Florian Käslin, & Philip Meier. FLUXNET-CH4 CH-Oe2 Oensingen crop. Switzerland.
<https://doi:10.18140/FLX/1669631>. 2020c.
- 1056 Hwang, Y., Ryu, Y., Huang, Y., Kim, J., Iwata, H., & Kang, M. Comprehensive assessments of carbon dynamics in
 1057 an intermittently-irrigated rice paddy. *Agr. Forest Met.*, 285–286, 107933.
<https://doi.org/10.1016/j.agrformet.2020.107933>. 2020.
- 1058 Iwata, H., Mano, M., Ono, K., Tokida, T., Kawazoe, T., Kosugi, Y., Sakabe, A., Takahashi, K., & Miyata, A.
 1059 Exploring sub-daily to seasonal variations in methane exchange in a single-crop rice paddy in central Japan.
 1060 *Atmos. Environ.*, 179, 156–165. <https://doi.org/10.1016/j.atmosenv.2018.02.015>. 2018.
- 1061 Iwata, Hiroki. FLUXNET-CH4 JP-Mse Mase rice paddy field. Japan. <https://doi:10.18140/FLX/1669647>. 2020a.
- 1062 Iwata, Hiroki. FLUXNET-CH4 JP-SwL Suwa Lake. Japan. <https://doi:10.18140/FLX/1669648>. 2020b.
- 1063 Iwata, Hiroki, Masahito Ueyama, & Yoshinobu Harazono. FLUXNET-CH4 US-Uaf University of Alaska,
 1064 Fairbanks. United States. <https://doi:10.18140/FLX/1669701>. 2020c.
- 1064 Jacotot, Adrien, Sébastien Gogo, & Fatima Laggoun-Défarge. FLUXNET-CH4 FR-LGt La Guette. France.
<https://doi:10.18140/FLX/1669641>. 2020.
- 1065 Jung, M., Reichstein, M., & Bondeau, A. Towards global empirical upscaling of FLUXNET eddy covariance
 1066 observations: validation of a model tree ensemble approach using a biosphere model. *Biogeosciences*, 6(10),
 1067 2001–2013. <https://doi.org/10.5194/bg-6-2001-2009>. 2009.
- 1068 Jung, M., Schwalm, C., Migliavacca, M., Walther, S., Camps-Valls, G., Koirala, S., Anthoni, P., Besnard, S.,
 1069 Bodesheim, P., Carvalhais, N., Chevallier, F., Gans, F., Goll, D. S., Haverd, V., Kohler, P., Ichii, K., Jain, A.,
 1070 Liu, J., Lombardozzi, D., Nabel, J. E. M. S., Nelson, J. A., O’Sullivan, M., Pallandt, M., Papale, D., Peters,
 1071 W., Pongrats, J., Rodenbeck, C., Sitch, S., Tramontana, G., Walker, A., Weber, U., & Reichstein, M. Scaling
 1072 carbon fluxes from eddy covariance sites to globe: synthesis and evaluation of the FLUXCOM approach.
 1073 *Biogeosciences*, 17(5), 1343–1365. <https://doi.org/10.5194/bg-17-1343-2020>. 2020.
- 1074 Kim, Y., Johnson, M. S., Knox, S. H., Andrew Black, T., Dalmagro, H. J., Kang, M., Kim, J., & Baldocchi, D. Gap-
 1075 filling approaches for eddy covariance methane fluxes: A comparison of three machine learning algorithms and
 1076 a traditional method with principal component analysis. *Glob. Change Biol.*, 26(3), 1499–1518.
 1077 <https://doi.org/10.1111/gcb.14845>. 2020.
- 1078 Kittler, F., Heimann, M., Kolle, O., Zimov, N., Zimov, S., & Göckede, M. Long-Term Drainage Reduces CO 2
 1079 Uptake and CH 4 Emissions in a Siberian Permafrost Ecosystem: Drainage impact on Arctic carbon cycle.
 1080 *Global Biogeochem. Cy.*, 31(12), 1704–1717. <https://doi.org/10.1002/2017GB005774>. 2017.
- 1081 Klatt, Janina, Hans Peter Schmid, Matthias Mauder, & Rainer Steinbrecher. FLUXNET-CH4 DE-SfN Schechenfilz
 1082 Nord. Germany. <https://doi:10.18140/FLX/1669635>. 2020.
- 1083 Knox, S. H., Sturtevant, C., Matthes, J. H., Koteen, L., Verfaillie, J., & Baldocchi, D. Agricultural peatland
 1084 restoration: effects of land-use change on greenhouse gas (CO2 and CH4) fluxes in the Sacramento-San
 1085 Joaquin Delta. *Glob. Change Biol.*, 21(2), 750–765. <https://doi.org/10.1111/gcb.12745>. 2015.
- 1086 Knox, S. H., Matthes, J. H., Sturtevant, C., Oikawa, P. Y., Verfaillie, J., & Baldocchi, D. Biophysical controls on
 1087 interannual variability in ecosystem-scale CO2and CH4exchange in a California rice paddy. *J. Geophys. Res.-*
 1088 *Biogeo.*, 121(3), 978–1001. <https://doi.org/10.1002/2015jg003247>. 2016.
- 1089 Knox, S. H., Jackson, R. B., Poulter, B., McNicol, G., Fluet-Chouinard, E., Zhang, Z., Hugelius, G., Bousquet, P.,
 1090 Canadell, J. G., Saunois, M., Papale, D., Chu, H., Keenan, T. F., Baldocchi, D., Torn, M. S., Mammarella, I.,
 1091 Trotta, C., Aurela, M., Bohrer, G., Campbell, D.I., Cescatti, A., Chamberlain, S., Chen, J., Chen, W., Dengel,

- 1098 S., Desai, A.R., Euskirchen, E., Friberg, T., Gasbarra, D., Goded, I., Goeckede, M., Heimann, M., Helbig, M.,
 1099 Hirano, T., Hollinger, D.Y., Iwata, H., & Others. FLUXNET-CH4 Synthesis Activity: Objectives,
 1100 Observations, and Future Directions. *B. Am. Meterol. Soc.*, 100(12), 2607–2632. <https://doi.org/10.1175/bams-d-18-0268.1>. 2019.
- 1102 Knox, Sara, Jaclyn Hatala Matthes, Joseph Verfaillie, & Dennis Baldocchi. FLUXNET-CH4 US-Twt Twitchell
 1103 Island. United States. <https://doi:10.18140/FLX/1669700>. 2020.
- 1104 Koebsch, F., Jurasinski, G., Koch, M., Hofmann, J., & Glatzel, S. Controls for multi-scale temporal variation in
 1105 ecosystem methane exchange during the growing season of a permanently inundated fen. *Agr. Forest
 1106 Meteorol.*, 204, 94–105. <https://doi.org/10.1016/j.agrformet.2015.02.002>. 2015.
- 1107 Koebsch, F., Winkel, M., Liebner, S., Liu, B., Westphal, J., Schmiedinger, I., Spitz, A., Gehre, M., Jurasinski, G.,
 1108 Köhler, S., & Others. Sulfate deprivation triggers high methane production in a disturbed and rewetted coastal
 1109 peatland. *Biogeosciences*, 16, 1937–1953. <https://doi.org/10.5194/bg-16-1937-2019>. 2019.
- 1110 Koebsch, Franziska, & Gerald Jurasinski. FLUXNET-CH4 DE-Hte Huetelmoor. Germany.
 1111 <https://doi:10.18140/FLX/1669634>. 2020.
- 1112 Kuznetsova A., Brockhoff P.B., & Christensen R. H. B. “lmerTest Package: Tests in Linear Mixed
 1113 Effects Models.” *Journal of Statistical Software*, 82(13), 1-26.
<https://doi.org/10.18637/jss.v082.i13>. 2017.
- 1115 Kwon, M. J., Beulig, F., Ilie, I., Wildner, M., Küsel, K., Merbold, L., Mahecha, M. D., Zimov, N., Zimov, S. A.,
 1116 Heimann, M., Schuur, E. A. G., Kostka, J. E., Kolle, O., Hilke, I., & Göckede, M. Plants, microorganisms, and
 1117 soil temperatures contribute to a decrease in methane fluxes on a drained Arctic floodplain. *Global Change
 1118 Biology*, 23(6), 2396–2412. <https://doi.org/10.1111/gcb.13558>. 2017.
- 1119 Lai, D. Y. F. Methane Dynamics in Northern Peatlands: A Review. *Pedosphere*, 19(4), 409–421.
 1120 [https://doi.org/10.1016/s1002-0160\(09\)00003-4](https://doi.org/10.1016/s1002-0160(09)00003-4). 2009.
- 1121 Lai, D. Y. F., Roulet, N. T., & Moore, T. R. The spatial and temporal relationships between CO₂ and CH₄
 1122 exchange in a temperate ombrotrophic bog. *Atmos. Environ.*, 89, 249–259.
 1123 <https://doi.org/10.1016/j.atmosenv.2014.02.034>. 2014.
- 1124 Lai, Derrick Y.F., & Jiangong Liu. FLUXNET-CH4 HK-MPM Mai Po Mangrove. Hong Kong.
 1125 <https://doi:10.18140/FLX/1669642>. 2020.
- 1126 Lasslop, G., Reichstein, M., Papale, D., Richardson, A. D., Arneth, A., Barr, A., Stoy, P., & Wohlfahrt, G.
 1127 Separation of net ecosystem exchange into assimilation and respiration using a light response curve approach:
 1128 critical issues and global evaluation. *Glob. Change Biol.*, 16(1), 187–208. [2486.2009.02041.x](https://doi.org/10.1111/j.1365-

 1129 2486.2009.02041.x). 2010.
- 1130 Liu, J., Zhou, Y., Valach, A., Shortt, R., Kasak, K., Rey-Sanchez, C., Hemes, K. S., Baldocchi, D., & Lai, D. Y. F.
 1131 Methane emissions reduce the radiative cooling effect of a subtropical estuarine mangrove wetland by half.
 1132 *Glob. Change Biol.*, 26(9), 4998–5016. <https://doi.org/10.1111/gcb.15247>. 2020.
- 1133 Madsen, K., Nielsen, H. B., & Tingleff, O. Methods for non-linear least squares problems. *Informatics and
 1134 Mathematical Modelling*, Technical University of Denmark. 2nd Edition. 2004.
- 1135 Magliulo, Vincenzo, Paul Di Tommasi, Daniela Famulari, Daniele Gasbarra, Luca Vitale, Antonio Manco,
 1136 Ferdinando di Matteo, Andrea Esposito, & Maurizio Tosca. FLUXNET-CH4 IT-BCi Borgo Cioffi. Italy.
 1137 <https://doi:10.18140/FLX/1669644>. 2020.
- 1138 Mahecha, M. D., Gans, F., Sippel, S., Donges, J. F., Kaminski, T., Metzger, S., Migliavacca, M., Papale, D.,
 1139 Rammig, A., & Zscheischler, J. Detecting impacts of extreme events with ecological in situ monitoring
 1140 networks. *Biogeosciences*, 14(18), 4255–4277. <https://doi.org/10.5194/bg-14-4255-2017>. 2017.
- 1141 Malhotra, A., & Roulet, N. T. Environmental correlates of peatland carbon fluxes in a thawing landscape: do
 1142 transitional thaw stages matter? *Biogeosciences*, 12(10), 3119–3130. <https://doi.org/10.5194/bg-12-3119-2015>.
 1143 2015.
- 1144 Mammarella, Ivan, Timo Vesala, Petri Keronen, Pasi Kolari, Samuli Launiainen, Jukka Pumpanen, Üllar Rannik,
 1145 Erkki Siivila, Janne Levula, & Toivo Pohja. FLUXNET-CH4 FI-Hyy Hyttiala. Finland.
 1146 <https://doi:10.18140/FLX/1669637>. 2020.
- 1147 Manca, Giovanni, & Ignacio Goded. FLUXNET-CH4 IT-Cas Castellaro. Italy. <https://doi:10.18140/FLX/1669645>.
 1148 2020.
- 1149 Mastepanov, M., Sigsgaard, C., Tagesson, T., Ström, L., Tamstorf, M. P., Lund, M., & Christensen, T. R.
 1150 Revisiting factors controlling methane emissions from high-Arctic tundra. *Biogeosciences*, 10(7), 5139–5158.
 1151 <https://doi.org/10.5194/bg-10-5139-2013>. 2013.

- 1152 Matthes, Jaclyn Hatala, Cove Sturtevant, Patty Oikawa, Samuel D Chamberlain, Daphne Szutu, Ariane Arias Ortiz,
 1153 Joseph Verfaillie, & Dennis Baldocchi. FLUXNET-CH4 US-Myb Mayberry Wetland. United States.
 1154 <https://doi:10.18140/FLX/1669685>. 2020.
- 1155 Matthews, E., Johnson, M. S., Genovese, V., Du, J., & Bastviken, D. Methane emission from high latitude lakes:
 1156 methane-centric lake classification and satellite-driven annual cycle of emissions. *Sci. Rep.- UK*, 10(1), 12465.
 1157 <https://doi.org/10.1038/s41598-020-68246-1>. 2020.
- 1158 Megonigal, J. P., Whalen, S. C., Tissue, D. T., Bovard, B. D., Allen, A. S., & Albert, D. B. A Plant-Soil-
 1159 Atmosphere Microcosm for Tracing Radiocarbon from Photosynthesis through Methanogenesis. *Soil Sci. Soc.*
 1160 *Am. J.* 63(3), 665–671. <https://doi.org/10.2136/sssaj1999.03615995006300030033x>. 1999.
- 1161 Meijide, A., Manca, G., Goded, I., Maglilio, V., Di Tommasi, P., Seufert, G., & Cescatti, A. Seasonal trends and
 1162 environmental controls of methane emissions in a rice paddy field in Northern Italy. *Biogeosciences*, 8(12),
 1163 3809. <https://doi.org/10.5194/bg-8-3809-2011>. 2011.
- 1164 Melloh, R. A., & Crill, P. M. Winter methane dynamics in a temperate peatland. *Global Biogeochem. Cy.*, 10(2),
 1165 247–254. <https://doi.org/10.1029/96gb00365>. 1996.
- 1166 Melton, J. R., Wania, R., Hodson, E. L., Poulter, B., Ringeval, B., Spahni, R., Bohn, T., Avis, C. A., Beerling, D. J.,
 1167 Chen, G., Eliseev, A. V., Denisov, S. N., Hopcroft, P. O., Lettenmaier, D. P., Riley, W. J., Singarayer, J. S.,
 1168 Subin, Z. M., Tian, H., Zürcher, S., & Others. Present state of global wetland extent and wetland methane
 1169 modelling: conclusions from a model inter-comparison project (WETCHIMP). *Biogeosciences*, 10(2), 753–
 1170 788. <https://doi.org/10.5194/bg-10-753-2013>. 2013.
- 1171 Merbold, Lutz, Corinna Rebmann, & Chiara Corradi. FLUXNET-CH4 RU-Che Cherski. Russian Federation.
 1172 <https://doi:10.18140/FLX/1669655>. 2020.
- 1173 Meyer, H., & Pebesma, E. Predicting into unknown space? Estimating the area of applicability of spatial prediction
 1174 models. *arXiv [stat.ML]*. arXiv. <http://arxiv.org/abs/2005.07939>. 2020.
- 1175 Mishra, S. R., Pattnaik, P., Sethunathan, N., & Adhya, T. K. Anion-Mediated Salinity Affecting Methane
 1176 Production in a Flooded Alluvial Soil. *Geomicrobiol. J.*, 20(6), 579–586. <https://doi.org/10.1080/713851167>.
 1177 2003.
- 1178 Moffat, A. M., Papale, D., Reichstein, M., Hollinger, D. Y., Richardson, A. D., Barr, A. G., Beckstein, C., Braswell,
 1179 B. H., Churkina, G., Desai, A. R., Falge, E., Gove, J. H., Heimann, M., Hui, D., Jarvis, A. J., Kattge, J.,
 1180 Noormets, A., & Stauch, V. J. Comprehensive comparison of gap-filling techniques for eddy covariance net
 1181 carbon fluxes. *Agr. Forest Meteorol.*, 147(3), 209–232. <https://doi.org/10.1016/j.agrformet.2007.08.011>. 2007.
- 1182 Myhre, G., D. Shindell, F.-M. Bréon, W. Collins, J. Fuglestvedt, J. Huang, D. Koch, J.-F. Lamarque, D. Lee, B.
 1183 Mendoza, T. Nakajima, A. Robock, G. Stephens, T. Takemura and H. Zhang. Anthropogenic and Natural
 1184 Radiative Forcing Supplementary Material. In Stocker, T.F., D. Qin, G.-K. Plattner, M. Tignor, S.K. Allen, J.
 1185 Boschung, A. Nauels, Y. Xia, V. Bex and P.M. Midgley (Ed.), *Climate Change 2013: The Physical Science*
 1186 Basis. Contribution of Working Group I to the Fifth Assessment Report of the Intergovernmental Panel on
 1187 Climate Change. 2013.
- 1188 Nemitz, E., Mammarella, I., Ibrom, A., Aurela, M., Burba, G. G., Dengel, S., Gielen, B., Grelle, A., Heinesch, B.,
 1189 Herbst, M., Hörtnagl, L., Klemedtsson, L., Lindroth, A., Lohila, A., McDermitt, D. K., Meier, P., Merbold, L.,
 1190 Nelson, D., Nicolini, G., & Others. Standardisation of eddy-covariance flux measurements of methane and
 1191 nitrous oxide. *Int. Agrophys.*, 32(4), 517–549. <https://doi.org/10.1515/intag-2017-0042>. 2018.
- 1192 Nielsen, H. B. Damping parameter in Marquardt's method. Department of Mathematical Modeling, IMM, Technical
 1193 University of Denmark. Technical Report, IMM-REP-1999-05. 1999.
- 1194 Nilsson, Mats B., & Matthias Peichl. FLUXNET-CH4 SE-Deg Degero. Sweden.
 1195 <https://doi:10.18140/FLX/1669659>. 2020.
- 1196 Niu, Shuli, & Weinan Chen. FLUXNET-CH4 CN-Hgu Hongyuan. China. <https://doi:10.18140/FLX/1669632>. 2020.
- 1197 Noormets, Asko, John King, Bhaskar Mitra, Guofang Miao, Maricar Aguilos, Kevan Minick, Prajaya Prajapati,
 1198 Jean-Christophe Domec, Jonathan Furst, & Maxwell Wightman. FLUXNET-CH4 US-NC4
 1199 NC_AlligatorRiver. United States. <https://doi:10.18140/FLX/1669686>. 2020.
- 1200 Oikawa, P. Y., Jenerette, G. D., Knox, S. H., Sturtevant, C., Verfaillie, J., Dronova, I., Poindexter, C. M.,
 1201 Eichelmann, E., & Baldocchi, D. D. Evaluation of a hierarchy of models reveals importance of substrate
 1202 limitation for predicting carbon dioxide and methane exchange in restored wetlands. *J. Geophys. Res.-Biogeog.*,
 1203 122(1), 145–167. <https://doi.org/10.1002/2016JG003438>. 2017.
- 1204 Oikawa, Patty. FLUXNET-CH4 US-EDN Eden Landing Ecological Reserve. United States.
 1205 <https://doi:10.18140/FLX/1669673>. 2020.

- 1206 Olefeldt, D., Turetsky, M. R., Crill, P. M., & McGuire, A. D. Environmental and physical controls on northern
1207 terrestrial methane emissions across permafrost zones. *Glob. Change Biol.*, 19(2), 589–603.
1208 <https://doi.org/10.1111/gcb.12071>. 2013.
- 1209 Papale, D., Andrew Black, T., Carvalhais, N., Cescatti, A., Chen, J., Jung, M., Kiely, G., Lasslop, G., Mahecha, M.
1210 D., Margolis, H., Merbold, L., Montagnani, L., Moors, E., Olesen, J. E., Reichstein, M., Tramontana, G., van
1211 Gorsel, E., Wohlfahrt, G., & Ráduly, B. Effect of spatial sampling from European flux towers for estimating
1212 carbon and water fluxes with artificial neural networks. *J. Geophys. Res.-Biogeosci.*, 120(10), 1941–1957.
1213 <https://doi.org/10.1002/2015jg002997>. 2015.
- 1214 Parmentier, F. J. W., van Huissteden, J., van der Molen, M. K., Schaepman-Strub, G., Karsanaev, S. A., Maximov,
1215 T. C., & Dolman, A. J. Spatial and temporal dynamics in eddy covariance observations of methane fluxes at a
1216 tundra site in northeastern Siberia. *J. Geophys. Res.*, 116(G3), 1368. <https://doi.org/10.1029/2010JG001637>.
1217 2011.
- 1218 Pastorello, G., Trotta, C., Canfora, E., Chu, H., Christianson, D., Cheah, Y.-W., Poindexter, C., Chen, J.,
1219 Elbashandy, A., Humphrey, M., Isaac, P., Polidori, D., Ribeca, A., van Ingen, C., Zhang, L., Amiro, B.,
1220 Ammann, C., Arain, M. A., Ardö, J., & Others. The FLUXNET2015 dataset and the ONEFlux processing
1221 pipeline for eddy covariance data. *Scientific Data*, 7(1), 225. <https://doi.org/10.1038/s41597-020-0534-3>. 2020.
- 1222 Pattnaik, P., Mishra, S. R., Bharati, K., Mohanty, S. R., Sethunathan, N., & Adhya, T. K. Influence of salinity on
1223 methanogenesis and associated microflora in tropical rice soils. *Microbiol. Res.*, 155(3), 215–220.
1224 [https://doi.org/10.1016/S0944-5013\(00\)80035-X](https://doi.org/10.1016/S0944-5013(00)80035-X). 2000.
- 1225 Poffenbarger, H. J., Needelman, B. A., & Patrick Megonigal, J. Salinity Influence on Methane Emissions from
1226 Tidal Marshes. *Wetlands*, 31(5), 831–842. <https://doi.org/10.1007/s13157-011-0197-0>. 2011.
- 1227 Poulter, B., Bousquet, P., Canadell, J. G., Ciais, P., Peregon, A., Saunois, M., Arora, V. K., Beerling, D. J., Brovkin,
1228 V., Jones, C. D., Joos, F., Gedney, N., Ito, A., Kleinen, T., Koven, C. D., McDonald, K., Melton, J. R., Peng,
1229 C., Peng, S., & Others. Global wetland contribution to 2000–2012 atmospheric methane growth rate dynamics.
1230 *Environ. Res. Lett.*, 12(9), 094013. <https://doi.org/10.1088/1748-9326/aa8391>. 2017.
- 1231 Reba, Michele, Benjamin Runkle, & Kosana Suvocarev. FLUXNET-CH4 US-HRC Humnoke Farm Rice Field –
1232 Field C. United States. <https://doi:10.18140/FLX/1669677>. 2020.
- 1233 Reichstein, M., Falge, E., Baldocchi, D., Papale, D., Aubinet, M., Berbigier, P., Bernhofer, C., Buchmann, N.,
1234 Gilmanov, T., Granier, A., Grunwald, T., Havrankova, K., Ilvesniemi, H., Janous, D., Knohl, A., Laurila, T.,
1235 Lohila, A., Loustau, D., Matteucci, G., & Others. On the separation of net ecosystem exchange into
1236 assimilation and ecosystem respiration: review and improved algorithm. *Glob. Change Biol.*, 11(9), 1424–
1237 1439. <https://doi.org/10.1111/j.1365-2486.2005.001002.x>. 2005.
- 1238 Rey-Sanchez, Camilo, Daphne Szutu, Robert Shortt, Samuel D. Chamberlain, Joseph Verfaillie, & Dennis
1239 Baldocchi. FLUXNET-CH4 US-Bi1 Bouldin Island Alfalfa. United States. <https://doi:10.18140/FLX/1669666>.
1240 2020a.
- 1241 Rey-Sanchez, Camilo, Daphne Szutu, Kyle Hemes, Joseph Verfaillie, & Dennis Baldocchi. FLUXNET-CH4 US-
1242 Bi2 Bouldin Island corn. United States. <https://doi:10.18140/FLX/1669667>. 2020b.
- 1243 Richardson, A. D., Hollinger, D. Y., Burba, G. G., Davis, K. J., Flanagan, L. B., Katul, G. G., William Munger, J.,
1244 Ricciuto, D. M., Stoy, P. C., Suyker, A. E., Verma, S. B., & Wofsy, S. C. A multi-site analysis of random error
1245 in tower-based measurements of carbon and energy fluxes. *Agr. Forest Meteorol.*, 136(1), 1–18.
1246 <https://doi.org/10.1016/j.agrformet.2006.01.007>. 2006.
- 1247 Richardson, A. D., & Hollinger, D. Y. A method to estimate the additional uncertainty in gap-filled NEE resulting
1248 from long gaps in the CO₂ flux record. *Agr. Forest Meteorol.*, 147(3), 199–208.
1249 <https://doi.org/10.1016/j.agrformet.2007.06.004>. 2007.
- 1250 Richardson, A. D., Mahecha, M. D., Falge, E., Kattge, J., Moffat, A. M., Papale, D., Reichstein, M., Stauch, V. J.,
1251 Braswell, B. H., Churkina, G., Kruijt, B., & Hollinger, D. Y. Statistical properties of random CO₂ flux
1252 measurement uncertainty inferred from model residuals. *Agr. Forest Meteorol.*, 148(1), 38–50.
1253 <https://doi.org/10.1016/j.agrformet.2007.09.001>. 2008.
- 1254 Richardson, A. D., Aubinet, M., Barr, A. G., Hollinger, D. Y., Ibrom, A., Lasslop, G., & Reichstein, M. Uncertainty
1255 quantification. *Eddy Covariance: A Practical Guide to Measurement and Data Analysis*. (eds) Aubinet, M.,
1256 Vesala, T., Papale, D. Springer Atmospheric Sciences. 2012.
- 1257 Richardson, Andrew D, & David Y Hollinger. FLUXNET-CH4 US-Ho1 Howland Forest (main tower). United
1258 States. <https://doi:10.18140/FLX/1669675>. 2020.
- 1259 Rinne, J., Riutta, T., Pihlatie, M., Aurela, M., Haapanala, S., Tuovinen, J.-P., Tuittila, E.-S., & Vesala, T. Annual
1260 cycle of methane emission from a boreal fen measured by the eddy covariance technique. *Tellus B*, 59(3), 449–
1261 457. <https://doi.org/10.1111/j.1600-0889.2007.00261.x>. 2007.

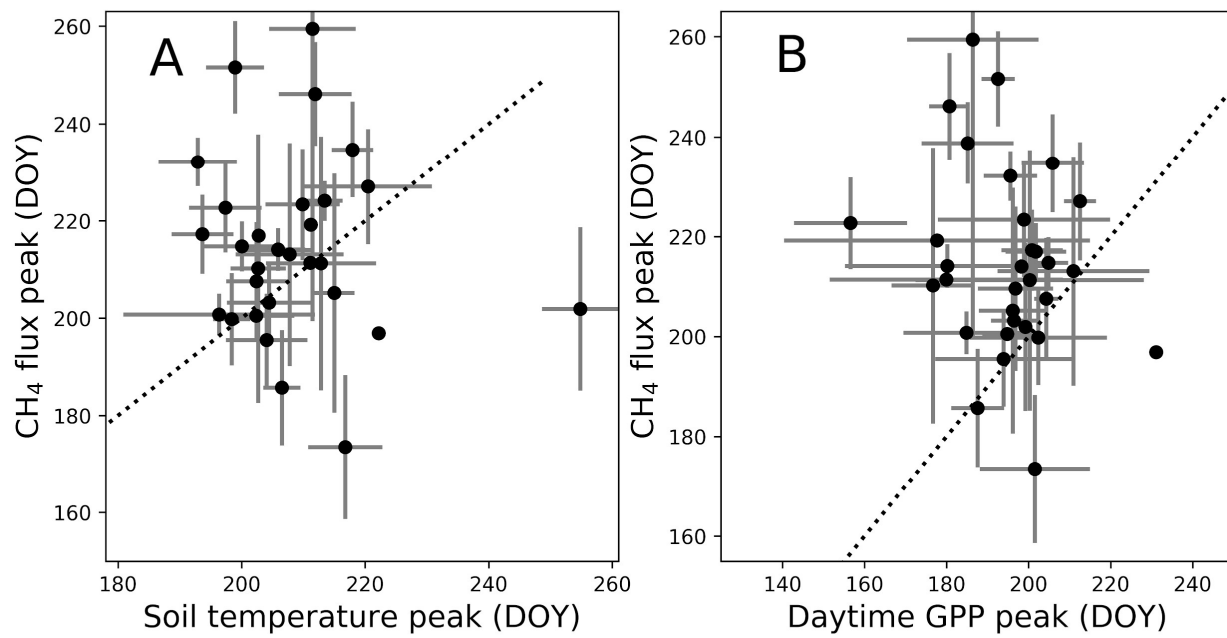
- 1262 Runkle, B. R. K., Suvočarev, K., Reba, M. L., Reavis, C. W., Smith, S. F., Chiu, Y.-L., & Fong, B. Methane
1263 Emission Reductions from the Alternate Wetting and Drying of Rice Fields Detected Using the Eddy
1264 Covariance Method. *Envir. Sci. Tech.*, 53(2), 671–681. <https://doi.org/10.1021/acs.est.8b05535>. 2019.
1265 Runkle, Benjamin, Michele Reba, & Kosana Suvocarev. FLUXNET-CH4 US-HRA Humnoke Farm Rice Field –
1266 Field A. United States. <https://doi:10.18140/FLX/1669676>. 2020.
1267 Ryu, Youngryel, Minseok Kang, & Jongho Kim. FLUXNET-CH4 KR-CRK Cheorwon Rice paddy. Korea,
1268 Republic of. <https://doi:10.18140/FLX/1669649>. 2020.
1269 Sachs, T., Giebels, M., Boike, J., & Kutzbach, L. Environmental controls on CH4 emission from polygonal tundra
1270 on the microsite scale in the Lena river delta, Siberia: CONTROLS ON TUNDRA CH4 FLUX AND
1271 SCALING. *Glob. Change Biol.*, 16(11) 3096 – 3110. <https://doi.org/10.1111/j.1365-2486.2010.02232.x>. 2010.
1272 Sachs, Torsten, Christian Wille, & Eric Larmanou. FLUXNET-CH4 DE-Dgw Dagowsee. Germany.
1273 <https://doi:10.18140/FLX/1669633>. 2020a.
1274 Sachs, Torsten, Christian Wille, Eric Larmanou, & Daniela Franz. FLUXNET-CH4 DE-Zrk Zarnekow. Germany.
1275 <https://doi:10.18140/FLX/1669636>. 2020b.
1276 Sakabe, Ayaka, Masayuki Itoh, Takashi Hirano, & Kitsos Kusin. FLUXNET-CH4 ID-Pag Palangkaraya undrained
1277 forest. Indonesia. <https://doi:10.18140/FLX/1669643>. 2020.
1278 Saunois, M., Bousquet, P., Poulter, B., Peregón, A., Ciais, P., Canadell, J. G., Dlugokencky, E. J., Etiöpe, G.,
1279 Bastviken, D., Houweling, S., Janssens-Maenhout, G., Tubiello, F. N., Castaldi, S., Jackson, R. B., Alexe, M.,
1280 Arora, V. K., Beerling, D. J., Bergamaschi, P., Blake, D. R., & Others. The global methane budget 2000–2012.
1281 *Earth Syst. Sci. Data*, 8, 697–751. <https://doi.org/10.5194/essd-8-697-2016>. 2016.
1282 Saunois, M., Stavert, A. R., Poulter, B., Bousquet, P., Canadell, J. G., Jackson, R. B., Raymond, P. A.,
1283 Dlugokencky, E. J., Houweling, S., Patra, P. K., Ciais, P., Arora, V. K., Bastviken, D., Bergamaschi, P., Blake,
1284 D. R., Brailsford, G., Bruhwiler, L., Carlson, K. M., Carroll, M., & Others. The Global Methane Budget 2000–
1285 2017. *Earth Syst. Sci. Data*, 12, 1561–1623. <https://doi.org/10.5194/essd-12-1561-2020>. 2020.
1286 Schafer, Karina. FLUXNET-CH4 US-MRM Marsh Resource Meadowlands Mitigation Bank. United States.
1287 <https://doi:10.18140/FLX/1669684>. 2020.
1288 Schuur, E.A. FLUXNET-CH4 US-EML Eight Mile Lake Permafrost thaw gradient, Healy Alaska. United States.
1289 <https://doi:10.18140/FLX/1669674>. 2020.
1290 Seyfferth, A. L., Bothfeld, F., Vargas, R., Stuckey, J. W., Wang, J., Kearns, K., Michael, H. A., Guimond, J., Yu,
1291 X., & Sparks, D. L. Spatial and temporal heterogeneity of geochemical controls on carbon cycling in a tidal
1292 salt marsh. *Geochim. Cosmochim. Ac.*, 282, 1–18. <https://doi.org/10.1016/j.gca.2020.05.013>. 2020.
1293 Shortt, Robert, Kyle Hemes, Daphne Szutu, Joseph Verfaillie, & Dennis Baldocchi. FLUXNET-CH4 US-Sne
1294 Sherman Island Restored Wetland. United States. <https://doi:10.18140/FLX/1669693>. 2020.
1295 Sims, D. A., Rahman, A. F., Cordova, V. D., El-Masri, B. Z., Baldocchi, D. D., Flanagan, L. B., Goldstein, A. H.,
1296 Hollinger, D. Y., Misson, L., Monson, R. K., Oechel, W. C., Schmid, H. P., Wofsy, S. C., & Xu, L. On the use
1297 of MODIS EVI to assess gross primary productivity of North American ecosystems. *J. Geophys. Res.-Biogeo.*
1298 111(G4). <https://doi.org/10.1029/2006jg000162>. 2006.
1299 Sonnentag, Oliver, & Manuel Helbig. FLUXNET-CH4 CA-SCB Scotty Creek Bog. Canada.
1300 <https://doi:10.18140/FLX/1669613>. 2020a.
1301 Sonnentag, Oliver, & Manuel Helbig. FLUXNET-CH4 CA-SCC Scotty Creek Landscape. Canada. <https://doi:10.18140/FLX/1669628>. 2020b.
1302 Spahni, R., Wania, R., Neef, L., van Weele, M., Pison, I., Bousquet, P., Frankenberg, C., Foster, P. N., Joos, F.,
1303 Prentice, I. C., & van Velthoven, P. Constraining global methane emissions and uptake by ecosystems. In
1304 *Biogeosciences*, 8(6), 1643–1665. <https://doi.org/10.5194/bg-8-1643-2011>. 2011.
1305 Sparks, Jed P. FLUXNET-CH4 US-MAC MacArthur Agro-Ecology. United States.
1306 <https://doi:10.18140/FLX/1669683>. 2020.
1307 Sturtevant, C. S., Ruddell, B. L., Knox, S. H., Verfaillie, J. G., Matthes, J. H., Oikawa, P. Y., & Baldocchi, D. D.
1308 Identifying scale-emergent, nonlinear, asynchronous processes of wetland methane exchange. *J. Geophys.
1309 Res.-Biogeo.*, 121, 188–204. <https://doi.org/10.1002/2015JG003054>. 2016.
1310 Tagesson, T., Mölder, M., Masteponov, M., Sigsgaard, C., Tamstorf, M. P., Lund, M., Falk, J. M., Lindroth, A.,
1311 Christensen, T. R., & Ström, L. Land-atmosphere exchange of methane from soil thawing to soil freezing in a
1312 high-Arctic wet tundra ecosystem. *Glob. Change Biol.*, 18(6), 1928–1940. [https://doi.org/10.1111/j.1365-2486.2012.02647.x](https://doi.org/10.1111/j.1365-
1313 2486.2012.02647.x). 2012.
1314

- 1315 Guan Xhuan Wong, Lulie Melling, Angela Che Ing Tang, Edward Baran Aeries, Joseph Wenceslaus Waili, Kevin
1316 Kemudang Musin, Kim San Lo, & Frankie Kiew. FLUXNET-CH4 MY-MLM Maludam National Park.
1317 Malaysia. <https://doi:10.18140/FLX/1669650>. 2020.
- 1318 Taoka, T., Iwata, H., Hirata, R., Takahashi, Y., Miyabara, Y., & Itoh, M. Environmental Controls on Diffusive and
1319 Ebullitive Methane Emission at a Sub-Daily Time Scale in the Littoral Zone of a Mid-Latitude Shallow Lake.
1320 *J. Geophys. Res.-Biogeo.*, 125(9), <https://doi.org/10.1029/2020JG005753>. 2020.
- 1321 Torn, Margaret, & Sigrid Dengel. FLUXNET-CH4 US-NGB NEE Arctic Barrow. United States. <https://doi:10.18140/FLX/1669687>. 2020a.
- 1322 Torn, Margaret, & Sigrid Dengel. FLUXNET-CH4 US-NGC NEE Arctic Council. United States.
1323 <https://doi:10.18140/FLX/1669688>. 2020b.
- 1324 Treat, C. C., Anthony Bloom, A., & Marushchak, M. E. Nongrowing season methane emissions-a significant
1325 component of annual emissions across northern ecosystems. *Glob. Change Biol.*, 24(8), 3331–3343.
1326 <https://doi.org/10.1111/gcb.14137>. 2018.
- 1327 Turetsky, M. R., Kotowska, A., Bubier, J., Dise, N. B., Crill, P., Hornbrook, E. R. C., Minkkinen, K., Moore, T. R.,
1328 Myers-Smith, I. H., Nykänen, H., Olefeldt, D., Rinne, J., Saarnio, S., Shurpali, N., Tuittila, E.-S., Waddington,
1329 J. M., White, J. R., Wickland, K. P., & Wilmking, M. A synthesis of methane emissions from 71 northern,
1330 temperate, and subtropical wetlands. *Glob. Change Biol.*, 20(7), 2183–2197.
1331 <https://doi.org/10.1111/gcb.12580>. 2014.
- 1332 Ueyama, Masahito, Takashi Hirano, & Yasuhiro Kominami. FLUXNET-CH4 JP-BBY Bibai bog. Japan.
1333 <https://doi:10.18140/FLX/1669646>. 2020.
- 1334 Valach, Alex, Daphne Szutu, Elke Eichelmann, Sara Knox, Joseph Verfaillie, & Dennis Baldocchi. FLUXNET-CH4
1335 US-Tw1 Twitchell Wetland West Pond. United States. <https://doi:10.18140/FLX/1669696>. 2020a.
- 1336 Valach, Alex, Kuno Kasak, Daphne Szutu, Joseph Verfaillie, & Dennis Baldocchi. FLUXNET-CH4 US-Tw5 East
1337 Pond Wetland. United States. <https://doi:10.18140/FLX/1669699>. 2020b.
- 1338 Varlagin, Andrej. FLUXNET-CH4 RU-Fy2 Fyodorovskoye dry spruce. Russian Federation.
1339 <https://doi:10.18140/FLX/1669657>. 2020.
- 1340 Vazquez-Lule, Alma, & Rodrigo Vargas. FLUXNET-CH4 US-StJ St Jones Reserve. United States.
1341 <https://doi:10.18140/FLX/1669695>. 2020.
- 1342 Vázquez-Lule, A., & Vargas, R. Biophysical drivers of net ecosystem and methane exchange across phenological
1343 phases in a tidal salt marsh. *Agricultural and Forest Meteorology*, 300, 108309.
1344 <https://doi.org/10.1016/j.agrformet.2020.108309>. 2021.
- 1345 Verma, S. B., Ullman, F. G., Billesbach, D., Clement, R. J., Kim, J., & Verry, E. S. Eddy correlation measurements
1346 of methane flux in a northern peatland ecosystem. *Bound. Lay. Meteorol.*, 58(3), 289–304.
1347 <https://doi.org/10.1007/BF02033829>. 1992.
- 1348 Vesala, Timo, Eeva-Stiina Tuittila, Ivan Mammarella, & Pavel Alekseychik. FLUXNET-CH4 FI-Si2 Siikaneva-2
1349 Bog. Finland. <https://doi:10.18140/FLX/1669639>. 2020a.
- 1350 Vesala, Timo, Eeva-Stiina Tuittila, Ivan Mammarella, & Janne Rinne. FLUXNET-CH4 FI-Sii Siikaneva. Finland.
1351 <https://doi:10.18140/FLX/1669640>. 2020b.
- 1352 Villarreal, S., Guevara, M., Alcaraz-Segura, D., Brunsell, N. A., Hayes, D., Loescher, H. W., & Vargas, R.
1353 Ecosystem functional diversity and the representativeness of environmental networks across the conterminous
1354 United States. *Agr. Forest Meteorol.*, 262, 423–433. <https://doi.org/10.1016/j.agrformet.2018.07.016>. 2018.
- 1355 Villarreal, S., Guevara, M., Alcaraz-Segura, D., & Vargas, R. Optimizing an Environmental Observatory Network
1356 Design Using Publicly Available Data. *J. Geophys. Res.-Biogeo.*, 124(7), 1812–1826.
1357 <https://doi.org/10.1029/2018JG004714>. 2019.
- 1358 Vourlitis, George, Hugo Dalmagro, Jose de S. Nogueira, Mark Johnson, & Paulo Arruda. FLUXNET-CH4 BR-Npw
1359 Northern Pantanal Wetland. Brazil. <https://doi:10.18140/FLX/1669368>. 2020.
- 1360 Vuichard, N., & Papale, D. Filling the gaps in meteorological continuous data measured at FLUXNET sites with
1361 ERA-Interim reanalysis. *Earth Syst. Sci. Data*, 7(2), 157–171. <https://doi.org/10.5194/essd-7-157-2015>. 2015.
- 1362 Weston, N. B., Dixon, R. E., & Joye, S. B. Ramifications of increased salinity in tidal freshwater sediments:
1363 Geochemistry and microbial pathways of organic matter mineralization. *J. Geophys. Res.*, 111(G1).
1364 <https://doi.org/10.1029/2005jg000071>. 2006.
- 1365 Weston, N. B., Vile, M. A., Neubauer, S. C., & Velinsky, D. J. Accelerated microbial organic matter mineralization
1366 following salt-water intrusion into tidal freshwater marsh soils. *Biogeochemistry*, 102, 135–151.
1367 <https://doi.org/10.1007/s10533-010-9427-4>. 2011.
- 1368 Wik, M., Crill, P. M., Varner, R. K., & Bastviken, D. Multiyear measurements of ebullitive methane flux from three
1369 subarctic lakes. *J. Geophys. Res.-Biogeo.* 118(3), 1307–1321. <https://doi.org/10.1002/jgrg.20103>. 2013.
- 1370

- 1371 Windham-Myers, Lisamarie, Ellen Stuart-Haëntjens, Brian Bergamaschi, Sara Knox, Frank Anderson, & Kyle
1372 Nakatsuka. FLUXNET-CH4 US-Srr Suisun marsh - Rush Ranch. United States.
1373 <https://doi:10.18140/FLX/1669694>. 2020.
- 1374 Wohlfahrt, Georg, Albin Hammerle, & Lukas Hörtnagl. FLUXNET-CH4 AT-Neu Neustift. Austria.
1375 <https://doi:10.18140/FLX/1669365>. 2020.
- 1376 Wutzler, T., Lucas-Moffat, A., Migliavacca, M., Knauer, J., Sickel, K., Šigut, L., Menzer, O., & Reichstein, M.
1377 Basic and extensible post-processing of eddy covariance flux data with REddyProc. Biogeosciences, 15, 5015–
1378 5030. <https://doi.org/10.5194/bg-2018-56-sc1>. 2018.
- 1379 Xu, X., Riley, W. J., Koven, C. D., Billesbach, D. P., -W. Chang, R. Y., Commane, R., Euskirchen, E. S., Hartery,
1380 S., Harazono, Y., Iwata, H., McDonald, K. C., Miller, C. E., Oechel, W. C., Poulter, B., Raz-Yaseef, N.,
1381 Sweeney, C., Torn, M., Wofsy, S. C., Zhang, Z., & Zona, D. A multi-scale comparison of modeled and
1382 observed seasonal methane emissions in northern wetlands. Biogeosciences, 13(17), 5043–5056.
1383 <https://doi.org/10.5194/bg-13-5043-2016>. 2016.
- 1384 Yvon-Durocher, G., Allen, A. P., Bastviken, D., Conrad, R., Gudasz, C., St-Pierre, A., Thanh-Duc, N., & del
1385 Giorgio, P. A. Methane fluxes show consistent temperature dependence across microbial to ecosystem scales.
1386 Nature, 507(7493), 488–491. <https://doi.org/10.1038/nature13164>. 2014.
- 1387 Zhang, Z. Fluet-Choinard, E., Jensen, K., McDonald, K., Hugelius, G., Gumbrecht, T., Carroll, M., Prigent, C.,
1388 Bartsch, A., & Poulter, B. Development of a global dataset of Wetland Area and Dynamics for Methane
1389 Modeling (WAD2M) [Data set]. Zenodo. <http://doi.org/10.5281/zenodo.3998454>. 2020.
- 1390 Zhang, Z. Fluet-Choinard, E., Jensen, K., McDonald, K., Hugelius, G., Gumbrecht, T., Carroll, M., Prigent, C.,
1391 Bartsch, A., & Poulter, B. Development of a global dataset of Wetland Area and Dynamics for Methane
1392 Modeling (WAD2M). Earth Syst. Sci. Data [In press]. 2021.
- 1393 Zona, D., Gioli, B., Commane, R., Lindaas, J., Wofsy, S. C., Miller, C. E., Dinardo, S. J., Dengel, S., Sweeney, C.,
1394 Karion, A., Chang, R. Y.-W., Henderson, J. M., Murphy, P. C., Goodrich, J. P., Moreaux, V., Liljedahl, A.,
1395 Watts, J. D., Kimball, J. S., Lipson, D. A., & Oechel, W. C. Cold season emissions dominate the Arctic tundra
1396 methane budget. P. Natl. A. Sci. USA., 113(1), 40–45. <https://doi.org/10.1073/pnas.1516017113>. 2016.
- 1397 Zona, Donatella, & Walter C Oechel. FLUXNET-CH4 US-Atq Atkasuk. United States.
1398 <https://doi:10.18140/FLX/1669663>. 2020a.
- 1399 Zona, Donatella, & Walter C Oechel. FLUXNET-CH4 US-Beo Barrow Environmental Observatory (BEO) tower.
1400 United States. <https://doi:10.18140/FLX/1669664>. 2020b.
- 1401 Zona, Donatella, & Walter C Oechel. FLUXNET-CH4 US-Bes Barrow-Bes (Biocomplexity Experiment South
1402 tower). United States. <https://doi:10.18140/FLX/1669665>. 2020c.
- 1403 Zona, Donatella, & Walter C Oechel. FLUXNET-CH4 US-Ivo Ivotuk. United States.
1404 <https://doi:10.18140/FLX/1669679>. 2020d.

1405 APPENDIX A

1406



1407

1408

1409 **Figure A1: Peak methane (CH_4) flux timing versus peak gross primary productivity (GPP) timing (A) and peak soil
1410 temperature timing by day of year (B). Points represent site average and error bars represent standard deviations. Dotted
1411 line represents 1:1 relationship.**

1412

1413 APPENDIX B

1414

1415 [Table B1: Data variable names, descriptions, and units](#)

1416 **FLUXNET-CH4 Data Variables**

1417 This webpage describes data variables and file formatting for the FLUXNET-CH4 Community Product.

1418 **1. Data Variable: Base names**

1419 Base names indicate fundamental quantities that are either measured or calculated/derived. They can also
1420 indicate quantified quality information.

1421 Table 1. Base names for data variables

<i>Variable</i>	<i>Description</i>	<i>Units</i>
-----------------	--------------------	--------------

TIMEKEEPING

TIMESTAMP_STAR T	ISO timestamp start of averaging period, used in half-hourly data	YYYYMMDDHHMM
TIMESTAMP_END	ISO timestamp end of averaging period, used in half-hourly data	YYYYMMDDHHMM
TIMESTAMP	ISO timestamp used in daily aggregation files	YYYYMMDD

MET_RAD

SW_IN	Shortwave radiation, incoming	W m-2
SW_OUT	Shortwave radiation, outgoing	W m-2
LW_IN	Longwave radiation, incoming	W m-2
LW_OUT	Longwave radiation, outgoing	W m-2

PPFD_IN	Photosynthetic photon flux density, incoming	$\mu\text{molPhoton m}^{-2} \text{s}^{-1}$
PPFD_OUT	Photosynthetic photon flux density, outgoing	$\mu\text{molPhoton m}^{-2} \text{s}^{-1}$
NETRAD	Net radiation	W m^{-2}

MET_WIND

USTAR	Friction velocity	m s^{-1}
WD	Wind direction	Decimal degrees
WS	Wind speed	m s^{-1}

HEAT

H	Sensible heat turbulent flux (with storage term if provided by site PI)	W m^{-2}
LE	Latent heat turbulent flux (with storage term if provided by site PI)	W m^{-2}
G	Soil heat flux	W m^{-2}

MET_ATM

PA	Atmospheric pressure	kPa
TA	Air temperature	deg C

VPD	Vapor Pressure Deficit	hPa
RH	Relative humidity, range 0-100	%

MET_PRECIP

P	Precipitation	mm
---	---------------	----

PRODUCTS

NEE	Net Ecosystem Exchange	$\mu\text{molCO}_2 \text{ m}^{-2} \text{ s}^{-1}$
GPP	Gross primary productivity	$\mu\text{molCO}_2 \text{ m}^{-2} \text{ s}^{-1}$
RECO	Ecosystem respiration	$\mu\text{molCO}_2 \text{ m}^{-2} \text{ s}^{-1}$

GASES

FCH4	Methane (CH_4) turbulent flux (no storage correction)	$\text{nmolCH}_4 \text{ m}^{-2} \text{ s}^{-1}$
------	------------------------------------------------------------------	-------------------------------------------------

MET_SOIL

TS	Soil temperature	deg C
WTD	Water table depth (negative values indicate below the surface)	m

1423 **2. Data Variable: Qualifiers**

1424 Qualifiers are suffixes appended to variable base names that provide additional information about the
1425 variable. For example, the _DT qualifier in the variable label GPP_DT indicates that gross primary
1426 production (GPP) has been partitioned using the flux partitioning method from Lasslop et al. 2010.

1427 Multiple qualifiers can be added, and they must **follow the order in which they are presented here**.

1428 **2.1. Qualifiers: General**

1429 General qualifiers indicate additional information about a variable.

1430 · **_F** : Variable has been gap-filled by the FLUXNET-CH4 team. Gaps in meteorological variables
1431 (including air temperature (TA), incoming shortwave (SW_IN) and longwave (LW_IN) radiation, vapor
1432 pressure deficit (VPD), pressure (PA), precipitation (P), and wind speed (WS)) were filled with ERA-
1433 Interim (ERA-I) reanalysis data ((Vuichard and Papale 2015)). Other variables were filled using the MDS
1434 approach in REddyProc (see Delwiche et al. 2020 for more details).

1435 · **_DT** : Variable acquired using the flux partitioning method from (Lasslop et al. 2010), with values
1436 estimated by fitting the light-response curve.

1437 · **_NT** : Variable acquired using the flux partitioning method from (Reichstein et al. 2005), with values
1438 estimated from night-time data and extrapolated to day time.

1439 · **RANDUNC**: Random uncertainty introduced from several different sources including errors
1440 associated with the flux measurement system (gas analyzer, sonic anemometer, data acquisition system,
1441 flux calculations), errors associated with turbulent transport, and statistical errors relating to the location
1442 and activity of the sites of flux exchange (“footprint heterogeneity”) (Hollinger and Richardson 2005).

1443 · **ANNOPTLM** : Gap-filled variable using an artificial neural net routine from Matlab with the
1444 Levenberg-Marquardt algorithm as the training function, and parameters optimized across runs (more
1445 detail in (Sara Helen Knox et al. 2016; Sara H. Knox et al. 2019)).

1446 · **_UNC** : Uncertainty introduced from ANNOPTLM gap-filling routine, as described in Knox et al.
1447 2016 and Knox et al. 2019.

1448 · **_QC** : Reports quality checks on FCH4 gap-filled data (**_ANNOPTLM**) based on length of data gap.
1449 1 = data gap shorter than 2 months, 3 = data gap exceeds 2 months which could lead to poor quality gap-
1450 filled data. Nondimensional.

1451

1452 **2.2. Qualifiers: Positional (_V)**

1453 Positional qualifiers are used to indicate relative positions of observations at the site. For FLUXNET-CH4,
1454 positional qualifiers are used to distinguish soil temperature probes for sites with more than one probe.
1455 Probe depths for each positional qualifier per site are included in the metadata file included with data
1456 download and also in Table B7 of Delwiche et al. 2020. For sites where the original database file release
1457 in Ameriflux, AsiaFlux, or EuroFlux contains multiple probes at the same _V depth, we average values
1458 and report only the average for each _V position. The one exception to this is site US-UAF where the
1459 original positional qualifier from the data we downloaded from Ameriflux had different depths for the

1460 same qualifier. We still averaged the probe data, so _V qualifiers from US-UAF represent an average of
1461 more than one depth.

1462 **3.0 Missing data**

1463 Missing data are reported using -9999. Data for all days in a leap year are reported.

1464 **4.0 References**

- 1465 Hollinger, D. Y., and A. D. Richardson. 2005. "Uncertainty in Eddy Covariance Measurements and Its
1466 Application to Physiological Models." *Tree Physiology* 25 (7): 873–85.
1467 Knox, Sara Helen, Jaclyn Hatala Matthes, Cove Sturtevant, Patricia Y. Oikawa, Joseph Verfaillie, and
1468 Dennis Baldocchi. 2016. "Biophysical Controls on Interannual Variability in Ecosystem-Scale
1469 CO₂ and CH₄ Exchange in a California Rice Paddy." *Journal of Geophysical Research: Biogeosciences*. <https://doi.org/10.1002/2015jg003247>.
1470 Knox, Sara H., Robert B. Jackson, Benjamin Poulter, Gavin McNicol, Etienne Fluet-Chouinard, Zhen
1471 Zhang, Gustaf Hugelius, et al. 2019. "FLUXNET-CH₄ Synthesis Activity: Objectives, Observations,
1472 and Future Directions." *Bulletin of the American Meteorological Society* 100 (12): 2607–32.
1473 Lasslop, Gitta, Markus Reichstein, Dario Papale, Andrew D. Richardson, Almut Arneth, Alan Barr, Paul
1474 Stoy, and Georg Wohlfahrt. 2010. "Separation of Net Ecosystem Exchange into Assimilation and
1475 Respiration Using a Light Response Curve Approach: Critical Issues and Global Evaluation." *Global
1476 Change Biology*. <https://doi.org/10.1111/j.1365-2486.2009.02041.x>.
1477 Reichstein, Markus, Eva Falge, Dennis Baldocchi, Dario Papale, Marc Aubinet, Paul Berbigier, Christian
1478 Bernhofer, et al. 2005. "On the Separation of Net Ecosystem Exchange into Assimilation and
1479 Ecosystem Respiration: Review and Improved Algorithm." *Global Change Biology*.
1480 <https://doi.org/10.1111/j.1365-2486.2005.001002.x>.
1481 Vuichard, N., and D. Papale. 2015. "Filling the Gaps in Meteorological Continuous Data Measured at
1482 FLUXNET Sites with ERA-Interim Reanalysis." *Earth System Science Data*.
1483 <https://doi.org/10.5194/essd-7-157-2015>.

Table B2 Site year annual sums and uncertainties

	SITE_ID	Year	Ann_Flux_g_C_m-2	Ann_Flux_Uncertainty_g_C_m-2	Mean_Soil_Temp_C	Mean_Water_Table_Depth_m
1	AT-Neu	2010	0.38	0.03	8.65	NaN
2	AT-Neu	2011	0.25	0.02	8.61	NaN
3	AT-Neu	2012	NaN	NaN	9.39	NaN
4	BR-Npw	2013	NaN	NaN	NaN	NaN
5	BR-Npw	2014	NaN	NaN	25.95	NaN
6	BR-Npw	2015	20.95	1.18	26.2	-0.47
7	BR-Npw	2016	17.48	1.14	25.31	-0.41
8	BW-Gum	2018	51.73	10.59	NaN	NaN
9	BW-Nxr	2018	47.32	3.70	NaN	NaN
10	CA-SCB	2014	10.42	0.66	9.6	-0.15
11	CA-SCB	2015	NaN	NaN	5.58	-0.1
12	CA-SCB	2016	12.12	0.31	5.38	-0.15
13	CA-SCB	2017	9.48	0.27	6.32	-0.21
14	CA-SCC	2013	NaN	NaN	7.2	NaN
15	CA-SCC	2014	4.94	0.12	4.38	NaN
16	CA-SCC	2015	6.76	0.15	3.15	NaN
17	CA-SCC	2016	6.76	0.12	NaN	NaN
18	CH-Cha	2012	2.13	0.38	11.88	NaN
19	CH-Cha	2013	2.30	0.36	10.89	NaN
20	CH-Cha	2014	3.46	0.40	12.2	NaN
21	CH-Cha	2015	3.93	0.68	11.93	NaN
22	CH-Cha	2016	NaN	NaN	12.28	NaN
23	CH-Dav	2016	1.21	0.40	4.33	NaN
24	CH-Dav	2017	NaN	NaN	4.41	NaN
25	CH-Oe2	2018	0.29	0.13	12.32	NaN
26	CN-Hgu	2015	NaN	NaN	NaN	NaN
27	CN-Hgu	2016	0.81	0.16	7.26	NaN
28	CN-Hgu	2017	0.82	0.45	7.66	NaN
29	DE-Dgw	2015	NaN	NaN	NaN	NaN
30	DE-Dgw	2016	7.51	0.22	NaN	NaN
31	DE-Dgw	2017	10.42	0.16	NaN	NaN
32	DE-Dgw	2018	NaN	NaN	NaN	NaN
33	DE-Hte	2011	59.85	6.39	NaN	-0.41
34	DE-Hte	2012	36.83	3.46	NaN	-0.21
35	DE-Hte	2013	49.72	2.34	NaN	-0.25
36	DE-Hte	2014	NaN	NaN	13.26	-0.19
37	DE-Hte	2015	51.37	1.75	10.78	-0.26
38	DE-Hte	2016	50.77	2.09	9.8	-0.25
39	DE-Hte	2017	46.61	1.40	10.39	-0.4
40	DE-Hte	2018	41.62	2.52	6.12	-0.22
41	DE-SfN	2012	NaN	NaN	NaN	-0.08

42	DE-SfN	2013	3.62	0.93	10.32	-0.05
43	DE-SfN	2014	NaN	NaN	8.16	NaN
44	DE-Zrk	2013	NaN	NaN	13.03	NaN
45	DE-Zrk	2014	NaN	NaN	11.67	NaN
46	DE-Zrk	2015	30.76	1.00	10.85	NaN
47	DE-Zrk	2016	31.14	1.23	11.28	0.12
48	DE-Zrk	2017	29.10	0.87	10.84	0.31
49	DE-Zrk	2018	31.10	1.20	10.54	0.25
50	FI-Hyy	2016	NaN	NaN	5.41	NaN
51	FI-Lom	2006	13.77	0.76	4.47	0
52	FI-Lom	2007	17.22	0.25	4.33	0.04
53	FI-Lom	2008	15.52	0.22	3.79	0.06
54	FI-Lom	2009	17.63	0.27	3.98	0.02
55	FI-Lom	2010	13.78	0.29	3.71	0.03
56	FI-Si2	2012	9.27	1.17	9.4	0.06
57	FI-Si2	2013	10.22	1.17	10.47	0.13
58	FI-Si2	2014	NaN	NaN	7.7	0.1
59	FI-Si2	2015	NaN	NaN	8.18	0.09
60	FI-Si2	2016	NaN	NaN	7.67	0.09
61	FI-Sii	2013	14.58	0.32	6.45	0.04
62	FI-Sii	2014	12.93	0.78	6.42	0.03
63	FI-Sii	2015	NaN	NaN	6.92	-0.02
64	FI-Sii	2016	16.56	0.68	5.87	-0.01
65	FI-Sii	2017	8.63	0.23	8.4	0.06
66	FI-Sii	2018	9.46	1.10	6.68	0.11
67	FR-LGt	2017	NaN	NaN	10.45	-0.24
68	FR-LGt	2018	2.45	0.60	10.87	-0.22
69	HK-MPM	2016	11.62	0.61	25.06	-0.61
70	HK-MPM	2017	10.60	0.30	23.14	-0.64
71	HK-MPM	2018	11.04	0.59	NaN	-0.8
72	ID-Pag*	2016	0.09	0.07	NaN	NaN
73	ID-Pag*	2017	0.09	0.09	NaN	NaN
74	IT-BCi	2017	NaN	NaN	17.16	NaN
75	IT-BCi	2018	NaN	NaN	17.36	NaN
76	IT-Cas	2009	25.44	1.46	9.62	NaN
77	IT-Cas	2010	17.80	1.26	12.37	NaN
78	JP-BBY	2015	9.53	0.29	10.12	0
79	JP-BBY	2016	16.42	0.45	10.02	0
80	JP-BBY	2017	19.61	0.65	9.33	-0.03
81	JP-BBY	2018	NaN	NaN	9.79	-0.04
82	JP-Mse	2012	9.50	1.97	14.52	0.03
83	JP-SwL	2016	66.68	4.29	NaN	1.91
84	KR-CRK	2015	NaN	NaN	14.41	0.02
85	KR-CRK	2016	29.12	0.91	12.48	0.03

86	KR-CRK	2017	25.84	0.86	13.94	0.02
87	KR-CRK	2018	28.82	1.15	11.32	0.02
88	MY-MLM	2014	9.55	0.59	26.8	-0.09
89	MY-MLM	2015	NaN	NaN	26.9	-0.01
90	NL-Hor	2007	NaN	NaN	12.4	NaN
91	NL-Hor	2008	NaN	NaN	10.37	NaN
92	NL-Hor	2009	NaN	NaN	11.61	NaN
93	NK-Kop	2012	23.98	1.38	12.17	-0.08
94	NK-Kop	2013	15.33	0.43	12.68	-0.13
95	NK-Kop	2014	15.67	0.39	12.38	-0.11
96	NK-Kop	2015	14.37	2.66	12.46	-0.1
97	PH-RiF	2012	NaN	NaN	27.78	NaN
98	PH-RiF	2013	12.41	0.99	28.17	NaN
99	PH-RiF	2014	NaN	NaN	27.47	NaN
100	RU-Ch2	2014	6.99	0.14	-4.21	NaN
101	RU-Ch2	2015	5.86	0.14	-4.87	NaN
102	RU-Ch2	2016	NaN	NaN	-2.88	NaN
103	RU-Che	2014	3.84	0.14	-3.31	NaN
104	RU-Che	2015	4.19	0.22	-3.28	NaN
105	RU-Che	2016	4.24	0.19	-1.65	NaN
106	RU-Cok	2008	NaN	NaN	NaN	NaN
107	RU-Cok	2009	NaN	NaN	NaN	NaN
108	RU-Cok	2010	NaN	NaN	NaN	NaN
109	RU-Cok	2011	NaN	NaN	NaN	NaN
110	RU-Cok	2012	NaN	NaN	-0.46	NaN
111	RU-Cok	2013	NaN	NaN	-5.73	NaN
112	RU-Cok	2014	NaN	NaN	-4.82	NaN
113	RU-Cok	2015	4.45	0.15	-4.4	NaN
114	RU-Cok	2016	NaN	NaN	-11.1	NaN
115	RU-Fy2	2015	NaN	NaN	9.83	NaN
116	RU-Fy2	2016	2.69	0.59	6.88	0.68
117	RU-Fy2	2017	2.17	0.52	6.1	0.19
118	RU-Fy2	2018	5.66	1.37	6.48	0.79
119	SE-Deg	2014	11.24	1.98	5.02	-0.02
120	SE-Deg	2015	11.11	0.08	5.04	0.02
121	SE-Deg	2016	11.19	0.15	5.19	-0.01
122	SE-Deg	2017	NaN	NaN	4.19	0
123	SE-Deg	2018	9.42	0.09	5.49	-0.03
124	UK-LBT	2011	NaN	NaN	NaN	NaN
125	UK-LBT	2012	NaN	NaN	NaN	NaN
126	UK-LBT	2013	50.50	0.97	NaN	NaN
127	UK-LBT	2014	42.57	2.25	NaN	NaN
128	US-A03	2015	NaN	NaN	-6.65	NaN
129	US-A03	2016	NaN	NaN	-6.14	NaN

130	US-A03	2017	7.26	2.58	-4.48	NaN
131	US-A03	2018	4.35	0.62	-4.93	NaN
132	US-A10	2012	NaN	NaN	NaN	NaN
133	US-A10	2013	NaN	NaN	NaN	NaN
134	US-A10	2014	NaN	NaN	NaN	NaN
135	US-A10	2015	NaN	NaN	NaN	NaN
136	US-A10	2016	NaN	NaN	NaN	NaN
137	US-A10	2017	NaN	NaN	NaN	NaN
138	US-A10	2018	NaN	NaN	NaN	NaN
139	US-Atq	2013	NaN	NaN	-5.65	NaN
140	US-Atq	2014	1.80	0.19	-4.48	NaN
141	US-Atq	2015	1.75	0.11	-0.43	NaN
142	US-Atq	2016	1.75	0.00	NaN	NaN
143	US-Beo	2013	NaN	NaN	-2.67	NaN
144	US-Beo	2014	2.74	0.05	-4.95	NaN
145	US-Bes	2013	NaN	NaN	-6.01	NaN
146	US-Bes	2014	3.32	0.04	-5.69	NaN
147	US-Bes	2015	3.06	0.54	-6.24	NaN
148	US-Bi1	2016	NaN	NaN	15.62	NaN
149	US-Bi1	2017	NaN	NaN	17.17	NaN
150	US-Bi1	2018	0.69	0.29	16.82	NaN
151	US-Bi2	2017	0.86	0.20	20.42	NaN
152	US-Bi2	2018	1.69	0.29	17.12	NaN
153	US-BZB	2014	8.02	4.61	4.03	NaN
154	US-BZB	2015	7.52	0.82	3.9	NaN
155	US-BZB	2016	11.61	2.25	4.89	NaN
156	US-BZF	2014	6.61	0.63	4.32	NaN
157	US-BZF	2015	10.82	0.90	3.99	NaN
158	US-BZF	2016	NaN	NaN	5.93	NaN
159	US-BZS	2015	0.68	0.68	0.48	NaN
160	US-BZS	2016	0.89	0.27	0.67	NaN
161	US-CRT	2011	2.21	0.15	11.49	-0.92
162	US-CRT	2012	2.21	0.11	12.38	-1.45
163	US-DPW	2013	NaN	NaN	NaN	NaN
164	US-DPW	2014	58.91	0.69	NaN	NaN
165	US-DPW	2015	NaN	NaN	NaN	NaN
166	US-DPW	2016	43.60	1.29	NaN	NaN
167	US-DPW	2017	43.60	0.06	NaN	NaN
168	US-EDN	2018	-0.04	0.06	NaN	NaN
169	US-EML	2015	NaN	NaN	5.71	NaN
170	US-EML	2016	1.04	0.08	3.07	NaN
171	US-EML	2017	0.36	0.27	3.8	NaN
172	US-EML	2018	0.36	0.07	NaN	NaN
173	US-Ho1	2012	NaN	NaN	NaN	-0.43

174	US-Ho1	2013	-0.05	0.02	NaN	-0.33
175	US-Ho1	2014	-0.04	0.02	NaN	-0.38
176	US-Ho1	2015	-0.16	0.01	NaN	-0.48
177	US-Ho1	2016	-0.22	0.01	NaN	-0.57
178	US-Ho1	2017	-0.24	0.01	NaN	-0.56
179	US-Ho1	2018	-0.24	0.01	NaN	NaN
180	US-HRA	2017	-0.24	0.56	NaN	NaN
181	US-HRC	2017	-0.24	0.81	NaN	NaN
182	US-ICs	2014	NaN	NaN	-1.55	NaN
183	US-ICs	2015	NaN	NaN	-0.62	NaN
184	US-ICs	2016	NaN	NaN	-1.48	NaN
185	US-Ivo	2013	NaN	NaN	3.19	NaN
186	US-Ivo	2014	5.05	0.22	0.02	NaN
187	US-Ivo	2015	3.89	0.27	0.47	NaN
188	US-Ivo	2016	5.77	0.55	-1.01	NaN
189	US-LA1	2011	NaN	NaN	18.92	NaN
190	US-LA1	2012	12.68	0.63	24.23	NaN
191	US-LA2	2011	12.68	0.19	NaN	NaN
192	US-LA2	2012	48.42	1.57	23.09	NaN
193	US-LA2	2013	43.34	1.32	23.19	NaN
194	US-Los	2014	6.66	1.48	8.3	-0.06
195	US-Los	2015	5.51	0.40	5.65	-0.1
196	US-Los	2016	8.67	0.35	6.3	-0.07
197	US-Los	2017	6.00	0.33	5.5	-0.09
198	US-Los	2018	5.71	0.37	4.29	-0.19
199	US-MAC	2013	5.71	2.68	NaN	NaN
200	US-MAC	2014	26.37	1.69	23.18	-0.71
201	US-MAC	2015	15.40	0.85	23.29	-0.55
202	US-MRM	2012	0.30	0.19	11.16	NaN
203	US-MRM	2013	0.37	0.14	8.99	NaN
204	US-Myb	2010	NaN	NaN	NaN	0.95
205	US-Myb	2011	33.83	0.72	17.18	1.23
206	US-Myb	2012	64.20	0.58	16.25	1.12
207	US-Myb	2013	59.81	0.92	15.7	1.19
208	US-Myb	2014	58.97	0.68	11.27	1.24
209	US-Myb	2015	60.85	0.55	NaN	1.3
210	US-Myb	2016	45.72	0.48	NaN	1.22
211	US-Myb	2017	30.32	0.84	18.5	1.35
212	US-Myb	2018	29.33	0.55	17.05	1.19
213	US-NC4	2012	38.28	1.70	17.12	NaN
214	US-NC4	2013	18.60	3.88	NaN	NaN
215	US-NC4	2014	26.98	0.60	18.02	NaN
216	US-NC4	2015	23.37	2.30	16.27	NaN
217	US-NC4	2016	62.20	2.78	16.35	NaN

218	US-NGB	2012	NaN	NaN	NaN	NaN
219	US-NGB	2013	NaN	NaN	NaN	NaN
220	US-NGB	2014	NaN	NaN	NaN	NaN
221	US-NGB	2015	NaN	NaN	NaN	NaN
222	US-NGB	2016	NaN	NaN	NaN	NaN
223	US-NGB	2017	2.31	0.11	NaN	NaN
224	US-NGB	2018	2.52	0.22	NaN	NaN
225	US-NGC	2017	2.52	0.06	NaN	NaN
226	US-NGC	2018	2.52	0.05	NaN	NaN
227	US-ORv	2011	3.53	0.54	16.64	NaN
228	US-ORv	2012	9.11	0.45	14.23	NaN
229	US-ORv	2013	7.70	0.41	13.19	NaN
230	US-ORv	2014	8.46	0.26	12	NaN
231	US-ORv	2015	NaN	NaN	13.36	NaN
232	US-OWC	2015	NaN	NaN	22.11	0.9
233	US-OWC	2016	113.99	3.25	21.19	0.54
234	US-PFa	2010	NaN	NaN	NaN	NaN
235	US-PFa	2011	0.34	0.05	NaN	NaN
236	US-PFa	2012	0.30	0.04	NaN	NaN
237	US-PFa	2013	0.31	0.05	NaN	NaN
238	US-PFa	2014	NaN	NaN	NaN	NaN
239	US-PFa	2015	0.63	0.03	NaN	NaN
240	US-PFa	2016	0.85	0.02	NaN	NaN
241	US-PFa	2017	0.80	0.06	NaN	NaN
242	US-PFa	2018	NaN	NaN	NaN	NaN
243	US-Snd	2010	NaN	NaN	16.85	NaN
244	US-Snd	2011	NaN	NaN	14.96	NaN
245	US-Snd	2012	6.34	0.25	16.06	NaN
246	US-Snd	2013	6.04	0.48	16.59	-0.65
247	US-Snd	2014	3.23	0.36	17.52	-0.78
248	US-Snd	2015	3.23	0.21	NaN	NaN
249	US-Sne	2016	NaN	NaN	17.85	-0.2
250	US-Sne	2017	45.96	0.40	17.05	0.16
251	US-Sne	2018	39.63	0.66	16.83	0.09
252	US-Srr	2014	0.71	0.10	NaN	NaN
253	US-Srr	2015	0.88	0.11	NaN	NaN
254	US-Srr	2016	0.86	0.10	16.3	-0.18
255	US-Srr	2017	0.86	0.11	NaN	NaN
256	US-StJ	2016	9.55	1.04	11.66	-0.26
257	US-Tw1	2011	26.09	2.70	14.01	NaN
258	US-Tw1	2012	NaN	NaN	11.58	0.24
259	US-Tw1	2013	33.93	1.78	11.92	0.25
260	US-Tw1	2014	49.60	1.67	13.14	0.25
261	US-Tw1	2015	54.80	2.58	12.79	0.33

262	US-Tw1	2016	45.93	1.90	12.91	0.41
263	US-Tw1	2017	38.66	2.09	12.53	0.38
264	US-Tw1	2018	27.60	1.64	12.1	0.24
265	US-Tw3	2013	NaN	NaN	19.63	NaN
266	US-Tw3	2014	NaN	NaN	17.91	NaN
267	US-Tw4	2013	NaN	NaN	NaN	NaN
268	US-Tw4	2014	16.26	0.39	NaN	0.48
269	US-Tw4	2015	27.61	0.43	17.2	0.36
270	US-Tw4	2016	33.49	0.37	14.8	0.18
271	US-Tw4	2017	47.95	0.58	13.78	0.07
272	US-Tw4	2018	37.41	0.48	13.02	0.08
273	US-Tw5	2018	59.72	1.15	16.67	0.69
274	US-Twt	2009	NaN	NaN	17.66	-0.01
275	US-Twt	2010	9.87	1.15	15.67	-0.18
276	US-Twt	2011	12.32	4.92	14.95	-0.11
277	US-Twt	2012	8.12	0.51	16.05	-0.04
278	US-Twt	2013	12.64	0.48	15.98	-0.11
279	US-Twt	2014	17.02	0.97	17.44	-0.09
280	US-Twt	2015	14.43	0.38	17.04	-0.14
281	US-Twt	2016	11.07	0.59	16.44	-0.29
282	US-Twt	2017	11.07	0.31	NaN	NaN
283	US-Uaf	2011	0.32	0.04	-2.14	-0.17
284	US-Uaf	2012	NaN	NaN	-2.43	-0.18
285	US-Uaf	2013	NaN	NaN	-1.15	-0.18
286	US-Uaf	2014	NaN	NaN	-1.18	-0.13
287	US-Uaf	2015	NaN	NaN	-0.49	-0.12
288	US-Uaf	2016	0.68	0.05	-0.05	-0.1
289	US-Uaf	2017	0.58	0.06	1.09	-0.13
290	US-Uaf	2018	NaN	NaN	0.87	-0.13
291	US-WPT	2011	41.05	1.57	17.22	0.43
292	US-WPT	2012	54.96	1.71	14.27	0.28
293	US-WPT	2013	52.76	1.29	12.89	0.44

*Data from ID-Pag spans 365 days from June 2016 to June 2017. Annual methane flux for each year is the sum of these 365 days, with uncertainty being calculated separately for each year.

Column Descriptions

SITE_ID	Site identification code as assigned by regional flux data network
Year	Data year
Ann_Flux_g_C_m-2	Total annual methane flux (gC/m^2)
Ann_Flux_Uncertainty_g_C_m-2	Gap-filling and rancom uncertainty associated with annual flux (gC/m^2)
Mean_Soil_Temp_C	Annual mean soil temperature (degree C). For sites with multiple probes, we use the probe closest to the surface
Mean_Water_Table_Depth_m	Annual mean water table depth (m)

Table B3-A: Site metadata, select data, and DOI links

SITE_ID	SITE_NAME	SITE_PERSONNEL	COUNTRY	LAT	LONG	DATA_DOI	YEAR_S	YEAR_E	UTC_O	ORIGINAL_DFFSET	ATA_SOURCE
1	AT-Neu	Neustift	Georg Wohlfahrt	Austria	47.117	11.318 10.18140/FLX/1669365	2010	2012	1	EuroFlux	
2	BR-Npw	Northern Pantanal Wetland	George Vourlitis	Brazil	-16.498	-56.412 10.18140/FLX/1669368	2013	2016	-4	AmeriFlux	
3	BW-Gum	Guma	Carole Heifter	Botswana	-18.965	22.371 10.18140/FLX/1669370	2018	2018	2	EuroFlux	
4	BW-Nxr	Nxaraga	Carole Heifter	Botswana	-19.548	23.179 10.18140/FLX/1669518	2018	2018	2	EuroFlux	
5	CA-SCB	Scotty Creek Bog	Oliver Sonnentag, Oliver Sonnentag, Manuel Helbig Oliver Sonnentag, Manuel Helbig	Canada	61.309	-121.298 10.18140/FLX/1669613	2014	2017	-7	AmeriFlux	
6	CA-SSC	Scotty Creek Landscape	Manuel Helbig	Canada	61.308	-121.299 10.18140/FLX/1669628	2013	2016	-7	AmeriFlux	
7	CH-Cha	Chamau	Nina Buchmann	Switzerland	47.210	8.410 10.18140/FLX/1669629	2012	2016	1	EuroFlux	
8	CH-Dav	Davos	Nina Buchmann	Switzerland	46.815	9.856 10.18140/FLX/1669630	2016	2017	1	EuroFlux	
9	CH-Oe2	Oensingen crop	Nina Buchmann	Switzerland	47.286	7.734 10.18140/FLX/1669631	2018	2018	1	EuroFlux	
10	CN-Hgu	Hongyuan	Shuli Niu, Weinan Chen	China	32.845	102.590 10.18140/FLX/1669632	2015	2017	8	EuroFlux	
11	DE-Dgw	Dagowsee	Torsten Sachs	Germany	53.151	13.054 10.18140/FLX/1669633	2015	2018	1	EuroFlux	
12	DE-Hte	Huetelmoor	Gerald Jurasinski	Germany	54.210	12.176 10.18140/FLX/1669634	2011	2018	1	EuroFlux	
13	DE-Sfn	Schechenfilz Nord	Hans Peter Schmid	Germany	47.806	11.328 10.18140/FLX/1669635	2012	2014	1	EuroFlux	
14	DE-Zrk	Zarnekow	Torsten Sachs	Germany	53.876	12.889 10.18140/FLX/1669636	2013	2018	1	EuroFlux	
15	FI-Hyy	Hyttiala	Timo Vesala, Ivan	Finland	61.847	24.295 10.18140/FLX/1669637	2016	2016	2	EuroFlux	
16	FI-Lom	Lompolojankka	Anna Lea Lohila	Finland	67.997	24.209 10.18140/FLX/1669638	2006	2010	2	EuroFlux	
17			Timo Vesala, Ivan								
18	FI-Si2	Silkaneva-2 Bog	Mammarella, Eeva-Stiina Tuittila	Finland	61.837	24.197 10.18140/FLX/1669639	2012	2016	2	EuroFlux	
19	FI-Sii	Silkaneva	Timo Vesala, Ivan	Finland	61.833	24.193 10.18140/FLX/1669640	2013	2018	2	EuroFlux	
			Mammarella, Eeva-Stiina Tuittila								
			Adrien Jacotot, Sébastien Gogo, Fatima Laggoun-Détage, Laurent Perdereau								
	FR-LGt	La Guette	France	47.323	2.284 10.18140/FLX/1669641	2017	2018	1	EuroFlux		

20	HK-MPM	Mai Po Mangrove	Derrick Lai, Jiangong Liu	Hong Kong	22.498	114.029 10.18140/FLX/1669642	2016	2018	8 EuroFlux
21	ID-Pag	Palangkaraya undrained forest	Takashi Hirano	Indonesia	-2.320	113.900 10.18140/FLX/1669643	2016	2017	7 EuroFlux
22	IT-BCi	Borgo Cioffi	Vincenzo Magliulo	Italy	40.524	14.957 10.18140/FLX/1669644	2017	2018	1 EuroFlux
23			Giovanni Manca, Ignacio Goded, Carsten Gruening, Ana Metijide	Italy	45.070	8.718 10.18140/FLX/1669645	2009	2010	1 EuroFlux
24	IT-Cas	Castellaro Bibai bog	Masahito Ueyama	Japan	43.323	141.811 10.18140/FLX/1669646	2015	2018	9 AsiaFlux
25	JP-BBY	Mase rice paddy field	Akira Miyata	Japan	36.054	140.027 10.18140/FLX/1669647	2012	2012	9 AsiaFlux
26	JP-Mse	Suwa Lake	Hiroki Iwata	Japan	36.047	138.108 10.18140/FLX/1669648	2016	2016	9 AsiaFlux
27	JP-SwL		Younghye Ryu, Minseok Kang	Korea	38.201	127.251 10.18140/FLX/1669649	2015	2018	9 AsiaFlux
28	KR-CRK	Cheorwon Rice paddy	Guan Xhuan Wong, Lulie Mellings, Angela C. I. Tang	Malaysia	1.454	111.149 10.18140/FLX/1669650	2014	2015	8 AsiaFlux
29	MY-MLM	Maludam National Park	Han Dolman	Netherlands	52.240	5.071 10.18140/FLX/1669651	2007	2009	1 EuroFlux
30	NL-Hor	Horstermeer	Dave Campbell	New Zealand	-37.388	175.554 10.18140/FLX/1669652	2012	2015	13 OzFlux
31	NZ-Kop	Koputawai Philippines Rice Institute flooded	Ma. Carmelita Alberto	Philippines	14.141	121.265 10.18140/FLX/1669653	2012	2014	8 EuroFlux
32	PH-Rif		Matthias Goeckede	Russia	68.617	161.351 10.18140/FLX/1669654	2014	2016	11 EuroFlux
33	RU-Ch2	Chersky reference	Matthias Goeckede	Russia	68.613	161.341 10.18140/FLX/1669655	2014	2016	11 EuroFlux
34	RU-Che	Cherski	Han Dolman	Russia	70.829	147.494 10.18140/FLX/1669656	2008	2016	11 EuroFlux
35	RU-Cok	Chokurdakh	Andrej Varlagin	Russia	56.448	32.902 10.18140/FLX/1669657	2015	2018	3 EuroFlux
36	RU-Fy2	Fyodorovskoye dry spruce	Matthias Peichl, Mats Nilsson	Sweden	64.182	19.557 10.18140/FLX/1669659	2014	2018	1 EuroFlux
37	SE-Deg	Degerö	Carole Helfter	UK	51.522	-0.139 10.18140/FLX/1670207	2011	2014	0 EuroFlux
38	UK-LBT	London_BT	Ryan Sullivan, David Cook, David Billesbach	USA	70.495	-149.882 10.18140/FLX/1669661	2015	2018	-9 AmeriFlux
39	US-A03	ARM-AMF3-Olkotk	Ryan Sullivan, David Cook, David Billesbach	USA					
	US-A10	ARM-NSA-Barrow							
40	US-Atq	Atqasuk	Donatella Zona	USA	71.324	-156.615 10.18140/FLX/1669662	2012	2018	-9 AmeriFlux
					70.470	-157.409 10.18140/FLX/1669663	2013	2016	-9 AmeriFlux

41	US-Beo	Barrow Environmental Observatory (BEO) tower	Donatella Zona	USA	71.281	-156.612 10.18140/FLX/1669664	2013	2014	-8 Ameriflux
42		Barrow-Bes (Biocomplexity Experiment South tower)	Donatella Zona	USA	71.281	-156.597 10.18140/FLX/1669665	2013	2015	-8 Ameriflux
43	US-Bes	Bouldin Island Alfalfa	Dennis Baldocchi	USA	38.099	-121.499 10.18140/FLX/1669666	2016	2018	-8 Ameriflux
44	US-Bi1	Bouldin Island corn	Dennis Baldocchi	USA	38.109	-121.535 10.18140/FLX/1669667	2017	2018	-8 Ameriflux
45	US-Bi2	Bonanza Creek Thermokarst Bog	Eugenie Euskirchen	USA	64.696	-148.321 10.18140/FLX/1669668	2014	2016	-9 Ameriflux
46	US-BZB	Bonanza Creek Rich Fen	Eugenie Euskirchen	USA	64.704	-148.313 10.18140/FLX/1669669	2014	2016	-9 Ameriflux
47	US-BZS	Bonanza Creek Black Spruce	Eugenie Euskirchen	USA	64.696	-148.324 10.18140/FLX/1669670	2015	2016	-9 Ameriflux
48	US-CRT	Curtice Walter-Berger cropland	Jiquen Chen, Housen Chu	USA	41.628	-83.347 10.18140/FLX/1669671	2011	2012	-5 Ameriflux
49			Charles Ross Hinkle, Rosvel Bracho, Scott Graham, Brian Benscoter	USA	28.052	-81.436 10.18140/FLX/1669672	2013	2017	-5 Ameriflux
	US-DPW	Disney Wilderness Preserve Wetland	Patty Oikawa	USA	37.616	-122.114 10.18140/FLX/1669673	2018	2018	-8 Ameriflux
50	US-EDN	Eden Landing Ecological Reserve							
51		Eight Mile Lake Permafrost thaw gradient, Healy Alaska.	Ted Schuur	USA	63.878	-149.254 10.18140/FLX/1669674	2015	2018	-9 Ameriflux
52	US-EML		Andrew Richardson, David Hollinger	USA	45.204	-68.740 10.18140/FLX/1669675	2012	2018	-5 Ameriflux
53	US-H01	Howland Forest (main tower)	Benjamin Runkle	USA	34.585	-91.752 10.18140/FLX/1669676	2017	2017	-6 Ameriflux
54	US-HRA	Hunnoke Farm Rice Field – Field A	Benjamin Runkle	USA	34.589	-91.752 10.18140/FLX/1669677	2017	2017	-6 Ameriflux
55		Imnavait Creek Watershed Wet Sedge Tundra	Eugenie Euskirchen	USA	68.606	-149.311 10.18140/FLX/1669678	2014	2016	-9 Ameriflux
56	US-Ivo	Ivotuk Pointe-aux-Chenes Brackish	Donatella Zona	USA	68.487	-155.750 10.18140/FLX/1669679	2013	2016	-9 Ameriflux
57	US-LA1	Marsh	Ken Krauss	USA	29.501	-90.445 10.18140/FLX/1669680	2011	2012	-6 Ameriflux
58	US-LA2	Salvador WMA Freshwater Marsh	Ken Krauss	USA	29.859	-90.287 10.18140/FLX/1669681	2011	2013	-6 Ameriflux
59	US-Los	Lost Creek	Ankur Desai	USA	46.083	-89.979 10.18140/FLX/1669682	2014	2018	-6 Ameriflux

60	US-MAC	MacArthur Agro-Ecology	Jed Sparks, Sam Chamberlain	USA	27.163	-81.187 10.18140/FLX/1669683	2013	2015	-5 Ameriflux	
61		Marsh Resource Meadowlands	Karina Schäfer	USA	40.816	-74.044 10.18140/FLX/1669684	2012	2013	5 Ameriflux	
62	US-MRM	Mitigation Bank	Dennis Baldocchi	USA	38.050	-121.765 10.18140/FLX/1669685	2010	2018	-8 Ameriflux	
63	US-Myb	Mayberry Wetland	Asko Noormets	USA	35.788	-75.904 10.18140/FLX/1669686	2012	2016	-5 Ameriflux	
64	US-NC4	NC_AlligatorRiver	Margaret Torn	USA	71.280	-156.609 10.18140/FLX/1669687	2012	2018	-9 Ameriflux	
65	US-NGB	NGEE Arctic Barrow	Margaret Torn	USA	64.861	-163.701 10.18140/FLX/1669688	2017	2018	-9 Ameriflux	
66	US-NGC	NGEE Arctic Council	Oleentangy River Wetland Research Park	Gil Bohrer	USA	40.020	-83.018 10.18140/FLX/1669689	2011	2015	-5 Ameriflux
67	US-ORv	Old Woman Creek	Gil Bohrer	USA	41.380	-82.512 10.18140/FLX/1669690	2015	2016	-5 Ameriflux	
68	US-OWC	Park Falls/WLEF	Ankur Desai	USA	45.946	-90.272 10.18140/FLX/1669691	2010	2018	-6 Ameriflux	
69	US-PFa	Sherman Island	Dennis Baldocchi	USA	38.037	-121.754 10.18140/FLX/1669692	2010	2015	-8 Ameriflux	
70	US-Snd	Sherman Island Restored Wetland	Dennis Baldocchi	USA	38.037	-121.755 10.18140/FLX/1669693	2016	2018	-8 Ameriflux	
71	US-Srr	Suisun marsh - Rush Ranch St.Jones Reserve	Lisamarie Windham-Myers	USA	38.201	-122.026 10.18140/FLX/1669694	2014	2017	-8 Ameriflux	
72	US-StJ		Rodrigo Vargas	USA	39.088	-75.437 10.18140/FLX/1669695	2016	2016	-5 Ameriflux	
73	US-Tw1	Twitchell Wetland West Pond	Dennis Baldocchi	USA	38.107	-121.647 10.18140/FLX/1669696	2011	2018	-8 Ameriflux	
74	US-Tw3	Twitchell Alfalfa	Dennis Baldocchi	USA	38.116	-121.647 10.18140/FLX/1669697	2013	2014	-8 Ameriflux	
75	US-Tw4	Twitchell East End Wetland	Dennis Baldocchi	USA	38.103	-121.641 10.18140/FLX/1669698	2013	2018	-8 Ameriflux	
76	US-Tw5	East Pond Wetland	Dennis Baldocchi	USA	38.107	-121.643 10.18140/FLX/1669699	2018	2018	-8 Ameriflux	
77	US-Twt	Twitchell Island	Dennis Baldocchi	USA	38.109	-121.653 10.18140/FLX/1669700	2009	2017	-8 Ameriflux	
78	US-Uaf	University of Alaska, Fairbanks	Masahito Ueyama	USA	64.866	-147.856 10.18140/FLX/1669701	2011	2018	-9 Ameriflux	
79	US-WPT	Winous Point North Marsh	Jiquen Chen, Housen Chu	USA	41.465	-82.996 10.18140/FLX/1669702	2011	2013	-5 Ameriflux	

Column Descriptions

SITE_ID
 SITE_NAME
 SITE_PERSONNEL
 COUNTRY
 LAT
 LON

Site identification code as assigned by regional flux data network
 Site name determined by site personnel
 People associated with site FLUXNET-CH4 data
 Site country
 Latitude
 Longitude

DATA_DOI
YEAR_START
YEAR_END
UTC_OFFSET
ORIGINAL_DATA_SOURCE

DOI link for site FLUXNET-CH4 data

Year data begins

Year data ends

Site data offset from Coordinated Universal Time (in hours)

Regional network hosting the site methane data that was incorporated into FLUXNET-CH4

Table B3-B: Site metadata, select data, and DOI links

SITE_ID	SITE_CLASSTIFICATION	UPLAND_CLASS	IGBP	KOPPEN	MEAN_ANNUAL_TEMPERATURE	MOSS_BROWNAGNUM	AERENC_HYMATORUS	ERI_SHRUB	TREE	DOM_VEG	IN_SEASONALITY_ANALYSIS
1	AT-Neu	Upland	Alpine meadow	GRA	Dfb	7.0	1029	0	1	0	0 aerenchymatous
2	BR-Npw	Swamp	WSA	Aw	25.2	1318	0	0	1	0	1 tree
3	BW-Gum	Swamp	WET	Bsh	23.1	459	0	0	1	0	1 aerenchymatous
4	BW-Nxr	Swamp	GRA	Bsh	23.5	433	0	0	1	0	1 aerenchymatous
5	CA-SCB	Bog	WET	Dfc	-2.8	414	0	1	1	1	0 moss_sphagnum
6	CA-SCC	Upland	Needleleaf forest	ENF	Dfc	-2.9	414	0	1	0	1 tree
7	CH-Cha	Upland	Grassland	GRA	Cfb	9.6	1194	0	0	1	0 aerenchymatous
8	CH-Dav	Upland	Needleleaf forest	ENF	ET	3.8	1053	1	0	0	1 tree
9	CH-Oe2	Upland	Crop-wheat	CRO	Cfb	9.1	1122	0	0	1	0 aerenchymatous
10	CN-Hgu	Upland	Alpine meadow	GRA	Cwc	2.8	702	0	0	1	0 aerenchymatous
11	DE-Dgw	Lake	WAT	Cfb	8.3	567	0	0	0	0	0 no vegetation
12	DE-Hte	Fen	WET	Dfb	8.5	584	0	0	1	0	0 aerenchymatous
13	DE-Sfn	Bog	WET	Cfb	8.3	1123	0	1	1	1	1 tree
14	DE-Zrk	Fen	WET	Dfb	8.3	580	0	0	1	0	0 aerenchymatous
15	FI-Hy	Upland	Needleleaf forest	ENF	Dfc	3.1	671	1	1	0	1 tree
16	FI-Lom	Fen	WET	Dfc	-1.0	512	1	1	1	1	0 aerenchymatous
17	FI-Si2	Bog	WET	Dfc	3.2	664	0	1	1	1	1 moss_sphagnum
18	FI-Sii	Fen	WET	Dfc	3.2	666	0	1	1	0	0 moss_sphagnum
19	FR-Lgt	Fen	WET	Cfb	11.0	707	0	1	1	1	0 aerenchymatous
20	HK-MPM	e	Mangrov	EBF	Cfa	22.7	1991	0	0	1	0 aerenchymatous
21	ID-Pag	Swamp	EBF	Af	27.4	2386	0	0	1	0	1 tree
22	IT-Bci	Upland	Crop - corn	CRO	Csa	16.3	1035	0	0	1	0 aerenchymatous
23	IT-Cas	Rice	CRO	Cfa	12.3	773	0	0	1	0	0 aerenchymatous

24	JP-BBY	Bog		WET	Dfb	6.7	1153	0	1	1	1	0 aerenchymatos	1
25	JP-Mse	Rice		CRO	Cfa	14.1	1305	0	0	1	0	0 aerenchymatos	0
26	JP-Swl	Lake		WAT	Dfb	10.2	1141	0	0	1	0	0 aerenchymatos	0
27	KR-CRK	Rice		CRO	Dwa	9.9	1234	0	0	1	0	0 aerenchymatos	0
28	MY-MLM	Swamp		EBF	Af	26.9	3401	0	0	0	0	1 tree	0
29	NL-Hor	Drained	Grassland	GRA	Cfb	9.7	827	0	0	1	0	0 aerenchymatos	0
30	NZ-Kop	Bog		EBF	Cfb	13.9	1343	0	1	1	0	0 aerenchymatos	1
31	PH-Rif	Rice		CRO	Am	26.9	2010	0	0	1	0	0 aerenchymatos	0
32		Wet	tundra	WET	Dfc	-12.3	172	0	0	1	1	0 aerenchymatos	1
33	RU-Che	Drained		WET	Dfc	-12.3	172	0	0	1	1	0 aerenchymatos	0
34		Wet	tundra	OSH	Dfc	-14.1	210	0	1	1	1	0 moss_sphagnum	0
35	RU-Fy2	Upland	Needleleaf	ENF	Dfb	4.3	694	0	1	0	1	1 tree	0
36	SE-Deg	Fen		GRA	Dfc	1.7	620	0	1	1	1	0 moss_sphagnum	1
37	UK-LBT	Upland	Urban	URB	Cfb	11.0	646	0	0	0	0	0 no vegetation	0
38		Wet	tundra	BSV	ET	-11.9	144	0	1	1	0	0 moss_sphagnum	0
39	US-A10	tundra		BSV	ET	-12.0	107	0	1	1	0	0 moss_sphagnum	0
40	US-Atq	Wet	tundra	WET	ET	-10.3	133	1	0	1	1	0 aerenchymatos	1
41	US-Beo	tundra		WET	ET	-11.9	109	1	1	1	0	0 aerenchymatos	1
42	US-Bes	Wet	tundra	WET	ET	-12.0	109	0	1	1	0	0 aerenchymatos	1
43	US-Bi1	Drained	Crop - alfalfa	CRO	Csa	15.5	382	0	0	1	0	0 aerenchymatos	0
44	US-Bi2	Drained	Crop - corn	CRO	Csa	15.5	380	0	0	1	0	0 aerenchymatos	0
45	US-BzB	Bog		WET	Dfd	-2.4	292	0	1	1	1	0 eri_shrub	1
46	US-Bzf	Fen	Needleleaf	ENF	Dfd	-2.5	294	1	1	1	0	0 aerenchymatos	1
47	US-Bzs	Upland	forest	CRO	Dfa	-2.4	292	1	0	0	0	1 tree	0
48	US-Crt	Upland	Crop - soy	WET	Cwa	9.7	855	0	0	1	0	0 aerenchymatos	0
49	US-Dpw	Marsh		WET	22.1	1223	0	0	1	0	0	0 aerenchymatos	1

50	US-EDN	Salt marsh	WET	Csa	14.9	403	0	0	1	1	0 aerenchymatous
51	US-EML	Upland	Tundra	OSH	-3.3	421	1	0	1	1	0 aerenchymatous
52	US-Ho1	Upland	Needleleaf forest	ENF	Dfb	5.7	1069	0	0	0	1 tree
53	US-HRA	Rice	CRO	Cfa	Cfa	16.8	1290	0	0	1	0 aerenchymatous
54	US-HRC	Rice	CRO	Cfa	Cfa	16.8	1290	0	0	1	0 aerenchymatous
55	US-ICs	Wet tundra	WET	ET	-8.9	242	0	0	1	1	0 aerenchymatous
56	US-Ivo	Wet tundra	WET	ET	-8.5	247	1	0	1	1	0 aerenchymatous
57	US-LA1	Salt marsh	WET	Cfa	20.4	1596	0	0	1	0	0 aerenchymatous
58	US-LA2	Marsh	WET	Cfa	20.0	1616	0	0	1	0	0 aerenchymatous
59	US-Los	Fen	WET	Dfb	4.1	833	0	0	1	1	1 eri_shrub
60	US-MAC	Drained Grassland	WET	Cwa	22.7	1207	0	0	1	0	0 aerenchymatous
61	US-MRM	Salt marsh	WET	Cfa	12.0	1211	0	0	1	0	0 aerenchymatous
62	US-Myb	Marsh	WET	Csa	15.4	346	0	0	1	0	0 aerenchymatous
63	US-NC4	Swamp	WET	Cfa	16.5	1322	0	0	1	0	1 aerenchymatous
64	US-NGB	Wet tundra	SNO	ET	-11.9	109	0	1	1	0	0 moss_sphagnum
65	US-NGC	tundra	GRA	ET	-3.1	413	0	1	1	1	0 eri_shrub
66	US-ORv	Marsh	WET	Cfa	11.0	954	0	0	1	0	0 aerenchymatous
67	US-OWC	Marsh	WET	Dfb	9.9	898	0	0	1	0	0 aerenchymatous
68	US-PFa	Upland forest	MF	Dfb	4.3	826	0	0	0	1	1 tree
69	US-Snd	Drained Grassland	GRA	Csa	15.5	340	0	0	1	0	0 aerenchymatous
70	US-Sne	Marsh	GRA	Csa	15.5	340	0	0	1	0	0 aerenchymatous
71	US-Srr	Salt marsh	WET	Csa	15.4	541	0	0	1	0	0 aerenchymatous
72	US-StJ	Salt marsh	WET	Cfa	13.0	1133	0	0	1	0	0 aerenchymatous
73	US-Tw1	Marsh	WET	Csa	15.4	371	0	0	1	0	0 aerenchymatous
74	US-Tw3	Drained Crop-alalfa	CRO	Csa	15.4	371	0	0	1	0	0 aerenchymatous

75	US-Tw4	Marsh	WET	Csa	15.4	370	0	0	1	0	0 aerenchymatos	1
76	US-Tw5	Marsh	WET	Csa	15.4	371	0	0	1	0	0 aerenchymatos	1
77	US-Twt	Rice	CRO	Csa	15.3	372	0	0	1	0	0 aerenchymatos	0
78	US-Uaf	Bog	ENF	Dwc	-2.8	298	1	1	1	1	1 moss_sphagnum	1
79	US-WPT	Marsh	WET	Dfa	9.9	881	0	0	1	0	0 aerenchymatos	1

Column Descriptions

SITE_ID	Site identification code as assigned by regional flux data network
SITE_CLASSIFICATION	Site classification based on literature description of sites
UPLAND_CLASS	For upland sites, category of upland type
IGBP	International Geosphere–Biosphere Programme (IGBP) ecosystem surface classification
KOPPEN	Koppen climate zone abbreviation
MEAN_ANNUAL_TEMP_C_W	Mean annual precipitation from WorldClim2 Global Climate Data
ORLDCLIM	Mean annual precipitation from WorldClim2 Global Climate Data
MEAN_ANNUAL_PRECIP_M	Mean annual precipitation from WorldClim2 Global Climate Data
M_WORLDCLIM	Mean annual precipitation from WorldClim2 Global Climate Data
MOSS_BROWN	Presence/absence (1/0) brown moss. Presence/absence designated by Avni Malhotra using site-literature
MOSS_SPHAGNUM	Presence/absence (1/0) sphagnum moss. Presence/absence designated by Avni Malhotra using site-literature
AERENCHYMATOUS	Presence/absence (1/0) aerenchymatos vegetation. Presence/absence designated by Avni Malhotra using site-literature
ERI_SHRUB	Presence/absence (1/0) ericaceous shrubs. Presence/absence designated by Avni Malhotra using site-literature
TREE	Presence/absence (1/0) trees. Presence/absence designated by Avni Malhotra using site-literature
DOM_VEG	Dominant vegetation type in tower footprint. Dom_veg provided to Avni Malhotra by site personnel via sur
IN_SEASONALITY_ANALYSIS	Is site in freshwater wetland seasonality analysis? 1 = yes, 0 = no.

Table B3-C: Site metadata, select data, and DOI links

SITE_ID	Mean_Air_Temp_C	Mean_Air_Temp_stddev_C	Ann_Flux_g_CH4-C_m-2	JFM_Flux_s_tdev_g_CH4-C_m-2	JFM_Flux_s_tdev_g_CH4-C_m-2	AMJ_Flux_s_tdev_g_CH4-C_m-2	JAS_Flux_s_tdev_g_CH4-C_m-2	JAS_Flux_s_tdev_g_CH4-C_m-2	OND_Flux_s_tdev_g_CH4-C_m-2
1	AT-Neu	6.60	0.51	0.32	0.09	0.03	0.05	0.04	0.07
2	BR-Npw	25.44	0.73	19.21	2.45	9.68	1.46	8.52	0.01
3	BW-Gum	22.79		51.73			19.32		0.16
4	BW-Nxr	23.06		47.32			8.88		0.15
5	CASCB	-0.75	1.92	10.67	1.34		2.96	0.70	18.09
6	CASSCC	-0.24	2.04	6.15	1.05		1.79	0.45	0.11
7	CH-Cha	9.74	0.54	2.95	0.88	0.75	0.18	0.99	0.25
8	CH-Dav	4.37	0.09	1.21		0.28	0.05	0.37	0.24
9	CH-Oe2	11.00		0.29				0.21	0.13
10	CN-Hgu	3.77	1.31	0.82	0.01		0.23	0.04	0.15
11	DE-Dgw	9.72	0.38	8.97	2.06	0.07	0.06	1.49	0.57
12	DE-Hte	10.04	0.54	48.11	7.41	2.98	0.72	17.18	3.66
13	DE-SfN	8.28	0.72	3.62		0.43	0.10	0.23	24.28
14	DE-Zrk	9.55	0.51	30.53	0.96	1.18	0.24	12.27	4.07
15	FI-Hyy	4.36						1.55	0.07
16	FI-Lom	-0.35	0.78	15.58	1.83	0.93	0.22	3.75	0.51
17	FI-Si2	5.14	0.84	9.74	0.67		2.71	0.59	0.76
18	FI-Sii	4.72	0.42	12.43	3.36	0.68	0.11	3.34	0.75
19	FR-Lgt	11.07	0.37		2.45		0.02	1.09	0.85
20	HK-MPM	23.75	0.10	11.09	0.51	0.97		2.33	0.52
21	ID-Pag	26.57	0.19	0.09	0.00	0.19	0.13	0.13	0.34
22	IT-BCi	16.69	0.39		-5.18			0.22	0.05
23	IT-Cas	12.58	0.58	21.62	5.40	0.60		5.59	-0.24
24	JP-BBY	7.11	0.44	15.19	5.15	1.60	0.39	2.61	0.45
25	JP-Mse	13.75		9.50				1.59	0.42
26	JP-Swl	11.67		66.68				7.42	0.03
27	KRCRK	10.96	0.46	27.92	1.81	0.92	0.15	8.81	1.77
28	MY-MLM	27.09	0.11	9.55		3.28		0.92	1.25
29	NL-Hor	10.75	0.60					16.69	0.11
30	NZ-Kop	13.68	0.28	17.34	4.46	3.99	0.84	3.03	0.52
								3.63	0.30

31	PH-RiF	26.54	0.15	12.41	3.57	1.02	2.58	2.66	5.53	0.01	3.34	
32	RU-Ch2	-9.88	1.26	6.43	0.79	0.29	0.87	0.09	4.65	0.48	1.44	0.28
33	RU-Che	-9.77	1.25	4.09	0.22	0.37	0.00	0.47	0.08	2.18	0.12	1.19
34	RU-Cok	-12.38	0.92	4.45			0.74	0.09	3.42			0.04
35	RU-Fy2	5.80	0.53	3.50	1.88	1.65	0.58	-0.27	0.04	-0.39	0.10	2.36
36	SE-Deg	2.57	0.77	10.74	0.88	0.59	0.55	3.30	0.29	5.70	0.78	1.44
37	UK-LBT	10.62	0.78	46.54	5.61	13.70	1.77	12.52		12.26	1.66	14.04
38	US-A03	-7.15	0.66	5.81	2.06		1.27	0.19	3.25	0.32		1.87
39	US-A10								1.08			
40	US-Atq	-10.88		2.23	1.77	0.03	0.00	0.30	0.07	1.05	0.03	0.55
41	US-Beo	-9.50	0.20	2.74		0.09	0.27		1.77		0.69	0.12
42	US-Bes	-10.46	0.21	3.19	0.18	0.09	0.58	0.26	2.20	0.18	0.71	
43	US-Bi1	13.87	1.20	0.69		0.45	0.43	-0.07	0.02	-0.13	0.17	0.05
44	US-Bi2	15.01	0.28	1.28	0.59	0.66		0.30	0.21	0.10	0.06	0.54
45	US-BZB	-0.62	0.55	9.05	2.23			2.41	0.39	6.06	1.43	
46	US-BZF	-0.31	0.55	8.72	2.98			3.21	2.77	6.35	2.24	
47	US-BZS	0.26	0.68	0.78	0.15			0.23	0.01	0.53	0.11	
48	US-CRT	11.32	0.91	2.21	0.00	0.58			0.26		0.59	
49	US-DPW	22.23	0.41	48.71	8.84	1.53	1.84	11.27	2.75	27.64	7.55	12.90
50	US-EDN	14.99		-0.04				-0.19		0.16		
51	US-EML	-1.72	3.76	0.59	0.39	-0.03	0.27	0.06	0.17	0.35	0.12	0.27
52	US-Ho1	6.48	1.32	-0.16	0.09	-0.04	0.01	-0.03	0.02	-0.02	0.05	-0.07
53	US-HRA	19.36		-0.24				1.28		6.08		
54	US-HRC	20.23		-0.24				3.07		8.38		
55	US-ICs	-6.02	0.48						1.23		0.30	
56	US-Ivo	-8.27	0.54	4.90	0.95	0.70	0.02	0.80	0.05	2.55	0.54	1.26
57	US-LA1	24.12	0.42	12.68		0.68	2.27		7.58		1.39	1.08
58	US-LA2	20.34	4.43	34.81	19.34	4.27		14.50	2.18	21.72	2.75	6.96
59	US-Los	5.01	1.23	6.51	1.28		0.36	0.07	1.71	0.46	3.57	0.96
60	US-MAC	23.15	0.96	15.82	10.34	1.32	0.02	3.71	2.07	14.70	5.53	2.81
61	US-MRM	13.14	0.88	0.34	0.05	0.09		0.07	0.01	0.11	0.01	
62	US-Myb	15.53	0.58	47.88	14.90	4.51	1.99	14.12	5.54	22.04	7.87	6.52
63	US-NC4	16.74	0.85	33.89	17.41	0.80	0.18	5.70	1.62	20.41	9.80	6.77
64	US-NGB	-9.45	0.92	2.41		0.15		0.26	0.15	2.00	0.26	

65	US-NGC	1.21	0.82	2.52	0.00					0.86	0.41		
66	US-ORv	12.20	0.92	7.20	2.51	0.88	0.10	2.55	0.93	3.14	1.16	0.99	0.17
67	US-OWC	13.02	1.72	113.99				31.03		66.03	10.07	9.81	
68	US-PFa	5.42	1.24	0.54	0.25	0.15	0.05	0.39	0.19	0.00	0.00		
69	US-Snd	14.76	1.16	4.71	1.71	2.00	1.79	1.11	0.74	1.35	0.61	1.74	1.14
70	US-Sne	15.04	0.45	42.80	4.48	2.44	0.71	14.95	5.12	12.61	10.68	4.71	3.54
71	US-Srr	15.93	0.45	0.83	0.08	0.09	0.06	0.31	0.04	0.42	0.09	0.08	0.07
72	US-StJ	13.96		9.55				1.40		5.24		2.92	
73	US-Tw1	15.16	0.74	39.51	11.03	4.92	1.91	10.13	3.74	18.02	4.08	7.11	2.49
74	US-Tw3	16.04	0.87									0.29	
75	US-Tw4	15.52	0.56	32.54	11.74	4.39	1.75	9.49	4.83	12.78	6.07	5.89	1.83
76	US-Tw5	15.03		59.72				21.49		29.78		8.45	
77	US-Twt	14.26	1.71	12.07	2.75	3.07	1.10	1.05	0.59	5.49	3.15	1.73	0.40
78	US-Uaf	-2.87	1.03	0.53	0.19			0.07		0.33	0.12		
79	US-WPT	11.40	0.99	49.59	7.48	1.66	0.22	16.31	3.99	28.75	3.05	3.26	0.12

Column Descriptions

SITE_ID	Site identification code as assigned by regional flux data network
Mean_Air_Temp_C	Mean annual air temperature, calculated from flux tower variable TA_F (C)
Ann_Flux_g_CH4-C_m-2	Mean annual methane flux (g CH4-C/m2/year)
JFM_flux_g_CH4-C_m-2	Mean methane flux in January, February, March (gCH4-C/m2/year)
AMJ_flux_g_CH4-C_m-2	Mean methane flux in April, May, June (gCH4-C/m2/year)
JAS_flux_g_CH4-C_m-2	Mean methane flux in July, August, September (gCH4-C/m2/year)
OND_flux_g_CH4-C_m-2	Mean methane flux in October, November, December (gCH4-C/m2/year)
Mean_Air_Temp_stdev_C	Standard deviation of annual air temperature (C)
Ann_Flux_stdev_g_CH4-C_m-2	Standard deviation of annual methane flux (gCH4-C/m2/year)
JFM_flux_stdev_g_CH4-C_m-2	Standard deviation of methane flux in January, February, March (gCH4-C/m2/year)
AMJ_flux_stdev_g_CH4-C_m-2	Standard deviation of methane flux in April, May, June (gCH4-C/m2/year)
JAS_flux_stdev_g_CH4-C_m-2	Standard deviation of methane flux in July, August, September (gCH4-C/m2/year)
OND_flux_stdev_g_CH4-C_m-2	Standard deviation of methane flux in October, November, December (gCH4-C/m2/year)

Table B3-D: Site metadata, select data, and DOI links

SITE_ID	SOIL_TEMP_PROBE_DEPTH\$
1 AT-Neu	TS_1 = -0.05cm; TS_2 = -0.1cm; TS_3 = -0.2cm;
2 BR-Npw	
3 BW-Gum	
4 BW-Nxr	
5 CA-SCB	TS_1 = 0cm; TS_2 = -0.02cm; TS_3 = -0.04cm; TS_4 = -0.08cm; TS_5 = -0.16cm; TS_6 = -0.32cm; TS_7 = -0.64cm; TS_8 = -1.28cm;
6 CA-SCC	TS_1 = -0.1cm; TS_2 = -0.15cm; TS_3 = -0.2cm; TS_4 = -0.25cm; TS_5 = -0.3cm; TS_6 = -0.5cm; TS_7 = -0.6cm; TS_8 = -0.7cm;
7 CH-Cha	TS_1 = -0.01cm; TS_2 = -0.02cm; TS_3 = -0.04cm; TS_4 = -0.07cm; TS_5 = -0.1cm; TS_6 = -0.15cm; TS_7 = -0.25cm; TS_8 = -0.4cm; TS_9 = -0.95cm;
8 CH-Dav	TS_1 = -0.05cm; TS_2 = -0.15cm; TS_3 = -0.5cm;
9 CH-Oe2	TS_1 = -0.05cm; TS_2 = -0.1cm; TS_3 = -0.15cm; TS_4 = -0.3cm; TS_5 = -0.5cm;
10 CN-Hgu	
11 DE-Dgw	
12 DE-Hte	TS_1 = 0cm; TS_2 = -0.1cm; TS_3 = -0.2cm;
13 DE-Sfn	TS_1 = -0.02cm; TS_3 = -0.1cm; TS_4 = -0.2cm; TS_5 = -0.5cm;
14 DE-Zrk	TS_1 = -0.05cm; TS_2 = -0.1cm; TS_3 = -0.2cm; TS_4 = -0.3cm; TS_5 = -0.5cm;
15 FI-Hyy	TS_1 = -0.02cm; TS_2 = -0.04cm; TS_3 = -0.12cm; TS_4 = -0.25cm; TS_5 = -0.5cm;
16 FI-Lom	TS_1 = -0.07cm; TS_2 = -0.3cm; TS_3 = -0.5cm;
17 FI-Si2	TS_1 = -0.05cm; TS_2 = -0.2cm; TS_3 = -0.35cm; TS_4 = -0.5cm; TS_1 = -0.05cm; TS_2 = -0.2cm; TS_3 = -0.35cm; TS_4 = -0.5cm; before 2016 (TS_1 = -0.05cm; TS_2 = -0.2cm; TS_3 = -0.35cm; TS_4 = -0.5cm; TS_2 = -0.2cm; TS_3 = -0.35cm; TS_4 = -0.5cm) after 2017 (TS_1 = 0cm; TS_2 = -0.5cm; TS_3 = -0.1cm; TS_4 = -0.15cm; TS_5 = -0.25cm; TS_6 = -0.45cm; TS_7 = -0.95cm)
18 FI-Sii	
19 FR-LGt	TS_1 = -0.02cm; TS_2 = -0.05cm; TS_3 = -0.1cm; TS_4 = -0.2cm; TS_5 = -0.4cm;
20 HK-MPM	
21 ID-Pag	TS_1 = -0.05cm;
22 IT-BCI	TS_1 = -0.05cm; TS_2 = -0.1cm; TS_3 = -0.3cm; TS_4 = -0.5cm; TS_5 = -1cm;
23 IT-Cas	TS_1 = -0.05cm; TS_2 = -0.3cm; TS_3 = -0.5cm;
24 JP-BBY	TS_1 = -0.183cm; TS_2 = -0.233cm; TS_3 = -0.283cm; TS_4 = -0.383cm; TS_5 = -0.483cm;
25 JP-Mse	TS_1 = -0.01cm; TS_2 = -0.025cm; TS_3 = -0.05cm; TS_4 = -0.1cm; TS_5 = -0.2cm; TS_6 = -0.4cm;
26 JP-Swl	
27 KR-CRK	TS_1 = -0.05cm; TS_2 = -0.15cm;
28 MY-MLM	TS_1 = -0.05cm;
29 NL-Hor	TS_1 = -0.01cm; TS_2 = -0.02cm; TS_3 = -0.04cm; TS_4 = -0.05cm; TS_5 = -0.1cm; TS_6 = -0.15cm; TS_7 = -0.25cm; TS_8 = -0.4cm; TS_9 = -0.6cm;
30 NZ-Kop	TS_1 = -0.5cm; TS_2 = -0.1cm; TS_3 = -0.2cm;
31 PH-Rif	

32	RU-Ch2	TS_1 = -0.04cm; TS_2 = -0.08cm; TS_3 = -0.16cm;
33	RU-Che	TS_1 = -0.04cm; TS_2 = -0.08cm; TS_3 = -0.16cm;
34	RU-Cok	
35	RU-Fy2	
36	SE-Deg	TS_1 = -0.02cm; TS_2 = -0.1cm; TS_4 = -0.15cm; TS_5 = -0.3cm; TS_6 = -0.5cm;
37	UK-LBT	
38	US-A03	TS_1 = -0.025cm; TS_2 = -0.1cm; TS_3 = -0.3cm;
39	US-A10	TS_1 = -0.025cm; TS_2 = -0.1cm; TS_3 = -0.3cm;
40	US-Atq	
41	US-Beo	
42	US-Bes	
43	US-Bi1	TS_1 = -0.02cm; TS_2 = -0.04cm; TS_3 = -0.08cm; TS_4 = -0.16cm; TS_5 = -0.32cm;
44	US-Bi2	TS_1 = -0.02cm; TS_2 = -0.04cm; TS_3 = -0.08cm; TS_4 = -0.16cm; TS_5 = -0.32cm;
45	US-BZB	TS_1 = -0.075cm; TS_2 = -0.05cm;
46	US-BZF	TS_1 = -0.075cm; TS_2 = -0.05cm;
47	US-BZS	
48	US-CRT	
49	US-DPW	
50	US-EDN	TS_1 = -0.25cm; TS_2 = -0.15cm; TS_3 = -0.05cm; TS_4 = 0cm; TS_5 = 0.05cm; TS_6 = 0.1cm; TS_7 = 0.2cm; TS_8 = 0.3cm;
51	US-EML	TS_1 = -0.05cm; TS_2 = -0.1cm; TS_3 = -0.2cm; TS_4 = -0.4cm;
52	US-Ho1	TS_1 = -0.05cm; TS_2 = -0.1cm;
53	US-HRA	
54	US-HRC	
55	US-ICs	TS_1 = -0.075cm; TS_2 = -0.05cm;
56	US-Ivo	TS_1 = -0.05cm; TS_2 = -0.1cm; TS_3 = -0.15cm; TS_4 = -0.3cm; TS_5 = -0.4cm;
57	US-LA1	TS = -0.1cm;
58	US-LA2	TS = -0.1cm;
59	US-Los	TS_1 = 0cm; TS_2 = -0.05cm; TS_3 = -0.1cm; TS_4 = -0.2cm; TS_5 = -0.5cm;
60	US-MAC	
61	US-MRM	
62	US-Myb	TS_1 = -0.02cm; TS_2 = -0.04cm; TS_3 = -0.08cm; TS_4 = -0.16cm; TS_5 = -0.32cm;
63	US-NC4	TS_1 = -0.05cm; TS_2 = -0.2cm;
64	US-NGB	
65	US-NGC	

66	US-ORv	TS_1 = -0.08cm;
67	US-OWC	TS_1 = -0.05cm; TS_2 = -0.3cm;
68	US-PFa	TS_1 = -0.08cm; TS_2 = -0.16cm; TS_3 = nancm; TS_4 = nancm; TS_5 = nancm; TS_6 = nancm;
69	US-Snd	TS_1 = -0.08cm; TS_2 = -0.04cm; TS_3 = -0.08cm; TS_4 = -0.16cm; TS_5 = -0.32cm;
70	US-Sne	TS_1 = -0.01cm; TS_2 = -0.02cm; TS_3 = -0.08cm; TS_4 = -0.16cm; TS_5 = -0.32cm;
71	US-Srr	TS_2 = -0.05cm; TS_3 = -0.1cm;
72	US-StJ	TS_1 = -0.02cm; TS_2 = -0.04cm; TS_3 = -0.08cm; TS_4 = -0.16cm; TS_5 = -0.32cm;
73	US-Tw1	TS_1 = -0.02cm; TS_2 = -0.04cm; TS_3 = -0.08cm; TS_4 = -0.16cm; TS_5 = -0.32cm;
74	US-Tw3	TS_1 = -0.02cm; TS_2 = -0.04cm; TS_3 = -0.08cm; TS_4 = -0.16cm; TS_5 = -0.32cm;
75	US-Tw4	TS_1 = -0.02cm; TS_2 = -0.04cm; TS_3 = -0.08cm; TS_4 = -0.16cm; TS_5 = -0.32cm;
76	US-Tw5	TS_1 = -0.02cm; TS_2 = -0.1cm; TS_3 = -0.02cm; TS_4 = -0.08cm; TS_5 = -0.16cm;
77	US-Twt	TS_1 = -0.02cm; TS_2 = -0.04cm; TS_3 = -0.08cm; TS_4 = -0.16cm; TS_5 = -0.32cm;
78	US-Uaf	TS_1 = -0.09cm; TS_2 = -0.183cm; TS_3 = -0.283cm; TS_4 = -0.367cm; TS_5 = -0.5cm; TS_6 = -0.6cm; TS_7 = -0.75cm; TS_8 = -0.925cm; TS_9 = -1cm;
79	US-WPT	TS_1 = -0.1cm; TS_2 = -0.3cm;

Column Descriptions

SITE_ID Site identification code as assigned by regional flux data network

SOIL_TEMP_PROBE_DEPTHS Depth of soil temperature probe (m), with negative values being under the surface

TS_1 = -0.09cm; TS_2 = -0.183cm; TS_3 = -0.283cm; TS_4 = -0.367cm; TS_5 = -0.5cm; TS_6 = -0.6cm; TS_7 = -0.75cm; TS_8 = -0.925cm; TS_9 = -1cm;

Table B4: Bioclimatic predictor data used in the Principal Component Analysis (PCA)

	SITE_ID	Enhanced_Vegetation_Index_(EVI)	Wong_Simple_Ratio_Water_Index_(SRWI)	Latent_Heat_(LE)	Mean_Annual_Temperature_(MAT)
1	BR-Npw	0.31	0.86	87.6	25.3
2	BW-Gum	0.28	0.87	60.9	23
3	BW-Nxr	0.22	0.82	52.6	23.5
4	CA-SCB	0.16	1.2	27.4	-2.7
5	DE-Hte	0.28	1.01	40.2	8.6
6	DE-SfN	0.41	1.03	48.5	8.2
7	DE-Zrk	0.33	1.05	42.5	8.2
8	FI-Lom	0.2	1.27	23.6	-1.5
9	FI-Si2	0.27	1.12	31.6	3.3
10	FI-Sii	0.27	1.12	31.6	3.3
11	FR-LGt	0.4	0.97	50	10.8
12	ID-Pag	0.5	1.1	119.7	27.2
13	JP-BBY	0.25	1.21	45.4	6.5
14	MY-MLM	0.42	1.17	116.6	26.9
15	NZ-Kop	0.53	1.06	71.2	13.9
16	RU-Ch2	-0.01	1.25	20	-12.1
17	RU-Cok	0.04	1.18	16.8	-14.2
18	SE-Deg	0.27	1.12	29	2
19	US-A03	-0.07	1.28	16.1	-11.4
20	US-Atq	-0.1	1.31	16.9	-10.2
21	US-BZB	0.17	1.09	26	-2.8
22	US-BZF	0.17	1.09	26	-2.8
23	US-DPW	0.32	0.88	71.8	22.2
24	US-ICs	-0.04	1.3	18.5	-8.8
25	US-Ivo	-0.08	1.34	18.4	-7.7
26	US-LA2	0.37	0.98	69.9	20
27	US-Los	0.29	1.1	46.6	4
28	US-Myb	0.23	0.86	51	15.5
29	US-NC4	0.34	0.96	68.4	16.5
30	US-NGC	0.1	1.24	22.3	-3.2
31	US-ORv	0.32	0.99	50.8	10.6
32	US-OWC	0.27	1.05	55.8	9.9
33	US-Sne	0.23	0.86	51	15.5
34	US-Tw1	0.26	0.91	51	15.5
35	US-Tw4	0.26	0.91	51	15.5
36	US-Tw5	0.26	0.91	51	15.5
37	US-Uaf	0.22	1.1	25.3	-2.8
38	US-WPT	0.27	0.96	55.8	9.8

Column Descriptions

SITE_ID

Site identification code as assigned by regional flux

Enhanced_Vegetation_Index_(EVI)	Enhanced vegetation index (unitless) from MOD13A3 (Didan 2015), 2001-2018 monthly data
Wong_Simple_Ratio_Water_Index_(SR WI)	Simple Ratio Water Index (unitless) from MOD09A1 (Vermote 2015), ~2001-2018 monthly data
Latent_Heat_(LE)	Latent heat in W m-2 from FLUXCOM (Jung et al., 2019), 2003-2013 monthly data
Mean_Annual_Temperature_(MAT)	Mean annual temperature (C) from BioClim (Fick & Hijman 2017), 2001-2018 monthly data

References

- Didan, K. MOD13A3 MODIS/Terra vegetation Indices Monthly L3 Global 1km SIN Grid V006 [Data 1 set]. NASA EOSDIS Land Processes DAAC. 2015.
- Fick, S.E. & R.J. Hijmans. WorldClim 2: new 1km spatial resolution climate surfaces for global land 2 areas. International Journal of Climatology, 37(12): 4302-4315. 2017.
- Jung, M., Koirala, S., Weber, U., Ichii, K., Gans, F., Camps-Valls, G., Papale, D., Schwalm, C., Tramontana, G., & Reichstein, M. The FLUXCOM ensemble of global land-atmosphere energy fluxes. 3 Scientific Data, 6(74). doi:10.1038/s41597-019-0076-8. 2019.
- Vermote. E. MOD09A1 MODIS Surface Reflectance 8-Day L3 Global 500m SIN Grid V006. NASA 4 EOSDIS Land Processes DAAC. <http://doi.org/10.5067/MODIS/MOD09A1.006> (Terra). 2015.

Table B5-A Timesat output for FCH4, GPP_DT, TA, and TS (TS from shallowest probe at each site)

SITE_ID	Year	Start_FCH4_(DOY)	End_FCH4_(DOY)	Base_value_FCH4_(nmolC/m2/s)	Ampl_FCH4_(n molCH4/m2/s)	Peak_FCH4_(DOY)	Peak_value_FCH4_(nmolCH4/m2/s)
1	AT-Neu	2010	NaN	NaN	NaN	NaN	NaN
2	AT-Neu	2011	NaN	NaN	NaN	NaN	NaN
3	AT-Neu	2012	NaN	NaN	NaN	NaN	NaN
4	BR-Npw	2014	NaN	NaN	NaN	NaN	NaN
5	BR-Npw	2015	NaN	NaN	NaN	NaN	NaN
6	BR-Npw	2016	192.7	345.8	-2.0	154.8	270.0
7	BW-Gum	2018	34.1	151.1	132.9	186.2	89.0
8	BW-Gum	2019	230.4	NaN	134.2	202.1	281.9
9	BW-Nxr	2018	65.1	NaN	29.2	208.7	287.5
10	CA-SCB	2014	138.8	299.1	17.5	72.3	222.4
11	CA-SCB	2015	NaN	NaN	NaN	NaN	NaN
12	CA-SCB	2016	109.2	290.4	11.8	82.0	207.9
13	CA-SCB	2017	119.0	300.4	14.0	58.9	221.5
14	CA-SCC	2013	NaN	NaN	NaN	203.4	44.8
15	CA-SCC	2014	128.4	313.1	3.1	40.1	215.0
16	CA-SCC	2015	98.0	303.9	1.7	54.6	210.9
17	CA-SCC	2016	102.7	NaN	1.7	NaN	208.0
18	DE-Dgw	2015	NaN	NaN	NaN	NaN	43.3
19	DE-Dgw	2016	NaN	NaN	NaN	NaN	56.3
20	DE-Dgw	2017	NaN	NaN	NaN	NaN	59.6
21	DE-Hte	2011	NaN	NaN	NaN	NaN	NaN
22	DE-Hte	2012	82.6	330.1	20.3	201.8	205.5
23	DE-Hte	2013	101.9	NaN	29.9	NaN	222.1
24	DE-Hte	2014	NaN	338.5	38.3	NaN	378.7
25	DE-Hte	2015	75.1	322.4	29.2	277.7	202.0
26	DE-Hte	2016	83.9	289.7	21.5	347.8	202.0
27	DE-Hte	2017	90.0	304.5	18.3	272.7	194.0
28	DE-Hte	2018	85.6	258.1	21.0	322.0	196.0
29	DE-Sfn	2012	79.6	340.7	4.3	10.2	217.0

30	DE-SfN	2013	Nan	2.7	3.0	301.9
31	DE-SfN	2014	Nan	Nan	Nan	Nan
32	DE-Zrk	2013	Nan	Nan	Nan	Nan
33	DE-Zrk	2014	Nan	Nan	Nan	Nan
34	DE-Zrk	2015	87.0	273.0	9.3	242.5
35	DE-Zrk	2016	107.9	274.0	9.9	224.2
36	DE-Zrk	2017	110.0	270.1	11.2	203.6
37	DE-Zrk	2018	88.1	261.0	8.5	250.8
38	Fl-Lom	2006	142.8	288.8	7.8	111.0
39	Fl-Lom	2007	139.3	270.6	10.9	165.0
40	Fl-Lom	2008	134.0	284.8	10.8	127.7
41	Fl-Lom	2009	121.5	291.0	12.1	132.3
42	Fl-Lom	2010	137.1	282.8	13.4	101.6
43	Fl-Si2	2012	Nan	Nan	Nan	220.6
44	Fl-Si2	2013	Nan	Nan	Nan	211.1
45	Fl-Si2	2014	Nan	280.7	7.2	212.8
46	Fl-Si2	2015	Nan	309.5	9.5	212.0
47	Fl-Si2	2016	Nan	Nan	Nan	Nan
48	Fl-Sii	2013	123.8	307.6	7.2	104.3
49	Fl-Sii	2014	118.8	Nan	2.3	NaN
50	Fl-Sii	2015	Nan	Nan	Nan	215.1
51	Fl-Sii	2016	114.5	311.3	8.9	121.1
52	Fl-Sii	2017	118.9	300.4	6.5	57.1
53	Fl-Sii	2018	116.3	295.1	7.5	53.8
54	HK-MPM	2016	Nan	Nan	Nan	Nan
55	HK-MPM	2017	Nan	Nan	Nan	Nan
56	HK-MPM	2018	Nan	Nan	Nan	Nan
57	ID-Pag	2016	274.1	Nan	-2.8	5.1
58	JP-BBY	2015	166.7	Nan	18.3	NaN
59	JP-BBY	2016	Nan	324.9	18.3	105.7
60	JP-BBY	2017	138.5	323.1	15.2	130.1
61	JP-BBY	2018	Nan	332.1	17.8	74.7
62	JP-Mse	2012	Nan	Nan	Nan	Nan
63	KR-CRK	2015	Nan	Nan	Nan	Nan

64	KR-CRK	2016	NaN	NaN	NaN	NaN	NaN	NaN
65	KR-CRK	2017	NaN	NaN	NaN	NaN	NaN	NaN
66	KR-CRK	2018	NaN	NaN	NaN	NaN	NaN	NaN
67	MY-MLM	2014	229.6	562.4	15.5	19.8	64.2	35.3
68	MY-MLM	2015	NaN	NaN	NaN	NaN	NaN	NaN
69	NZ-Kop	2012	-94.5	227.6	36.9	28.3	176.2	65.2
70	NZ-Kop	2013	7.2	251.5	21.1	61.7	182.0	82.8
71	NZ-Kop	2014	10.0	228.4	22.6	42.7	161.0	65.2
72	NZ-Kop	2015	-8.5	NaN	23.0	34.7	150.0	57.8
73	PH-Rif	2012	154.2	303.9	4.0	62.9	239.1	66.9
74	PH-Rif	2013	304.1	455.0	5.3	54.0	380.3	59.3
75	PH-Rif	2014	133.9	265.7	6.1	121.8	178.3	127.9
76	PH-Rif	2015	NaN	NaN	3.8	56.3	NaN	60.1
77	RU-Ch2	2014	150.8	312.2	0.7	70.2	216.5	70.9
78	RU-Ch2	2015	153.3	NaN	8.0	NaN	209.0	56.1
79	RU-Ch2	2016	NaN	NaN	NaN	NaN	218.8	68.3
80	RU-Che	2014	NaN	NaN	NaN	NaN	NaN	NaN
81	RU-Che	2015	NaN	NaN	NaN	NaN	NaN	NaN
82	RU-Che	2016	NaN	NaN	NaN	NaN	NaN	NaN
83	SE-Deg	2014	NaN	NaN	NaN	80.8	204.2	91.7
84	SE-Deg	2015	103.3	318.7	5.1	73.7	211.3	78.8
85	SE-Deg	2016	102.5	324.1	4.3	74.3	205.3	78.7
86	SE-Deg	2017	NaN	NaN	NaN	NaN	NaN	NaN
87	SE-Deg	2018	117.2	327.6	6.9	50.9	192.0	57.8
88	US-Atq	2013	NaN	NaN	NaN	NaN	NaN	NaN
89	US-Atq	2014	145.7	328.7	0.9	13.2	215.0	14.1
90	US-Atq	2015	153.3	264.0	1.0	18.6	193.2	19.6
91	US-Beo	2013	NaN	NaN	NaN	NaN	NaN	NaN
92	US-Beo	2014	157.0	356.3	0.4	23.0	211.4	23.4
93	US-Bes	2013	NaN	NaN	NaN	NaN	NaN	NaN
94	US-Bes	2014	157.3	312.6	0.6	34.3	206.5	34.9
95	US-Bes	2015	146.8	283.8	0.6	35.0	193.1	35.7
96	US-BzB	2014	NaN	NaN	NaN	NaN	226.9	67.5
97	US-BzB	2015	NaN	NaN	NaN	NaN	219.4	68.4

98	US-BZB	2016	NaN	NaN	NaN	98.4
99	US-BZF	2014	NaN	NaN	NaN	57.7
100	US-BZF	2015	NaN	NaN	NaN	87.0
101	US-BZF	2016	NaN	NaN	NaN	119.1
102	US-BZS	2015	NaN	NaN	NaN	NaN
103	US-BZS	2016	NaN	NaN	NaN	NaN
104	US-DPW	2013	151.7	364.0	16.4	395.0
105	US-DPW	2014	98.9	332.5	34.5	338.0
106	US-DPW	2015	NaN	376.3	25.0	240.7
107	US-DPW	2016	84.2	389.2	23.5	248.6
108	US-HRA	2017	NaN	NaN	184.3	237.0
109	US-HRC	2018	NaN	NaN	NaN	207.8
110	US-ICs	2014	NaN	NaN	NaN	411.4
111	US-ICs	2015	NaN	NaN	NaN	372.4
112	US-ICs	2016	138.2	302.1	0.2	247.3
113	US-Ivo	2013	NaN	400.0	1.9	240.7
114	US-Ivo	2014	158.5	301.8	6.7	228.9
115	US-Ivo	2015	156.8	278.0	6.9	248.6
116	US-Ivo	2016	164.7	352.4	6.1	237.0
117	US-LA1	2012	NaN	NaN	NaN	207.8
118	US-LA2	2012	62.8	NaN	NaN	411.4
119	US-LA2	2013	NaN	NaN	NaN	372.4
120	US-Los	2014	127.1	309.8	4.0	247.3
121	US-Los	2015	143.4	324.4	3.2	248.6
122	US-Los	2016	143.8	310.1	3.3	237.0
123	US-Los	2017	134.1	255.2	3.6	207.8
124	US-Los	2018	143.0	288.8	3.0	240.7
125	US-MAC	2013	NaN	NaN	NaN	304.3
126	US-MAC	2014	NaN	NaN	NaN	192.5
127	US-MAC	2015	NaN	NaN	NaN	385.5
128	US-Myb	2010	NaN	NaN	NaN	220.2
129	US-Myb	2011	72.4	369.3	18.3	174.2
130	US-Myb	2012	97.2	345.3	18.9	214.7
131	US-Myb	2013	46.8	336.3	39.0	265.4

132	US-Myb	2014	57.4	334.7	37.1	276.9	206.0	314.0
133	US-Myb	2015	23.7	330.0	21.6	285.7	201.0	307.3
134	US-Myb	2016	36.9	306.0	21.9	216.0	191.0	237.9
135	US-Myb	2017	175.8	332.2	30.5	191.7	235.0	222.2
136	US-Myb	2018	33.1	322.6	28.8	99.3	169.0	128.1
137	US-NC4	2012	132.9	307.9	9.5	323.8	232.2	333.3
138	US-NC4	2013	97.2	365.1	4.3	113.3	240.7	117.5
139	US-NC4	2014	110.6	332.3	-0.1	181.8	253.9	181.6
140	US-NC4	2015	68.4	414.1	-0.8	122.5	245.0	121.7
141	US-NC4	2016	128.4	350.6	2.7	373.6	259.0	376.2
142	US-Orv	2011	NaN	297.3	7.3	15.2	178.5	22.4
143	US-Orv	2012	120.1	269.1	8.3	65.2	189.7	73.4
144	US-Orv	2013	72.4	308.4	9.0	27.4	189.4	36.4
145	US-Orv	2014	87.6	292.2	9.1	32.4	201.0	41.5
146	US-Orv	2015	86.0	NaN	8.9	38.5	170.0	47.4
147	US-Owc	2015	NaN	NaN	NaN	NaN	NaN	NaN
148	US-Owc	2016	NaN	NaN	NaN	NaN	219.2	882.8
149	US-Sne	2016	NaN	NaN	NaN	NaN	NaN	NaN
150	US-Sne	2017	76.2	337.1	14.9	244.2	187.8	259.0
151	US-Sne	2018	60.6	341.6	21.4	168.3	222.6	189.8
152	US-Srr	2014	NaN	NaN	NaN	NaN	NaN	NaN
153	US-Srr	2015	NaN	NaN	NaN	NaN	NaN	NaN
154	US-Srr	2016	NaN	NaN	NaN	NaN	NaN	NaN
155	US-Srr	2017	NaN	NaN	NaN	NaN	NaN	NaN
156	US-Stj	2016	NaN	NaN	NaN	NaN	NaN	NaN
157	US-Tw1	2011	140.5	352.4	36.3	104.5	233.8	140.8
158	US-Tw1	2012	NaN	309.6	28.1	243.5	242.9	271.6
159	US-Tw1	2013	33.4	307.1	42.2	114.3	218.0	156.5
160	US-Tw1	2014	174.6	331.5	65.3	253.2	240.0	318.5
161	US-Tw1	2015	62.3	330.3	63.8	204.1	207.0	267.9
162	US-Tw1	2016	32.3	323.8	48.5	160.0	221.0	208.5
163	US-Tw1	2017	27.8	305.0	43.1	138.1	226.0	181.1
164	US-Tw1	2018	155.0	314.9	38.7	127.5	228.0	166.3
165	US-Tw4	2014	93.8	461.3	27.4	36.5	226.8	63.8

166	US-Tw4	2015	114.5	334.1	39.8	86.5	228.2
167	US-Tw4	2016	42.8	357.1	43.2	101.8	215.6
168	US-Tw4	2017	110.7	318.8	55.1	201.2	222.0
169	US-Tw4	2018	63.0	237.3	53.0	165.1	173.0
170	US-Tw5	2018	NaN	331.9	26.5	339.3	196.9
171	US-Twt	2009	NaN	NaN	NaN	NaN	NaN
172	US-Twt	2010	NaN	NaN	NaN	NaN	NaN
173	US-Twt	2011	NaN	NaN	NaN	NaN	NaN
174	US-Twt	2012	NaN	NaN	NaN	NaN	NaN
175	US-Twt	2013	NaN	NaN	NaN	NaN	NaN
176	US-Twt	2014	NaN	NaN	NaN	NaN	NaN
177	US-Twt	2015	NaN	NaN	NaN	NaN	NaN
178	US-Twt	2016	NaN	NaN	NaN	NaN	NaN
179	US-Uaf	2011	157.6	NaN	0.8	2.1	242.0
180	US-Uaf	2012	151.8	NaN	0.7	1.6	265.9
181	US-Uaf	2013	167.0	NaN	0.8	1.4	267.0
182	US-Uaf	2014	182.2	NaN	0.9	3.2	247.0
183	US-Uaf	2015	176.0	NaN	0.8	3.5	245.0
184	US-Uaf	2016	184.7	NaN	0.9	7.3	248.0
185	US-Uaf	2017	182.0	NaN	0.9	6.0	248.0
186	US-Uaf	2018	158.5	NaN	0.9	4.9	250.0
187	US-WPT	2011	103.5	294.1	5.6	355.3	207.1
188	US-WPT	2012	90.0	296.5	9.0	380.5	195.6
189	US-WPT	2013	72.5	297.0	7.5	343.3	220.0

Column Descriptions

SITE_ID
 Year
 Start_FCH4_(DOY)
 End_FCH4_(DOY)
 Base_value_FCH4_(nmolCH4/m2/s)

Site identification code as assigned by regional flux data network

Data year

Season start for elevated methane fluxes (DOY), point "f" in Figure 1

Season end for elevated methane fluxes (DOY), point "h" in Figure 1

Baseline methane flux during non-elevated season (nmol CH4/m2/s), average of points "a" and "b" in Figure 1

Amp1_FCH4_(nmolCH4/m2/s)

Amplitude of methane flux during elevated flux season (nmol CH4/m2/s), difference between point "e" in Figure 1 and Base_value_FCH4

Peak_FCH4_(DOY)

Day of maximum elevated methane flux (DOY), point "g" in Figure 1
Maximum value of methane flux (nmol CH4/m2/s), point "e" in Figure 1

Peak_value_FCH4_(nmolCH4/m2/s)

Table B5-B Timesat output for FCH4, GPP_DT, TA, and TS (TS from shallowest probe at each site)

SITE_ID	Year	Start_GPP_D T_(DOY)	End_GPP_D DT_(DOY)	Base_value_G PP_DT_(μmol CO2/m2/s)	Ampl_GPP_D T_(μmolCO2/ m2/s)	Peak_GPP_D T_(DOY)	Peak_value_G PP_DT_(μmol CO2/m2/s)
1	AT-Neu	2010	61.39	332.24	-0.22	9.75	175.90
2	AT-Neu	2011	76.71	303.74	0.18	11.36	167.90
3	AT-Neu	2012	84.67	305.48	0.29	9.75	179.00
4	BR-Npw	2014	59.47	367.83	2.03	5.10	242.90
5	BR-Npw	2015	61.54	385.15	2.05	5.15	228.00
6	BR-Npw	2016	83.78	375.61	2.44	4.74	203.00
7	BW-Gum	2018	NaN	NaN	NaN	NaN	NaN
8	BW-Gum	2019	NaN	NaN	NaN	NaN	NaN
9	BW-Nxr	2018	NaN	NaN	NaN	NaN	NaN
10	CA-SCB	2014	127.53	266.07	0.10	2.69	210.00
11	CA-SCB	2015	60.15	275.15	0.10	3.35	199.40
12	CA-SCB	2016	123.04	277.07	0.05	3.66	191.90
13	CA-SCB	2017	113.78	274.63	0.04	2.99	202.00
14	CA-SCC	2013	126.43	273.72	0.20	3.21	198.80
15	CA-SCC	2014	130.06	269.31	0.30	3.22	194.30
16	CA-SCC	2015	104.41	269.97	0.28	4.54	196.90
17	CA-SCC	2016	106.89	284.75	0.09	3.67	191.00
18	DE-Dgw	2015	13.43	348.62	0.04	0.40	227.30
19	DE-Dgw	2016	31.35	294.27	0.04	0.49	167.60
20	DE-Dgw	2017	80.56	293.50	0.04	0.46	191.00
21	DE-Hte	2011	111.70	280.46	0.05	6.87	170.10
22	DE-Hte	2012	122.64	296.52	0.31	7.11	200.10
23	DE-Hte	2013	133.51	293.97	0.29	6.10	206.40
24	DE-Hte	2014	37.51	277.70	0.27	5.50	160.00
25	DE-Hte	2015	127.82	303.30	0.27	5.35	191.00
26	DE-Hte	2016	117.96	328.49	0.16	5.39	184.00
27	DE-Hte	2017	123.83	301.59	0.11	5.71	177.00
28	DE-Hte	2018	121.03	334.06	0.06	6.99	190.00
29	DE-SfN	2012	-13.79	320.94	0.37	4.34	168.10

30	DE-SfN	2013	64.35	316.65	0.31	3.96	198.00	4.27
31	DE-SfN	2014	43.97	335.84	0.41	4.10	193.00	4.51
32	DE-Zrk	2013	110.23	283.50	0.09	4.30	186.30	4.39
33	DE-Zrk	2014	86.61	309.76	0.06	3.56	180.40	3.62
34	DE-Zrk	2015	99.44	264.19	0.10	3.54	186.60	3.64
35	DE-Zrk	2016	90.31	301.90	0.13	4.38	218.00	4.51
36	DE-Zrk	2017	92.93	303.86	0.11	4.07	180.00	4.18
37	DE-Zrk	2018	105.21	314.58	0.06	6.90	212.00	6.96
38	Fl-Lom	2006	147.75	261.40	0.06	5.89	197.40	5.95
39	Fl-Lom	2007	145.82	257.55	0.06	6.36	197.90	6.43
40	Fl-Lom	2008	151.61	258.87	0.06	7.24	200.00	7.30
41	Fl-Lom	2009	147.57	262.55	0.02	6.55	197.00	6.57
42	Fl-Lom	2010	153.94	262.64	0.03	6.39	199.00	6.41
43	Fl-Si2	2012	33.66	276.85	0.07	1.52	209.00	1.59
44	Fl-Si2	2013	106.78	338.07	0.13	1.63	182.90	1.76
45	Fl-Si2	2014	40.93	290.00	0.13	2.19	146.00	2.32
46	Fl-Si2	2015	113.24	267.77	0.13	1.93	197.00	2.06
47	Fl-Si2	2016	43.90	284.85	0.13	1.85	166.00	1.98
48	Fl-Sii	2013	118.98	282.46	-0.03	3.70	185.70	3.67
49	Fl-Sii	2014	100.30	294.41	0.00	2.43	199.70	2.44
50	Fl-Sii	2015	84.64	321.89	0.06	2.63	204.30	2.69
51	Fl-Sii	2016	118.70	284.09	0.09	3.43	200.00	3.52
52	Fl-Sii	2017	117.46	290.52	0.05	3.04	206.00	3.09
53	Fl-Sii	2018	113.63	295.59	0.04	2.32	185.00	2.36
54	HK-MPM	2016	NaN	NaN	NaN	NaN	NaN	NaN
55	HK-MPM	2017	NaN	NaN	NaN	NaN	NaN	NaN
56	HK-MPM	2018	NaN	NaN	NaN	NaN	NaN	NaN
57	ID-Pag	2016	NaN	NaN	NaN	NaN	NaN	NaN
58	JP-BBY	2015	123.64	304.32	0.23	5.32	203.40	5.56
59	JP-BBY	2016	114.13	302.43	0.03	7.94	203.20	7.98
60	JP-BBY	2017	119.90	300.38	0.03	7.58	199.80	7.61
61	JP-BBY	2018	96.26	311.58	0.01	5.44	217.00	5.45
62	JP-Mse	2012	144.63	266.88	0.63	9.81	209.70	10.44
63	KR-CRK	2015	134.99	267.83	0.10	10.68	202.10	10.78

64	KR-CRK	2016	137.21	262.37	0.06	12.44	198.80	12.50
65	KR-CRK	2017	143.28	266.25	0.13	12.20	193.50	12.33
66	KR-CRK	2018	138.97	263.80	0.17	10.96	198.00	11.13
67	MY-MLM	2014	179.97	437.86	8.48	2.67	272.60	11.16
68	MY-MLM	2015	194.24	NaN	8.76	8.31	271.10	17.07
69	NZ-Kop	2012	38.67	334.88	1.33	2.50	194.80	3.83
70	NZ-Kop	2013	58.12	351.65	1.50	2.61	190.00	4.10
71	NZ-Kop	2014	42.25	355.00	1.41	2.78	209.00	4.18
72	NZ-Kop	2015	44.32	366.21	1.19	3.28	193.00	4.47
73	PH-Rif	2012	NaN	NaN	NaN	NaN	NaN	NaN
74	PH-Rif	2013	NaN	NaN	NaN	NaN	NaN	NaN
75	PH-Rif	2014	NaN	NaN	NaN	NaN	NaN	NaN
76	PH-Rif	2015	NaN	NaN	NaN	NaN	NaN	NaN
77	RU-Ch2	2014	142.91	252.79	0.02	5.10	210.30	5.11
78	RU-Ch2	2015	157.47	247.95	-0.02	5.00	202.60	4.97
79	RU-Ch2	2016	145.27	257.90	-0.04	4.15	201.50	4.11
80	RU-Che	2014	161.74	258.77	0.14	5.51	206.90	5.65
81	RU-Che	2015	157.04	250.25	0.01	5.39	203.30	5.40
82	RU-Che	2016	140.55	258.30	-0.10	6.94	188.60	6.84
83	SE-Deg	2014	115.38	285.94	0.02	2.78	196.30	2.79
84	SE-Deg	2015	113.50	278.71	0.02	2.69	203.40	2.70
85	SE-Deg	2016	118.80	290.27	0.02	2.32	195.50	2.35
86	SE-Deg	2017	121.86	276.14	0.02	2.45	199.00	2.47
87	SE-Deg	2018	118.54	276.63	0.00	1.72	188.00	1.72
88	US-Atq	2013	33.24	256.46	0.03	3.05	161.70	3.09
89	US-Atq	2014	139.11	244.88	0.09	1.77	194.30	1.86
90	US-Atq	2015	132.75	243.97	0.08	3.41	191.00	3.48
91	US-Beo	2013	39.33	285.28	0.01	0.88	159.80	0.88
92	US-Beo	2014	88.23	261.54	0.02	1.99	200.00	2.02
93	US-Bes	2013	49.45	269.44	0.04	0.84	187.90	0.87
94	US-Bes	2014	174.64	262.25	0.04	1.60	220.70	1.64
95	US-Bes	2015	160.53	248.82	0.04	2.53	198.40	2.57
96	US-BZB	2014	NaN	NaN	NaN	NaN	NaN	NaN
97	US-BZB	2015	NaN	NaN	NaN	NaN	NaN	NaN

98	US-BZB	2016	NaN	NaN	NaN	NaN	NaN	NaN	NaN
99	US-BZF	2014	132.71	201.27	0.18	5.84	167.50	6.01	
100	US-BZF	2015	129.12	258.65	0.16	6.93	187.50	7.10	
101	US-BZF	2016	128.63	227.99	0.18	9.14	175.00	9.32	
102	US-BZS	2015	NaN	NaN	NaN	NaN	NaN	NaN	
103	US-BZS	2016	NaN	NaN	NaN	NaN	NaN	NaN	
104	US-DPW	2013	NaN	NaN	NaN	NaN	NaN	NaN	
105	US-DPW	2014	55.72	332.08	0.65	4.60	183.50	5.24	
106	US-DPW	2015	53.69	372.93	0.73	4.77	174.80	5.50	
107	US-DPW	2016	71.21	343.87	0.85	4.83	197.00	5.68	
108	US-HRA	2017	131.27	244.82	0.39	20.14	183.10	20.53	
109	US-HRC	2018	135.69	237.65	1.34	18.79	182.20	20.13	
110	US-ICs	2014	150.35	253.40	0.21	3.46	201.60	3.66	
111	US-ICs	2015	142.83	263.16	0.15	4.42	189.90	4.57	
112	US-ICs	2016	154.39	245.71	0.12	3.22	192.80	3.34	
113	US-Ivo	2013	149.10	257.98	0.06	3.85	201.90	3.91	
114	US-Ivo	2014	151.63	257.85	0.11	3.63	199.10	3.73	
115	US-Ivo	2015	121.66	248.35	0.07	3.97	187.10	4.03	
116	US-Ivo	2016	154.70	254.51	0.09	5.30	194.00	5.39	
117	US-LA1	2012	-7.96	216.91	0.49	2.29	142.80	2.78	
118	US-LA2	2012	46.97	334.04	0.34	5.64	146.80	5.98	
119	US-LA2	2013	93.73	335.84	0.31	6.94	166.30	7.25	
120	US-Los	2014	131.45	288.06	-0.01	6.65	198.20	6.64	
121	US-Los	2015	130.36	288.12	0.11	6.26	201.50	6.37	
122	US-Los	2016	130.87	291.48	0.17	7.17	198.20	7.33	
123	US-Los	2017	136.00	292.41	0.13	7.38	199.00	7.51	
124	US-Los	2018	134.97	285.61	0.13	7.17	199.00	7.29	
125	US-MAC	2013	NaN	378.12	2.50	5.43	222.70	9.45	
126	US-MAC	2014	47.02	334.19	2.51	9.17	180.70	11.68	
127	US-MAC	2015	46.53	356.65	2.92	5.92	154.10	8.84	
128	US-Myb	2010	28.65	305.24	0.56	1.41	183.40	1.97	
129	US-Myb	2011	200.41	367.27	0.28	3.62	265.50	3.89	
130	US-Myb	2012	88.45	331.93	-0.06	13.68	204.50	13.62	
131	US-Myb	2013	47.39	341.89	-0.12	7.95	200.00	7.83	

132	US-Myb	2014	86.80	310.73	0.16	168.00	8.36
133	US-Myb	2015	76.10	323.19	0.17	7.31	7.47
134	US-Myb	2016	24.11	328.43	0.00	4.03	4.03
135	US-Myb	2017	67.46	395.16	-0.24	5.79	5.55
136	US-Myb	2018	83.66	331.31	-0.25	10.50	10.25
137	US-NC4	2012	NaN	NaN	NaN	NaN	NaN
138	US-NC4	2013	94.35	304.81	0.78	6.97	181.00
139	US-NC4	2014	97.51	354.46	0.64	6.09	173.70
140	US-NC4	2015	92.03	315.08	0.74	9.73	185.00
141	US-NC4	2016	99.57	326.98	0.92	8.22	183.00
142	US-Orv	2011	88.77	316.45	-0.06	7.39	180.40
143	US-Orv	2012	93.50	303.39	0.27	9.29	181.00
144	US-Orv	2013	107.62	305.23	0.36	10.11	192.40
145	US-Orv	2014	109.31	299.17	0.24	10.14	190.00
146	US-Orv	2015	105.01	301.56	0.27	9.64	194.00
147	US-Owc	2015	NaN	301.35	0.26	6.72	151.30
148	US-Owc	2016	116.05	309.20	0.30	6.44	204.00
149	US-Sne	2016	-21.79	306.16	0.34	7.99	190.30
150	US-Sne	2017	NaN	NaN	NaN	NaN	NaN
151	US-Sne	2018	84.63	370.31	0.32	2.43	202.00
152	US-Srr	2014	47.02	307.53	0.78	6.04	175.60
153	US-Srr	2015	35.50	320.88	0.33	7.96	158.60
154	US-Srr	2016	44.76	318.87	0.38	8.86	170.80
155	US-Srr	2017	56.75	309.79	0.30	10.46	185.00
156	US-StJ	2016	120.72	280.75	1.30	12.01	193.80
157	US-Tw1	2011	NaN	NaN	NaN	NaN	NaN
158	US-Tw1	2012	102.12	325.54	0.00	12.83	216.10
159	US-Tw1	2013	98.35	338.02	-0.18	13.11	208.40
160	US-Tw1	2014	95.66	326.27	0.12	10.46	208.00
161	US-Tw1	2015	105.53	344.13	0.26	9.88	215.00
162	US-Tw1	2016	91.82	313.13	-0.01	10.10	209.00
163	US-Tw1	2017	93.36	329.76	-0.04	11.26	214.00
164	US-Tw1	2018	119.04	363.78	-0.02	12.73	217.00
165	US-Tw4	2014	160.04	363.23	0.00	4.70	236.60

SITE_ID	Year	Start_GPP_DT_(DOY)	End_GPP_DT_(DOY)	Base_value_GPP_DT_(μmolCO2/m2/s)
166	US-Tw4	2015	57.22	335.89
167	US-Tw4	2016	76.15	311.33
168	US-Tw4	2017	100.19	332.90
169	US-Tw4	2018	98.39	337.78
170	US-Tw5	2018	115.94	321.33
171	US-Twt	2009	149.98	293.01
172	US-Twt	2010	141.10	311.91
173	US-Twt	2011	158.51	288.69
174	US-Twt	2012	166.84	308.78
175	US-Twt	2013	138.24	272.38
176	US-Twt	2014	148.14	281.40
177	US-Twt	2015	137.11	277.23
178	US-Twt	2016	169.14	289.90
179	US-Uaf	2011	114.56	283.49
180	US-Uaf	2012	88.03	271.24
181	US-Uaf	2013	124.13	271.61
182	US-Uaf	2014	84.63	269.30
183	US-Uaf	2015	90.52	264.29
184	US-Uaf	2016	103.06	270.75
185	US-Uaf	2017	102.29	275.58
186	US-Uaf	2018	111.65	291.46
187	US-WPT	2011	134.98	285.59
188	US-WPT	2012	129.04	293.67
189	US-WPT	2013	134.87	278.12

Column Descriptions

SITE_ID	Site identification code as assigned by regional flux data network
Year	Data year
Start_GPP_DT_(DOY)	Season start for elevated GPP_DT (DOY), point "f" in Figure 1
End_GPP_DT_(DOY)	Season end for elevated GPP_DT fluxes (DOY), point "h" in Figure 1
Base_value_GPP_DT_(μmolCO2/m2/s)	Baseline GPP_DT flux during non-elevated season (μmol CO2/m2/s), average of points "a" and "b" in Figure 1

Amp1_GPP_DT_(μmolCO₂/m²/s)

Amplitude of GPP_DT flux during elevated flux season (μmol CO₂/m²/s), difference between point "e" in Figure 1 and Base_value_GPP_DT

Peak_GPP_DT_(DOY)
Peak_value_GPP_DT_(μmolCO₂/m²/s)

Day of maximum elevated GPP_DT flux (DOY), point "g" in Figure 1
Maximum value of GPP_DT flux (μmol CO₂/m²/s), point "e" in Figure 1

Table B5-C Timesat output for FCH4, GPP_DT, TA, and TS (TS from shallowest probe at each site)

SITE_ID	Year	Start_TA_(DOY)	End_TA_(DOY)	Base_value_TA_(C)	Amp_TA_(C)	Peak_TA_(DOY)	Peak_value_TA_(C)
1	AT-Neu	2010	43.17	351.66	-4.84	20.94	195.90
2	AT-Neu	2011	18.47	359.91	-5.08	20.55	198.50
3	AT-Neu	2012	38.03	366.62	-5.57	22.35	197.20
4	BR-Npw	2014	NaN	NaN	NaN	NaN	NaN
5	BR-Npw	2015	NaN	NaN	NaN	NaN	NaN
6	BR-Npw	2016	7.49	348.67	19.56	7.53	211.00
7	BW-Gum	2018	NaN	NaN	NaN	NaN	NaN
8	BW-Gum	2019	NaN	NaN	NaN	NaN	NaN
9	BW-Nxr	2018	NaN	NaN	NaN	NaN	NaN
10	CA-SCB	2014	60.23	335.31	-23.33	41.29	197.40
11	CA-SCB	2015	45.11	360.83	-21.75	39.11	186.40
12	CA-SCB	2016	49.77	335.79	-18.88	37.28	193.90
13	CA-SCB	2017	64.68	327.30	-18.45	35.95	201.00
14	CA-SCC	2013	67.57	338.23	-21.08	39.13	203.80
15	CA-SCC	2014	54.14	337.83	-22.27	40.98	196.70
16	CA-SCC	2015	46.41	359.38	-20.09	37.86	187.10
17	CA-SCC	2016	47.31	350.23	-18.76	37.65	194.00
18	DE-Dgw	2015	72.47	347.56	2.18	16.25	203.80
19	DE-Dgw	2016	64.46	324.69	1.34	17.37	205.40
20	DE-Dgw	2017	43.79	375.32	-0.17	18.47	202.20
21	DE-Hte	2011	NaN	NaN	NaN	NaN	NaN
22	DE-Hte	2012	50.34	352.49	0.77	17.03	207.60
23	DE-Hte	2013	83.53	365.30	1.64	17.09	202.50
24	DE-Hte	2014	48.71	352.47	2.86	15.82	213.00
25	DE-Hte	2015	57.62	366.35	2.59	15.33	211.00
26	DE-Hte	2016	67.53	323.10	2.75	16.01	211.00
27	DE-Hte	2017	58.94	370.07	1.81	16.22	212.00
28	DE-Hte	2018	74.55	368.02	0.91	19.14	203.00
29	DE-Sfn	2012	54.86	355.18	-2.09	20.25	196.30
30	DE-Sfn	2013	64.64	344.04	-0.35	18.57	202.80
31	DE-Sfn	2014	NaN	NaN	NaN	NaN	NaN

32	DE-Zrk	2013	NaN	NaN	NaN	NaN	NaN	NaN	NaN	NaN	NaN	NaN
33	DE-Zrk	2014	NaN	NaN	NaN	NaN	NaN	NaN	NaN	NaN	NaN	NaN
34	DE-Zrk	2015	49.71	355.39	2.13	15.33	203.40	17.46				
35	DE-Zrk	2016	63.30	323.76	1.85	16.45	204.00	18.31				
36	DE-Zrk	2017	45.25	372.48	0.47	17.44	205.00	17.91				
37	DE-Zrk	2018	75.77	358.90	-0.10	18.78	190.00	18.68				
38	Fl-Lom	2006	72.49	355.63	-12.19	26.67	195.00	14.48				
39	Fl-Lom	2007	56.24	372.50	-11.01	22.60	193.40	11.59				
40	Fl-Lom	2008	73.45	348.05	-10.36	22.30	200.40	11.95				
41	Fl-Lom	2009	56.72	356.29	-13.61	27.09	205.00	13.48				
42	Fl-Lom	2010	54.81	346.00	-16.10	27.81	200.00	11.71				
43	Fl-Si2	2012	70.38	349.74	-6.91	22.72	199.10	15.81				
44	Fl-Si2	2013	88.15	369.48	-5.99	23.74	188.60	17.76				
45	Fl-Si2	2014	53.29	350.42	-4.39	21.50	200.30	17.11				
46	Fl-Si2	2015	39.64	359.19	-5.00	19.39	212.00	14.39				
47	Fl-Si2	2016	42.62	345.02	-6.72	23.17	199.00	16.45				
48	Fl-Sii	2013	89.28	363.91	-5.74	22.24	189.10	16.50				
49	Fl-Sii	2014	52.05	339.85	-4.36	21.52	200.90	17.15				
50	Fl-Sii	2015	34.40	357.72	-5.42	19.66	209.50	14.25				
51	Fl-Sii	2016	55.00	320.65	-5.24	20.90	195.00	15.66				
52	Fl-Sii	2017	61.62	377.27	-6.32	20.93	208.00	14.61				
53	Fl-Sii	2018	74.22	378.66	-8.98	27.37	195.00	18.39				
54	HK-MPM	2016	53.59	378.86	15.97	13.27	198.10	29.24				
55	HK-MPM	2017	49.13	357.32	16.27	13.07	215.60	29.34				
56	HK-MPM	2018	42.11	383.02	15.25	14.05	199.00	29.30				
57	ID-Pag	2016	NaN	NaN	NaN	NaN	NaN	NaN				
58	JP-BBY	2015	56.18	355.66	-5.30	25.89	209.50	20.58				
59	JP-BBY	2016	46.06	348.04	-7.13	28.01	212.00	20.89				
60	JP-BBY	2017	44.65	361.65	-7.47	28.20	208.70	20.73				
61	JP-BBY	2018	45.63	367.94	-7.55	27.12	210.00	19.57				
62	JP-Mse	2012	54.48	351.81	1.48	24.59	219.90	26.08				
63	KR-CRK	2015	NaN	NaN	NaN	NaN	NaN	NaN				
64	KR-CRK	2016	NaN	NaN	NaN	NaN	NaN	NaN				
65	KR-CRK	2017	NaN	NaN	NaN	NaN	NaN	NaN				

66	KR-CRK	2018	NaN	NaN	NaN	NaN	NaN	NaN	NaN	NaN	NaN	NaN
67	MV-MLM	2014	17.51	365.80	25.97	1.95	179.40	27.91				
68	MV-MLM	2015	NaN	NaN	NaN	NaN	NaN	NaN				
69	NZ-Kop	2012	50.84	347.05	9.12	9.72	219.90	18.84				
70	NZ-Kop	2013	39.31	352.93	9.31	8.28	209.60	17.60				
71	NZ-Kop	2014	53.45	352.71	9.08	9.68	215.00	18.76				
72	NZ-Kop	2015	51.01	357.77	8.55	10.41	212.00	18.96				
73	PH-RiF	2012	NaN	NaN	NaN	NaN	NaN	NaN				
74	PH-RiF	2013	NaN	NaN	NaN	NaN	NaN	NaN				
75	PH-RiF	2014	NaN	NaN	NaN	NaN	NaN	NaN				
76	PH-RiF	2015	NaN	NaN	NaN	NaN	NaN	NaN				
77	RU-Ch2	2014	62.07	339.91	-31.58	46.02	208.40	14.44				
78	RU-Ch2	2015	54.09	340.02	-34.37	47.59	204.40	13.23				
79	RU-Ch2	2016	56.44	373.19	-34.38	48.39	201.90	14.00				
80	RU-Che	2014	61.35	339.96	-31.54	45.92	208.00	14.37				
81	RU-Che	2015	53.19	340.10	-34.28	47.55	204.30	13.26				
82	RU-Che	2016	55.88	372.30	-34.29	48.37	201.70	14.08				
83	SE-Deg	2014	69.57	327.67	-5.24	21.42	201.00	16.18				
84	SE-Deg	2015	29.69	352.18	-7.38	19.31	213.90	11.93				
85	SE-Deg	2016	54.69	331.26	-7.34	20.99	197.10	13.65				
86	SE-Deg	2017	61.87	353.17	-8.35	21.32	210.00	12.98				
87	SE-Deg	2018	74.36	373.70	-11.34	26.53	193.00	15.18				
88	US-Atq	2013	NaN	NaN	NaN	NaN	NaN	NaN				
89	US-Atq	2014	70.05	360.75	-25.81	32.20	203.40	6.38				
90	US-Atq	2015	84.07	347.24	-26.07	34.70	196.70	8.63				
91	US-Beo	2013	NaN	NaN	NaN	NaN	NaN	NaN				
92	US-Beo	2014	63.26	351.27	-22.70	25.61	203.20	2.91				
93	US-Bes	2013	NaN	NaN	NaN	NaN	NaN	NaN				
94	US-Bes	2014	76.62	357.34	-24.74	26.57	208.30	1.83				
95	US-Bes	2015	82.66	344.05	-25.16	29.49	203.30	4.32				
96	US-BZB	2014	65.05	339.25	-17.12	32.08	189.60	14.95				
97	US-BZB	2015	52.17	340.04	-17.27	33.86	181.60	16.58				
98	US-BZB	2016	35.70	321.04	-16.88	33.52	192.50	16.64				
99	US-BZF	2014	64.65	341.50	-16.78	31.98	190.50	15.20				

100	US-BZF	2015	52.19	340.98	-16.93	33.41	181.50	16.48
101	US-BZF	2016	34.60	321.31	-16.57	33.21	194.00	16.63
102	US-BZS	2015	46.24	343.61	-17.41	34.59	180.20	17.18
103	US-BZS	2016	32.55	320.26	-15.91	33.02	193.80	17.11
104	US-DPW	2013	59.45	361.72	16.30	10.86	220.80	27.16
105	US-DPW	2014	38.66	326.75	15.99	11.79	210.30	27.78
106	US-DPW	2015	33.62	381.23	15.93	9.98	211.80	25.91
107	US-DPW	2016	45.53	367.09	15.72	12.81	203.00	28.53
108	US-HRA	2017	NaN	NaN	NaN	NaN	NaN	NaN
109	US-HRC	2018	NaN	NaN	NaN	NaN	NaN	NaN
110	US-ICs	2014	NaN	NaN	NaN	NaN	NaN	NaN
111	US-ICs	2015	NaN	NaN	NaN	NaN	NaN	NaN
112	US-ICs	2016	68.13	328.76	-16.90	26.34	196.80	9.44
113	US-Ivo	2013	93.13	360.42	-23.36	36.20	193.60	12.84
114	US-Ivo	2014	69.00	341.89	-21.44	30.70	193.50	9.26
115	US-Ivo	2015	90.83	326.77	-21.52	31.94	188.60	10.42
116	US-Ivo	2016	90.00	339.98	-21.61	31.33	197.00	9.72
117	US-LA1	2012	31.05	302.54	19.07	8.85	177.60	27.92
118	US-LA2	2012	35.18	316.87	16.70	11.55	197.40	28.25
119	US-LA2	2013	71.41	321.17	15.91	13.32	210.60	29.23
120	US-Los	2014	58.01	365.46	-14.20	33.10	195.40	18.89
121	US-Los	2015	50.36	367.57	-10.76	29.37	203.50	18.60
122	US-Los	2016	39.16	356.37	-9.11	29.07	209.40	19.96
123	US-Los	2017	30.73	345.36	-9.80	28.09	212.00	18.29
124	US-Los	2018	69.61	336.03	-9.75	29.76	197.00	20.02
125	US-MAC	2013	NaN	NaN	NaN	NaN	NaN	NaN
126	US-MAC	2014	42.39	323.96	17.10	9.77	211.20	26.87
127	US-MAC	2015	39.48	328.01	16.94	9.62	200.60	26.56
128	US-Myb	2010	NaN	NaN	NaN	NaN	NaN	NaN
129	US-Myb	2011	31.10	331.80	8.15	12.63	223.60	20.78
130	US-Myb	2012	16.54	358.52	7.18	13.47	214.90	20.66
131	US-Myb	2013	24.44	342.29	7.26	13.44	197.00	20.70
132	US-Myb	2014	11.52	353.52	8.78	12.76	211.00	21.54
133	US-Myb	2015	-0.97	325.62	8.88	13.12	228.00	21.99

134	US-Myb	2016	-3.34	351.73	7.96	12.97	208.00	20.93
135	US-Myb	2017	27.35	345.82	8.30	13.88	214.00	22.19
136	US-Myb	2018	44.40	332.57	9.03	11.46	218.00	20.49
137	US-NC4	2012	57.32	339.28	9.01	17.49	208.70	26.50
138	US-NC4	2013	69.27	352.37	6.79	19.01	204.60	25.79
139	US-NC4	2014	49.17	367.68	5.41	18.30	206.30	23.71
140	US-NC4	2015	64.43	392.18	6.92	19.42	202.00	26.33
141	US-NC4	2016	53.97	350.61	8.14	19.07	215.00	27.21
142	US-ORv	2011	63.96	358.28	0.50	25.07	195.20	25.57
143	US-ORv	2012	32.88	351.31	0.84	24.92	195.90	25.76
144	US-ORv	2013	51.21	355.78	-2.44	25.94	203.60	23.50
145	US-ORv	2014	51.30	370.00	-4.35	27.96	196.00	23.61
146	US-ORv	2015	62.52	393.56	-4.58	27.87	199.00	23.29
147	US-OWC	2015	NaN	NaN	NaN	NaN	NaN	NaN
148	US-OWC	2016	56.19	365.00	2.20	22.65	211.80	24.85
149	US-Sne	2016	NaN	NaN	NaN	NaN	NaN	NaN
150	US-Sne	2017	9.23	344.35	7.29	14.52	217.90	21.80
151	US-Sne	2018	49.63	357.43	7.14	13.97	220.90	21.11
152	US-Srr	2014	50.56	337.45	10.74	10.06	217.30	20.80
153	US-Srr	2015	4.98	323.35	9.49	12.20	235.30	21.69
154	US-Srr	2016	-6.23	346.21	8.26	11.70	211.90	19.96
155	US-Srr	2017	17.23	346.39	7.94	13.42	216.00	21.36
156	US-StJ	2016	67.33	347.07	3.01	23.37	214.00	26.37
157	US-Tw1	2011	59.53	328.03	7.82	13.46	222.10	21.28
158	US-Tw1	2012	18.52	356.80	6.67	14.88	216.30	21.56
159	US-Tw1	2013	29.27	344.79	7.09	14.34	196.80	21.43
160	US-Tw1	2014	14.74	349.77	8.52	13.61	204.00	22.13
161	US-Tw1	2015	7.05	324.07	8.19	13.45	222.00	21.63
162	US-Tw1	2016	4.40	350.56	7.22	13.89	203.00	21.11
163	US-Tw1	2017	25.14	343.29	7.24	15.12	206.00	22.36
164	US-Tw1	2018	50.84	337.80	7.43	13.37	211.00	20.80
165	US-Tw4	2014	15.67	348.81	8.65	13.44	206.80	22.09
166	US-Tw4	2015	5.29	324.60	8.49	13.42	224.80	21.90
167	US-Tw4	2016	2.66	347.62	7.58	14.06	201.00	21.64

168	US-Tw4	2017	30.79	337.78	7.88	15.11	208.00	22.99
169	US-Tw4	2018	44.48	331.60	8.26	13.08	213.00	21.33
170	US-Tw5	2018	76.28	338.55	9.15	12.61	208.50	21.76
171	US-Twt	2009	NaN	NaN	NaN	NaN	NaN	NaN
172	US-Twt	2010	NaN	NaN	NaN	NaN	NaN	NaN
173	US-Twt	2011	NaN	NaN	NaN	NaN	NaN	NaN
174	US-Twt	2012	NaN	NaN	NaN	NaN	NaN	NaN
175	US-Twt	2013	NaN	NaN	NaN	NaN	NaN	NaN
176	US-Twt	2014	NaN	NaN	NaN	NaN	NaN	NaN
177	US-Twt	2015	NaN	NaN	NaN	NaN	NaN	NaN
178	US-Twt	2016	NaN	NaN	NaN	NaN	NaN	NaN
179	US-Uaf	2011	59.01	330.80	-23.42	38.45	191.90	15.02
180	US-Uaf	2012	43.13	311.75	-23.94	38.57	192.30	14.63
181	US-Uaf	2013	64.43	344.15	-22.12	39.63	195.90	17.51
182	US-Uaf	2014	49.85	342.99	-20.55	34.19	190.00	13.65
183	US-Uaf	2015	51.31	346.65	-19.52	34.90	182.00	15.38
184	US-Uaf	2016	27.33	325.47	-20.83	36.13	193.00	15.31
185	US-Uaf	2017	59.18	357.64	-22.10	38.30	191.00	16.20
186	US-Uaf	2018	35.38	354.57	-21.58	36.74	196.00	15.16
187	US-WPT	2011	62.29	362.57	-1.13	26.31	199.10	25.18
188	US-WPT	2012	34.86	355.23	-0.44	25.53	198.40	25.09
189	US-WPT	2013	64.19	341.07	-1.92	24.49	205.00	22.57

Column Description

SITE_ID	Site identification code as assigned by regional flux data network
Year	Data year
Start_TA_(DOY)	Season start for elevated TA (DOY), point "f" in Figure 1
End_TA_(DOY)	Season end for elevated TA (DOY), point "h" in Figure 1
Base_value_TA_(C)	Baseline TA during non-elevated season (C), average of points "a" and "b" in Figure 1
Ampl_TA_(C)	Amplitude of TA during elevated temperature season (C), difference between point "e" in Figure 1 and Base_value_TA
Peak_TA_(DOY)	Day of maximum elevated TA (DOY), point "g" in Figure 1
Peak_value_TA_(C)	Maximum value of TA (C) point "e" in Figure 1

100	US-BZF	2015	TS_1	-0.08	108.39	331.07	-1.20	14.88	197.50	13.68
101	US-BZF	2016	TS_1	-0.08	95.50	315.89	-1.03	17.18	205.10	16.15
102	US-BZS	2015	TS_1	NaN	116.48	275.22	-0.07	4.87	202.90	4.79
103	US-BZS	2016	TS_1	NaN	119.07	278.90	-0.05	5.58	208.40	5.54
104	US-DPW	2013	Nan	NaN	NaN	NaN	NaN	NaN	NaN	NaN
105	US-DPW	2014	Nan	NaN	NaN	NaN	NaN	NaN	NaN	NaN
106	US-DPW	2015	Nan	NaN	NaN	NaN	NaN	NaN	NaN	NaN
107	US-DPW	2016	Nan	NaN	NaN	NaN	NaN	NaN	NaN	NaN
108	US-HRA	2017	Nan	NaN	NaN	NaN	NaN	NaN	NaN	NaN
109	US-HRC	2018	Nan	NaN	NaN	NaN	NaN	NaN	NaN	NaN
110	US-ICs	2014	TS_1	-0.08	147.27	263.08	-0.08	5.47	205.60	5.39
111	US-ICs	2015	TS_1	-0.08	141.61	255.70	-0.02	6.12	195.20	6.10
112	US-ICs	2016	TS_1	-0.08	146.75	265.86	-0.05	5.67	206.20	5.62
113	US-Ivo	2013	Nan	NaN	NaN	NaN	NaN	NaN	NaN	NaN
114	US-Ivo	2014	TS_1	-0.05	136.92	264.34	-0.20	10.84	195.70	10.64
115	US-Ivo	2015	TS_1	-0.05	139.42	257.06	-0.14	14.86	185.60	14.72
116	US-Ivo	2016	TS_1	-0.05	133.60	262.43	-0.10	8.90	197.30	8.80
117	US-LA1	2012	TS_1	-0.10	29.15	331.44	15.59	13.50	197.20	29.08
118	US-LA2	2012	TS_1	-0.10	36.65	336.05	15.04	14.35	193.20	29.39
119	US-LA2	2013	TS_1	-0.10	65.79	377.93	14.70	16.06	201.50	30.76
120	US-Los	2014	TS_1	0.00	136.18	417.40	1.95	8.26	244.30	10.22
121	US-Los	2015	TS_1	0.00	148.23	422.27	2.43	7.76	258.70	10.19
122	US-Los	2016	TS_1	0.00	135.20	415.75	2.47	8.08	255.10	10.56
123	US-Los	2017	TS_1	0.00	141.15	414.62	1.89	7.45	256.00	9.34
124	US-Los	2018	TS_1	0.00	169.83	421.79	1.46	7.42	260.00	8.88
125	US-MAC	2013	Nan	NaN	NaN	NaN	NaN	NaN	NaN	NaN
126	US-MAC	2014	Nan	NaN	NaN	NaN	NaN	NaN	NaN	NaN
127	US-MAC	2015	Nan	NaN	NaN	NaN	NaN	NaN	NaN	NaN
128	US-Myb	2010	Nan	NaN	NaN	NaN	NaN	NaN	NaN	NaN
129	US-Myb	2011	TS_3	-0.08	NaN	329.50	12.12	8.86	231.70	20.98
130	US-Myb	2012	TS_3	-0.08	35.60	372.21	9.39	10.96	216.10	20.36
131	US-Myb	2013	TS_3	-0.08	34.38	354.74	9.25	11.28	210.90	20.52
132	US-Myb	2014	TS_3	-0.08	26.04	365.88	9.64	12.28	210.00	21.93
133	US-Myb	2015	TS_3	-0.08	17.34	340.72	9.77	11.85	212.00	21.62

134	US-Myb	2016	TS_3	-0.08	5.05	357.82	9.61	11.19	201.00	20.80
135	US-Myb	2017	TS_3	-0.08	27.31	352.90	9.86	13.10	214.00	22.96
136	US-Myb	2018	TS_3	-0.08	36.27	326.10	10.20	10.72	207.00	20.92
137	US-NC4	2012	TS_-1	-0.05	42.43	336.03	7.87	15.75	215.40	23.62
138	US-NC4	2013	TS_-1	-0.05	59.96	368.85	6.92	16.83	210.50	23.74
139	US-NC4	2014	TS_-1	-0.05	54.42	362.34	6.73	16.81	208.50	23.54
140	US-NC4	2015	TS_-1	-0.05	68.13	387.31	8.27	16.06	205.00	24.33
141	US-NC4	2016	TS_-1	-0.05	52.97	351.38	9.41	15.04	220.00	24.45
142	US-ORv	2011	NaN	NaN	NaN	NaN	NaN	NaN	NaN	NaN
143	US-ORv	2012	TS	NaN	57.42	352.55	4.36	20.61	203.90	24.97
144	US-ORv	2013	TS	NaN	63.67	356.74	2.93	19.98	210.80	22.90
145	US-ORv	2014	TS	NaN	68.11	364.96	2.11	20.17	205.30	22.28
146	US-ORv	2015	TS	NaN	68.77	387.78	1.77	21.26	206.00	23.04
147	US-OWC	2015	NaN	NaN	NaN	NaN	NaN	NaN	NaN	NaN
148	US-OWC	2016	TS_-1	-0.05	0.00	0.00	0.00	0.00	211.20	23.91
149	US-Sne	2016	NaN	NaN	NaN	NaN	NaN	NaN	NaN	NaN
150	US-Sne	2017	TS_-1	-0.01	46.07	337.92	10.33	13.14	212.70	23.47
151	US-Sne	2018	TS_-1	-0.01	48.41	325.09	10.28	12.15	217.30	22.43
152	US-Srr	2014	NaN	NaN	NaN	NaN	NaN	NaN	NaN	NaN
153	US-Srr	2015	NaN	NaN	NaN	NaN	NaN	NaN	NaN	NaN
154	US-Srr	2016	TS_-1	NaN	326.29	10.03	10.71	200.50	20.74	
155	US-Srr	2017	TS_-1	NaN	11.34	346.85	7.22	13.71	199.50	20.93
156	US-StJ	2016	TS_-2	-0.05	68.37	347.38	4.05	16.22	213.70	20.27
157	US-Tw1	2011	NaN	NaN	NaN	NaN	NaN	NaN	NaN	NaN
158	US-Tw1	2012	TS_-1	-0.02	50.54	359.96	5.99	11.52	225.20	17.51
159	US-Tw1	2013	TS_-1	-0.02	35.80	337.57	4.39	14.59	206.60	18.97
160	US-Tw1	2014	TS_-1	-0.02	41.23	395.41	6.67	10.89	208.30	17.56
161	US-Tw1	2015	TS_-1	-0.02	50.66	342.55	9.02	7.83	235.00	16.85
162	US-Tw1	2016	TS_-1	-0.02	34.57	361.06	8.78	7.94	218.00	16.72
163	US-Tw1	2017	TS_-1	-0.02	41.17	343.75	7.55	10.22	228.00	17.77
164	US-Tw1	2018	TS_-1	-0.02	60.47	327.43	6.70	10.42	222.00	17.12
165	US-Tw4	2014	NaN	NaN	NaN	NaN	NaN	NaN	NaN	NaN
166	US-Tw4	2015	TS_-1	-0.02	15.93	327.22	10.04	11.56	199.40	21.60
167	US-Tw4	2016	TS_-1	-0.02	9.56	358.75	8.16	11.29	201.70	19.45

	SITE_ID	Year	Probe_name	Soil_temp_depth_m	Start_TS_(DOY)	End_TS_(DOY)	Base_value_TS_(C)	Ampl_TS_(C)
168	US-Tw4	2017	TS_1	-0.02	38.35	347.31	8.07	11.52
169	US-Tw4	2018	TS_1	-0.02	58.11	344.87	8.00	10.93
170	US-Tw5	2018	TS_1	-0.02	NaN	414.83	0.00	8.89
171	US-Twt	2009	NaN	NaN	NaN	NaN	NaN	NaN
172	US-Twt	2010	NaN	NaN	NaN	NaN	NaN	NaN
173	US-Twt	2011	NaN	NaN	NaN	NaN	NaN	NaN
174	US-Twt	2012	NaN	NaN	NaN	NaN	NaN	NaN
175	US-Twt	2013	NaN	NaN	NaN	NaN	NaN	NaN
176	US-Twt	2014	NaN	NaN	NaN	NaN	NaN	NaN
177	US-Twt	2015	NaN	NaN	NaN	NaN	NaN	NaN
178	US-Twt	2016	NaN	NaN	NaN	NaN	NaN	NaN
179	US-Uaf	2011	TS_1	-0.09	86.20	372.46	-12.29	21.95
180	US-Uaf	2012	TS_1	-0.09	73.77	338.53	-11.83	20.86
181	US-Uaf	2013	TS_1	-0.09	109.63	395.51	-10.08	20.52
182	US-Uaf	2014	TS_1	-0.09	76.07	365.40	-10.94	19.94
183	US-Uaf	2015	TS_1	-0.09	80.99	423.19	-9.77	19.76
184	US-Uaf	2016	TS_1	-0.09	77.38	315.75	-7.74	19.13
185	US-Uaf	2017	TS_1	-0.09	84.88	380.17	-7.39	19.08
186	US-Uaf	2018	TS_1	-0.09	96.04	333.33	-5.60	17.72
187	US-WPT	2011	TS_1	-0.10	80.95	342.17	5.27	19.27
188	US-WPT	2012	TS_1	-0.10	40.29	345.57	3.70	21.60
189	US-WPT	2013	TS_1	-0.10	74.61	340.47	3.73	18.23
							207.20	207.20
								21.96

Column Descriptions

SITE_ID	Site identification code as assigned by regional flux data network
Year	Data year
Probe_name	Temperature probe name as given in data files
Soil_temp_depth_m	Depth of soil temperature probe (m), with negative values being under the surface
Start_TS_(DOY)	Season start for elevated TS (DOY), point "f" in Figure 1
End_TS_(DOY)	Season end for elevated TS (DOY), point "h" in Figure 1
Base_value_TS_(C)	Baseline TS during non-elevated season (C), average of points "a" and "b" in Figure 1
Ampl_TS_(C)	Amplitude of TS during elevated temperature season (C), difference between point "e" in Figure 1 and Base_value_TS

Peak_TS_(DOY)
Peak_value_TS_(C)

Day of maximum elevated TS (DOY), point "g" in Figure 1
Maximum value of TS (C) point "e" in Figure 1

Table B6: Timesat output for all soil temperature probes

	SITE_ID	Year	Probe_name	Soil_temp_depth_m	Start_TS_(DOY)	End_TS_(DOY)	Base_value_TS_(C)	Ampl_TS_(C)	Peak_TS_(DOY)	Peak_value_TS_(C)
1	AT-Neu	2010	TS_1	-0.05	61.32	339.44	0.15	17.54	200.9	17.7
2	AT-Neu	2011	TS_1	-0.05	51.04	328.84	0.40	16.37	201	16.77
3	AT-Neu	2012	TS_1	-0.05	61.12	341.88	0.73	17.57	202.9	18.3
4	BR-Npw	2016	TS_1	NaN	18.41	343.22	22.41	5.982	188	28.4
5	CA-SCB	2014	TS_1	0	105.94	292.18	-0.63	20.62	196.6	19.99
6	CA-SCB	2014	TS_2	-0.02	105.15	294.06	-0.74	20.42	197.5	19.68
7	CA-SCB	2014	TS_3	-0.04	112.00	294.38	0.05	19.07	199.6	19.11
8	CA-SCB	2014	TS_5	-0.16	123.21	317.72	-1.38	18.6	205.3	17.23
9	CA-SCB	2015	TS_1	0	106.92	287.14	-0.39	17.23	186.8	16.84
10	CA-SCB	2015	TS_2	-0.02	107.06	287.40	-0.42	17.08	187.4	16.66
11	CA-SCB	2015	TS_3	-0.04	107.45	289.83	-0.51	16.81	188.9	16.3
12	CA-SCB	2015	TS_5	-0.16	114.95	305.55	-0.39	15.84	195.7	15.45
13	CA-SCB	2016	TS_1	0	101.64	284.09	-0.31	19.07	193.2	18.77
14	CA-SCB	2016	TS_2	-0.02	101.81	284.11	-0.30	18.96	193.5	18.66
15	CA-SCB	2016	TS_3	-0.04	102.22	285.19	-0.30	18.6	194.3	18.3
16	CA-SCB	2016	TS_5	-0.16	101.16	298.99	-0.24	16.99	201.1	16.74
17	CA-SCB	2017	TS_1	0	107.44	289.72	-0.25	17.67	198	17.42
18	CA-SCB	2017	TS_2	-0.02	107.22	288.88	-0.25	17.59	198	17.33
19	CA-SCB	2017	TS_3	-0.04	108.58	289.29	-0.26	17.28	199	17.02
20	CA-SCB	2017	TS_5	-0.16	116.34	300.28	-0.24	14.95	214	14.71
21	CA-SCC	2014	TS_1	-0.1	123.36	287.06	-0.55	15.64	203	15.09
22	CA-SCC	2014	TS_2	-0.15	114.89	287.71	-0.83	14.49	200.8	13.66
23	CA-SCC	2014	TS_3	-0.2	111.36	288.63	-0.69	11.52	194.9	10.84
24	CA-SCC	2014	TS_4	-0.25	129.50	287.24	-0.22	8.612	207.4	8.391
25	CA-SCC	2014	TS_5	-0.3	142.36	287.99	-0.10	6.329	212.1	6.225
26	CA-SCC	2015	TS_1	-0.1	113.88	285.22	-0.28	16.26	189.2	15.98
27	CA-SCC	2015	TS_2	-0.15	113.05	284.18	-0.24	14.56	192.8	14.32
28	CA-SCC	2015	TS_3	-0.2	111.76	285.45	-0.22	12.71	199.1	12.48
29	CA-SCC	2015	TS_4	-0.25	120.81	287.09	-0.16	10.08	204.8	9.922
30	CA-SCC	2015	TS_5	-0.3	131.92	285.42	-0.09	7.705	209.2	7.616
31	CA-SCC	2016	TS_1	-0.1	108.09	260.12	-0.33	18.37	190.9	18.04
32	CA-SCC	2016	TS_2	-0.15	108.96	260.19	-0.30	17.31	192.1	17.01
33	CA-SCC	2016	TS_3	-0.2	110.49	260.44	-0.26	15.4	194.1	15.14
34	CA-SCC	2016	TS_4	-0.25	119.21	260.34	-0.20	13.38	200.2	13.18
35	CA-SCC	2016	TS_5	-0.3	130.75	261.73	-0.12	10.03	202.2	9.906
36	DE-Hte	2012	TS_3	-0.2	76.96	344.01	4.98	12.26	215.5	17.23
37	DE-Hte	2013	TS_3	-0.2	60.92	377.99	3.96	11.99	207.9	15.95
38	DE-Hte	2014	TS_1	0	NaN	327.83	8.52	8.342	205.6	16.87
39	DE-Hte	2015	TS_1	0	62.92	360.55	5.17	11.67	187.4	16.84
40	DE-Hte	2016	TS_1	0	71.87	NaN	4.94	12.36	175.6	17.3
41	DE-Hte	2017	TS_1	0	61.55	343.32	4.50	11.76	186	16.26
42	DE-SfN	2012	TS_1	-0.02	NaN	372.59	0.00	23.55	206.5	15.29
43	DE-SfN	2012	TS_3	-0.1	NaN	366.65	1.64	12.91	219.7	14.55

44	DE-SfN	2012 TS_4	-0.2	NaN	367.40	4.86	7.276	242.7	12.14
45	DE-SfN	2012 TS_5	-0.5	NaN	367.40	4.86	7.276	242.7	12.14
46	DE-SfN	2013 TS_1	-0.02	55.84	381.50	0.92	13.62	216.4	14.54
47	DE-SfN	2013 TS_3	-0.1	60.45	384.77	1.56	12.5	221.1	14.06
48	DE-SfN	2013 TS_4	-0.2	83.55	394.53	3.62	8.417	243.4	12.04
49	DE-SfN	2013 TS_5	-0.5	83.55	394.53	3.62	8.417	243.4	12.04
50	DE-Zrk	2014 TS_1	-0.05	54.79	361.65	4.36	13.93	202.3	18.29
51	DE-Zrk	2014 TS_2	-0.1	59.27	366.51	4.87	12.65	207.3	17.52
52	DE-Zrk	2014 TS_3	-0.2	62.95	371.30	5.53	11.5	211.7	17.03
53	DE-Zrk	2014 TS_4	-0.3	67.45	375.14	6.05	10.4	216.5	16.45
54	DE-Zrk	2014 TS_5	-0.5	72.50	378.95	6.57	9.359	221	15.93
55	DE-Zrk	2015 TS_1	-0.05	58.29	359.29	4.28	13.24	215.5	17.52
56	DE-Zrk	2015 TS_2	-0.1	62.61	364.99	4.79	12	219.8	16.8
57	DE-Zrk	2015 TS_3	-0.2	66.01	369.78	5.42	10.87	223.7	16.29
58	DE-Zrk	2015 TS_4	-0.3	70.47	374.40	5.93	9.771	228	15.7
59	DE-Zrk	2015 TS_5	-0.5	74.71	378.76	6.43	8.751	232.2	15.19
60	DE-Zrk	2016 TS_1	-0.05	72.81	332.00	4.28	14.93	200.4	19.2
61	DE-Zrk	2016 TS_2	-0.1	76.31	337.37	4.79	13.6	204.4	18.39
62	DE-Zrk	2016 TS_3	-0.2	79.73	343.16	5.43	12.33	208.1	17.77
63	DE-Zrk	2016 TS_4	-0.3	83.58	347.57	5.94	11.14	212	17.09
64	DE-Zrk	2016 TS_5	-0.5	87.15	354.22	6.40	10.07	216	16.47
65	DE-Zrk	2017 TS_1	-0.05	69.10	351.44	4.40	14.72	199	19.12
66	DE-Zrk	2017 TS_2	-0.1	73.29	356.52	4.91	13.33	204	18.23
67	DE-Zrk	2017 TS_3	-0.2	77.19	362.40	5.56	12.02	208	17.58
68	DE-Zrk	2017 TS_4	-0.3	82.20	367.20	6.04	10.8	212	16.84
69	DE-Zrk	2017 TS_5	-0.5	86.22	372.96	6.48	9.675	217	16.15
70	DE-Zrk	2018 TS_1	-0.05	84.47	336.14	4.83	12.32	203	17.14
71	DE-Zrk	2018 TS_2	-0.1	86.60	342.59	5.30	11.27	208	16.57
72	DE-Zrk	2018 TS_3	-0.2	87.68	348.07	5.89	10.25	212	16.14
73	DE-Zrk	2018 TS_4	-0.3	89.82	354.77	6.31	9.308	217	15.61
74	DE-Zrk	2018 TS_5	-0.5	92.01	360.46	6.69	8.412	222	15.11
75	Fl-Lom	2006 TS_1	-0.07	114.15	290.83	-0.11	13.42	204.8	13.31
76	Fl-Lom	2006 TS_2	-0.3	117.21	307.88	0.27	12.01	214.1	12.28
77	Fl-Lom	2006 TS_3	-0.5	128.82	329.03	1.06	9.071	225.8	10.13
78	Fl-Lom	2007 TS_1	-0.07	126.84	302.05	0.11	13.05	200	13.16
79	Fl-Lom	2007 TS_2	-0.3	134.00	321.03	0.42	11.5	207.5	11.92
80	Fl-Lom	2007 TS_3	-0.5	138.37	348.03	1.06	8.873	221.1	9.936
81	Fl-Lom	2008 TS_1	-0.07	135.62	296.74	0.16	12.73	202.9	12.88
82	Fl-Lom	2008 TS_2	-0.3	141.46	318.74	0.58	10.62	209.6	11.2
83	Fl-Lom	2008 TS_3	-0.5	146.70	349.21	1.17	8.214	221.2	9.382
84	Fl-Lom	2009 TS_1	-0.07	117.16	291.86	0.14	11.73	214	11.87
85	Fl-Lom	2009 TS_2	-0.3	123.51	314.51	0.67	9.692	221	10.36
86	Fl-Lom	2009 TS_3	-0.5	133.69	336.65	1.30	7.896	233	9.193
87	Fl-Lom	2010 TS_1	-0.07	129.91	318.54	0.05	12.13	208	12.18
88	Fl-Lom	2010 TS_2	-0.3	138.09	338.24	0.52	9.962	218	10.48
89	Fl-Lom	2010 TS_3	-0.5	147.34	359.95	1.19	7.344	231	8.532
90	Fl-Si2	2012 TS_1	-0.05	NaN	323.46	0.00	19.85	204.6	16.02

91	FI-Si2	2012 TS_2	-0.2	103.64	333.52	-0.04	15.75	217.5	15.71
92	FI-Si2	2012 TS_3	-0.35	105.57	NaN	0.00	19.38	230.6	15.09
93	FI-Si2	2012 TS_4	-0.5	110.87	NaN	0.00	17.26	237.5	14.66
94	FI-Si2	2013 TS_1	-0.05	106.90	341.05	-0.05	16.04	199.4	15.98
95	FI-Si2	2013 TS_2	-0.2	102.57	356.13	0.23	14.91	207.3	15.14
96	FI-Si2	2013 TS_3	-0.35	NaN	376.47	0.00	18.26	209.6	14.23
97	FI-Si2	2013 TS_4	-0.5	NaN	392.35	0.00	16.71	216.4	13.48
98	FI-Si2	2014 TS_1	-0.05	104.63	331.10	-0.04	17.07	208.5	17.03
99	FI-Si2	2014 TS_2	-0.2	107.82	359.78	0.59	15.33	215.3	15.92
100	FI-Si2	2014 TS_3	-0.35	112.02	385.94	0.99	13.61	222.2	14.61
101	FI-Si2	2014 TS_4	-0.5	118.24	400.15	1.59	12.01	229.1	13.59
102	FI-Si2	2015 TS_1	-0.05	76.49	352.34	-0.87	16.31	211	15.44
103	FI-Si2	2015 TS_2	-0.2	80.08	364.72	-0.41	14.83	218	14.42
104	FI-Si2	2015 TS_3	-0.35	82.01	374.79	0.12	13.27	225	13.39
105	FI-Si2	2015 TS_4	-0.5	88.25	382.37	0.84	11.7	233	12.53
106	FI-Si2	2016 TS_1	-0.05	102.64	329.42	-0.88	16.48	206	15.6
107	FI-Si2	2016 TS_2	-0.2	102.16	361.04	-0.77	16.02	212	15.25
108	FI-Si2	2016 TS_3	-0.35	103.15	383.82	-0.63	14.7	219	14.07
109	FI-Si2	2016 TS_4	-0.5	104.76	399.01	-0.20	13.36	227	13.16
110	HK-MPM	2016 TS_2	NaN	NaN	566.87	0.00	7.789	219.8	28.92
111	HK-MPM	2016 TS_3	NaN	NaN	373.06	20.56	7.386	227.3	27.95
112	HK-MPM	2017 TS_2	NaN	NaN	NaN	0.00	8.726	218.5	29.13
113	HK-MPM	2017 TS_3	NaN	69.55	364.53	19.53	8.572	233.6	28.1
114	HK-MPM	2018 TS_2	NaN	NaN	NaN	0.00	7.231	204.9	28.66
115	HK-MPM	2018 TS_3	NaN	64.82	383.39	19.17	8.406	221.4	27.58
116	JP-BBY	2015 TS_1	-0.183	87.83	340.83	0.94	21.59	218.1	22.53
117	JP-BBY	2015 TS_2	-0.233	90.59	340.99	1.34	20.9	219.9	22.25
118	JP-BBY	2015 TS_3	-0.283	90.34	341.60	1.58	20.42	221.4	22
119	JP-BBY	2015 TS_4	-0.383	96.01	341.35	2.39	19.09	225.1	21.48
120	JP-BBY	2015 TS_5	-0.483	95.83	341.49	2.91	18.09	228.9	21
121	JP-BBY	2016 TS_1	-0.183	80.75	330.60	0.36	22.19	217.8	22.55
122	JP-BBY	2016 TS_2	-0.233	82.30	335.40	0.67	21.64	220.8	22.3
123	JP-BBY	2016 TS_3	-0.283	84.28	332.64	0.99	21.1	222	22.09
124	JP-BBY	2016 TS_4	-0.383	89.00	332.43	1.76	19.92	225.6	21.68
125	JP-BBY	2016 TS_5	-0.483	94.29	331.91	2.44	18.83	228.9	21.27
126	JP-BBY	2017 TS_1	-0.183	80.38	347.77	0.20	21.75	213.8	21.95
127	JP-BBY	2017 TS_2	-0.233	84.54	347.79	0.82	21.02	214.6	21.83
128	JP-BBY	2017 TS_3	-0.283	86.19	347.10	1.06	20.56	216.3	21.62
129	JP-BBY	2017 TS_4	-0.383	92.20	346.01	1.97	19.34	218.5	21.31
130	JP-BBY	2017 TS_5	-0.483	98.15	345.18	2.70	18.34	221	21.03
131	JP-BBY	2018 TS_1	-0.183	78.28	355.38	0.50	20.38	222	20.88
132	JP-BBY	2018 TS_2	-0.233	83.55	357.60	1.48	19.23	224	20.7
133	JP-BBY	2018 TS_3	-0.283	85.93	355.90	1.69	18.78	225	20.47
134	JP-BBY	2018 TS_4	-0.383	95.89	351.34	2.81	17.25	229	20.07
135	JP-BBY	2018 TS_5	-0.483	103.83	349.39	3.63	16.1	232	19.73
136	JP-Mse	2012 TS_1	-0.01	60.38	348.86	2.15	23.76	211.8	25.91
137	MY-MLM	2014 TS	NaN	NaN	358.37	25.06	3.968	194.5	29.03

138	MY-MLM	2015 TS	NaN	27.32	NaN	25.57	1.973	172.7	27.55
139	NZ-Kop	2012 TS_1	-0.5	62.54	360.29	8.30	8.394	219.8	16.7
140	NZ-Kop	2012 TS_2	-0.1	65.53	362.35	8.45	8.093	222.1	16.54
141	NZ-Kop	2012 TS_3	-0.2	68.77	365.64	8.73	7.243	228.2	15.98
142	NZ-Kop	2013 TS_1	-0.5	45.63	367.00	8.41	7.635	210.5	16.04
143	NZ-Kop	2013 TS_2	-0.1	47.60	370.98	8.54	7.486	212.3	16.03
144	NZ-Kop	2013 TS_3	-0.2	52.74	377.20	8.82	6.87	217.8	15.69
145	NZ-Kop	2014 TS_1	-0.5	56.88	365.68	8.16	8.79	219	16.95
146	NZ-Kop	2014 TS_2	-0.1	59.45	367.47	8.29	8.512	221	16.8
147	NZ-Kop	2014 TS_3	-0.2	62.93	372.48	8.55	7.792	226	16.34
148	NZ-Kop	2015 TS_1	-0.5	56.49	371.82	7.73	9.355	214	17.09
149	NZ-Kop	2015 TS_2	-0.1	58.32	374.74	7.87	9.063	217	16.93
150	NZ-Kop	2015 TS_3	-0.2	62.67	378.44	8.19	8.217	222	16.4
151	RU-Ch2	2014 TS_1	-0.04	138.76	263.76	-0.13	14.42	206.6	14.29
152	RU-Ch2	2014 TS_2	-0.08	146.08	262.11	-0.14	13.03	206.5	12.9
153	RU-Ch2	2014 TS_3	-0.16	155.95	264.51	-0.05	4.581	210.5	4.535
154	RU-Ch2	2015 TS_1	-0.04	143.88	269.56	-0.14	13.97	193.3	13.83
155	RU-Ch2	2015 TS_2	-0.08	147.34	265.69	-0.10	12.3	195.7	12.2
156	RU-Ch2	2015 TS_3	-0.16	159.93	266.60	-0.04	3.995	205.2	3.96
157	RU-Ch2	2016 TS_1	-0.04	126.98	273.54	-0.16	11.64	200.2	11.48
158	RU-Ch2	2016 TS_2	-0.08	133.92	272.58	-0.10	10.06	203.2	9.964
159	RU-Ch2	2016 TS_3	-0.16	147.99	275.45	-0.04	4.042	217.7	4.001
160	RU-Che	2014 TS_1	-0.04	138.05	267.57	-0.12	15.04	208	14.92
161	RU-Che	2014 TS_2	-0.08	149.72	263.67	-0.09	8.959	206.6	8.873
162	RU-Che	2014 TS_3	-0.16	154.97	265.49	-0.07	7.006	210.3	6.938
163	RU-Che	2015 TS_1	-0.04	143.85	274.68	-0.17	14.81	193.7	14.64
164	RU-Che	2015 TS_2	-0.08	149.49	267.08	-0.06	8.336	197.9	8.273
165	RU-Che	2015 TS_3	-0.16	154.48	271.03	-0.04	5.942	202.4	5.9
166	RU-Che	2016 TS_1	-0.04	126.72	274.03	-0.19	12.95	200.4	12.76
167	RU-Che	2016 TS_2	-0.08	137.01	273.70	-0.07	7.076	205.4	7.01
168	RU-Che	2016 TS_3	-0.16	142.51	275.62	-0.05	5.498	211.8	5.451
169	SE-Deg	2014 TS_1	-0.02	111.85	303.55	-0.53	17.22	201.6	16.69
170	SE-Deg	2014 TS_2	-0.05	119.11	308.12	-0.31	13.23	207.4	12.93
171	SE-Deg	2014 TS_3	-0.1	125.46	315.55	-0.10	12.54	212	12.44
172	SE-Deg	2014 TS_4	-0.15	134.61	321.20	0.29	11.63	215.6	11.93
173	SE-Deg	2014 TS_5	-0.3	126.75	330.85	0.52	11.61	220	12.13
174	SE-Deg	2014 TS_6	-0.5	130.62	341.66	0.89	11.33	223.1	12.21
175	SE-Deg	2015 TS_1	-0.02	104.25	310.59	-0.28	15.2	207.2	14.91
176	SE-Deg	2015 TS_2	-0.05	110.64	312.57	0.09	13.86	209.5	13.95
177	SE-Deg	2015 TS_3	-0.1	112.94	321.41	0.41	12.94	212.9	13.36
178	SE-Deg	2015 TS_4	-0.15	115.72	329.21	0.60	11.94	216.6	12.54
179	SE-Deg	2015 TS_5	-0.3	118.31	339.17	0.90	11.08	220.5	11.98
180	SE-Deg	2015 TS_6	-0.5	121.80	347.97	1.30	10.19	224.6	11.48
181	SE-Deg	2016 TS_1	-0.02	108.14	306.39	-0.19	14.88	200.3	14.68
182	SE-Deg	2017 TS_1	-0.02	133.38	326.87	-0.20	12.35	215	12.15
183	SE-Deg	2018 TS_1	-0.02	111.67	310.21	-0.17	14.7	198	14.52
184	US-Atq	2014 TS_1	NaN	10.75	139.53	-0.20	8.068	61	7.864

185	US-Atq	2014 TS_2	NaN	18.00	137.32	-0.08	4.191	74.3	4.109
186	US-Atq	2014 TS_3	NaN	28.49	138.48	-0.03	2.366	83.5	2.334
187	US-Beo	2014 TS_1	NaN	155.09	270.13	-0.04	4.874	211.1	4.829
188	US-Beo	2014 TS_2	NaN	168.62	270.60	-0.02	2.94	219.6	2.922
189	US-Beo	2014 TS_3	NaN	170.53	269.49	-0.02	3.128	219.9	3.104
190	US-Bes	2013 TS_1	NaN	143.22	261.99	-0.05	5.649	201.3	5.602
191	US-Bes	2013 TS_2	NaN	150.57	267.49	-0.04	6.744	205.7	6.706
192	US-Bes	2013 TS_3	NaN	146.03	267.28	-0.06	8.248	202.3	8.187
193	US-Bes	2014 TS_1	NaN	151.79	282.29	-0.10	3.924	198.5	3.822
194	US-Bes	2015 TS_1	NaN	140.45	270.98	-0.11	4.763	195.3	4.65
195	US-Bes	2015 TS_2	NaN	148.76	269.64	-0.11	5.512	202.8	5.401
196	US-Bes	2015 TS_3	NaN	146.77	271.72	-0.16	7.182	197.8	7.027
197	US-BZB	2014 TS_1	-0.075	123.11	298.35	-0.44	15.35	215.8	14.91
198	US-BZB	2014 TS_2	-0.05	115.15	292.07	-0.59	15.49	209.9	14.9
199	US-BZB	2015 TS_1	-0.075	107.82	295.60	-0.38	14.04	210.2	13.67
200	US-BZB	2015 TS_2	-0.05	98.63	293.17	-0.67	14.56	203.5	13.9
201	US-BZB	2016 TS_1	-0.075	125.09	292.39	-0.33	16.39	214.3	16.06
202	US-BZB	2016 TS_2	-0.05	109.89	290.95	-0.74	16.89	211.7	16.15
203	US-BZF	2014 TS_1	-0.075	96.05	322.79	-1.56	16.12	205.4	14.56
204	US-BZF	2014 TS_2	-0.05	112.68	322.83	-1.22	15.9	208.3	14.68
205	US-BZF	2015 TS_1	-0.075	108.39	331.07	-1.20	14.88	197.5	13.68
206	US-BZF	2015 TS_2	-0.05	111.46	336.09	-1.12	14.83	200.2	13.72
207	US-BZF	2016 TS_1	-0.075	95.50	315.89	-1.03	17.18	205.1	16.15
208	US-BZF	2016 TS_2	-0.05	100.12	317.57	-0.90	17.72	206	16.81
209	US-BZS	2015 TS_1	NaN	116.48	275.22	-0.07	4.866	202.9	4.792
210	US-BZS	2015 TS_2	NaN	97.29	283.75	-0.27	8.135	187.7	7.862
211	US-BZS	2015 TS_3	NaN	105.93	272.47	-0.13	10.61	193.1	10.47
212	US-BZS	2016 TS_1	NaN	119.07	278.90	-0.05	5.584	208.4	5.535
213	US-BZS	2016 TS_2	NaN	87.59	278.96	-0.25	12.09	203.1	11.84
214	US-BZS	2016 TS_3	NaN	98.29	277.92	-0.16	11.67	198.8	11.51
215	US-ICs	2014 TS_1	-0.075	147.27	263.08	-0.08	5.467	205.6	5.39
216	US-ICs	2014 TS_2	-0.05	147.13	262.66	-0.01	6.41	205.1	6.402
217	US-ICs	2015 TS_1	-0.075	141.61	255.70	-0.02	6.12	195.2	6.098
218	US-ICs	2015 TS_2	-0.05	140.38	256.88	-0.02	7.07	193.1	7.047
219	US-ICs	2016 TS_1	-0.075	146.75	265.86	-0.05	5.67	206.2	5.623
220	US-ICs	2016 TS_2	-0.05	146.79	265.67	-0.05	6.654	206.1	6.599
221	US-Ivo	2014 TS_1	-0.05	136.92	264.34	-0.20	10.84	195.7	10.64
222	US-Ivo	2014 TS_1	-0.4	136.92	264.34	-0.20	10.84	195.7	10.64
223	US-Ivo	2014 TS_2	-0.1	142.52	266.53	-0.16	9.908	195.5	9.744
224	US-Ivo	2014 TS_3	-0.15	144.98	262.74	-0.19	6.761	204.8	6.574
225	US-Ivo	2014 TS_4	-0.3	166.58	262.05	-0.03	4.068	214.3	4.034
226	US-Ivo	2015 TS_1	-0.05	139.42	257.06	-0.14	14.86	185.6	14.72
227	US-Ivo	2015 TS_1	-0.4	139.42	257.06	-0.14	14.86	185.6	14.72
228	US-Ivo	2015 TS_2	-0.1	141.20	256.70	-0.09	11.99	189.1	11.9
229	US-Ivo	2015 TS_3	-0.15	145.76	260.99	-0.07	6.85	199.1	6.785
230	US-Ivo	2015 TS_4	-0.3	158.88	259.63	-0.03	4.032	208.2	3.997
231	US-Ivo	2016 TS_1	-0.05	133.60	262.43	-0.10	8.895	197.3	8.796

232	US-Ivo	2016 TS_1	-0.4	133.60	262.43	-0.10	8.895	197.3	8.796
233	US-Ivo	2016 TS_2	-0.1	139.70	264.19	-0.04	6.76	202.2	6.719
234	US-Ivo	2016 TS_3	-0.15	153.78	269.47	-0.05	4.305	211.5	4.253
235	US-Ivo	2016 TS_4	-0.3	171.24	271.03	-0.01	2.644	221.2	2.631
236	US-LA1	2012 TS_1	-0.1	29.15	331.44	15.59	13.5	197.2	29.08
237	US-LA2	2012 TS_1	-0.1	36.65	336.05	15.04	14.35	193.2	29.39
238	US-LA2	2013 TS_1	-0.1	65.79	377.93	14.70	16.06	201.5	30.76
239	US-Los	2014 TS_1	0	136.18	417.40	1.95	8.263	244.3	10.22
240	US-Los	2015 TS_1	0	148.23	422.27	2.43	7.761	258.7	10.19
241	US-Los	2016 TS_1	0	135.20	415.75	2.47	8.083	255.1	10.56
242	US-Los	2017 TS_1	0	141.15	414.62	1.89	7.451	256	9.343
243	US-Los	2018 TS_1	0	169.83	421.79	1.46	7.419	260	8.883
244	US-Myb	2011 TS_3	-0.08	NaN	329.50	12.12	8.859	231.7	20.98
245	US-Myb	2011 TS_4	-0.16	NaN	333.87	12.36	8.288	235.8	20.65
246	US-Myb	2011 TS_5	-0.32	NaN	338.98	12.72	7.56	241.4	20.28
247	US-Myb	2011 TS_1	-0.02	NaN	326.62	11.96	9.156	229.3	21.12
248	US-Myb	2012 TS_3	-0.08	35.60	372.21	9.39	10.96	216.1	20.36
249	US-Myb	2012 TS_4	-0.16	40.39	375.48	9.90	10.23	220.7	20.13
250	US-Myb	2012 TS_5	-0.32	47.39	379.29	10.56	9.212	227.2	19.78
251	US-Myb	2012 TS_1	-0.02	29.91	372.10	8.98	11.77	214.4	20.74
252	US-Myb	2013 TS_3	-0.08	34.38	354.74	9.25	11.28	210.9	20.52
253	US-Myb	2013 TS_4	-0.16	40.07	359.02	9.87	10.41	215	20.28
254	US-Myb	2013 TS_5	-0.32	45.10	363.81	10.53	9.441	221.9	19.97
255	US-Myb	2013 TS_1	-0.02	NaN	355.11	8.47	12.24	208.2	20.7
256	US-Myb	2014 TS_3	-0.08	26.04	365.88	9.64	12.28	210	21.93
257	US-Myb	2014 TS_4	-0.16	38.09	364.15	10.74	11.23	211	21.97
258	US-Myb	2014 TS_5	-0.32	44.34	366.12	11.25	10.25	218	21.5
259	US-Myb	2015 TS_3	-0.08	17.34	340.72	9.77	11.85	212	21.62
260	US-Myb	2015 TS_4	-0.16	12.76	339.04	10.79	10.84	221	21.63
261	US-Myb	2015 TS_5	-0.32	18.83	343.94	11.35	9.93	226	21.28
262	US-Myb	2016 TS_3	-0.08	5.05	357.82	9.61	11.19	201	20.8
263	US-Myb	2016 TS_4	-0.16	3.39	356.20	9.84	10.87	208	20.72
264	US-Myb	2016 TS_5	-0.32	12.02	360.46	10.73	9.627	214	20.36
265	US-Myb	2017 TS_3	-0.08	27.31	352.90	9.86	13.1	214	22.96
266	US-Myb	2017 TS_4	-0.16	28.29	357.41	9.92	12.74	215	22.66
267	US-Myb	2017 TS_5	-0.32	36.79	360.41	10.85	11.23	223	22.08
268	US-Myb	2017 TS_1	-0.02	62.79	325.72	12.70	10.71	216.8	23.41
269	US-Myb	2018 TS_3	-0.08	36.27	326.10	10.20	10.72	207	20.92
270	US-Myb	2018 TS_4	-0.16	41.30	332.83	10.47	10.35	209	20.82
271	US-Myb	2018 TS_5	-0.32	48.43	336.09	11.18	9.293	215	20.47
272	US-Myb	2018 TS_1	-0.02	38.38	344.86	10.05	11.93	200.3	21.98
273	US-NC4	2012 TS_1	-0.05	42.43	336.03	7.87	15.75	215.4	23.62
274	US-NC4	2013 TS_1	-0.05	59.96	368.85	6.92	16.83	210.5	23.74
275	US-NC4	2014 TS_1	-0.05	54.42	362.34	6.73	16.81	208.5	23.54
276	US-NC4	2015 TS_1	-0.05	68.13	387.31	8.27	16.06	205	24.33
277	US-NC4	2016 TS_1	-0.05	52.97	351.38	9.41	15.04	220	24.45
278	US-ORv	2012 TS	NaN	57.42	352.55	4.36	20.61	203.9	24.97

279	US-ORv	2013 TS	NaN	63.67	356.74	2.93	19.98	210.8	22.9
280	US-ORv	2014 TS	NaN	68.11	364.96	2.11	20.17	205.3	22.28
281	US-ORv	2015 TS	NaN	68.77	387.78	1.77	21.26	206	23.04
282	US-OWC	2016 TS_1	-0.05	0.00	0.00	0.00	0	211.2	23.91
283	US-Sne	2017 TS_1	-0.01	46.07	337.92	10.33	13.14	212.7	23.47
284	US-Sne	2017 TS_2	-0.02	41.06	341.82	10.76	12.66	205.7	23.41
285	US-Sne	2017 TS_3	-0.08	42.89	343.85	11.04	12.17	208.5	23.22
286	US-Sne	2017 TS_4	-0.16	46.36	346.18	11.39	11.79	211	23.18
287	US-Sne	2017 TS_5	-0.32	50.59	350.46	11.98	10.7	216	22.67
288	US-Sne	2018 TS_1	-0.01	48.41	325.09	10.28	12.15	217.3	22.43
289	US-Sne	2018 TS_2	-0.02	33.91	331.01	10.55	11.34	210.2	21.89
290	US-Sne	2018 TS_3	-0.08	36.76	331.50	10.87	10.63	212.1	21.5
291	US-Sne	2018 TS_4	-0.16	35.64	335.45	11.23	10.09	220.1	21.32
292	US-Sne	2018 TS_5	-0.32	49.09	335.94	11.88	9.045	218	20.92
293	US-Srr	2016 TS_1	NaN	NaN	326.29	10.03	10.71	200.5	20.74
294	US-Srr	2017 TS_1	NaN	11.34	346.85	7.22	13.71	199.5	20.93
295	US-StJ	2016 TS_2	-0.05	68.37	347.38	4.05	16.22	213.7	20.27
296	US-StJ	2016 TS_3	-0.1	68.38	347.38	5.84	14.1	213.7	19.94
297	US-Tw1	2012 TS_1	-0.02	50.54	359.96	5.99	11.52	225.2	17.51
298	US-Tw1	2012 TS_2	-0.04	48.02	358.76	6.14	11.32	227	17.46
299	US-Tw1	2012 TS_3	-0.08	50.07	367.92	5.18	12.31	222.1	17.49
300	US-Tw1	2012 TS_4	-0.16	49.05	367.52	5.31	12.19	224.5	17.5
301	US-Tw1	2012 TS_5	-0.32	-79.10	347.23	7.89	9.513	225.3	17.4
302	US-Tw1	2013 TS_1	-0.02	35.80	337.57	4.39	14.59	206.6	18.97
303	US-Tw1	2013 TS_2	-0.04	36.08	337.66	4.39	14.57	206.8	18.96
304	US-Tw1	2013 TS_3	-0.08	36.81	338.09	4.40	14.54	207.5	18.94
305	US-Tw1	2013 TS_4	-0.16	37.57	338.82	4.41	14.59	208.4	19.01
306	US-Tw1	2013 TS_5	-0.32	38.64	340.06	4.46	14.62	209.6	19.07
307	US-Tw1	2014 TS_1	-0.02	41.23	395.41	6.67	10.89	208.3	17.56
308	US-Tw1	2014 TS_2	-0.04	41.86	397.14	6.70	10.85	208.6	17.55
309	US-Tw1	2014 TS_3	-0.08	43.55	400.01	6.78	10.72	209.8	17.49
310	US-Tw1	2014 TS_4	-0.16	45.61	404.82	6.88	10.56	211.3	17.44
311	US-Tw1	2014 TS_5	-0.32	49.62	416.29	7.09	10.24	213.9	17.33
312	US-Tw1	2015 TS_1	-0.02	50.66	342.55	9.02	7.831	235	16.85
313	US-Tw1	2015 TS_2	-0.04	52.00	342.38	9.09	7.706	235	16.8
314	US-Tw1	2015 TS_3	-0.08	55.61	341.98	9.26	7.385	238	16.64
315	US-Tw1	2015 TS_4	-0.16	59.57	342.95	9.51	6.972	240	16.48
316	US-Tw1	2015 TS_5	-0.32	69.39	345.18	10.00	6.208	246	16.21
317	US-Tw1	2016 TS_1	-0.02	34.57	361.06	8.78	7.943	218	16.72
318	US-Tw1	2016 TS_2	-0.04	35.49	362.19	8.86	7.837	219	16.69
319	US-Tw1	2016 TS_3	-0.08	38.58	363.10	9.04	7.546	221	16.59
320	US-Tw1	2016 TS_4	-0.16	44.73	365.88	9.33	7.14	223	16.47
321	US-Tw1	2016 TS_5	-0.32	56.22	370.54	9.86	6.35	229	16.21
322	US-Tw1	2017 TS_1	-0.02	41.17	343.75	7.55	10.22	228	17.77
323	US-Tw1	2017 TS_2	-0.04	41.75	344.56	7.61	10.11	229	17.72
324	US-Tw1	2017 TS_3	-0.08	42.61	345.02	7.75	9.803	231	17.55
325	US-Tw1	2017 TS_4	-0.16	45.05	347.17	7.97	9.368	234	17.34

326	US-Tw1	2017 TS_5	-0.32	48.82	349.23	8.38	8.5	240	16.88
327	US-Tw1	2018 TS_1	-0.02	60.47	327.43	6.70	10.42	222	17.12
328	US-Tw1	2018 TS_2	-0.04	61.54	327.44	6.75	10.36	223	17.1
329	US-Tw1	2018 TS_3	-0.08	64.60	328.44	6.85	10.18	225	17.03
330	US-Tw1	2018 TS_4	-0.16	67.67	329.40	7.01	9.925	227	16.93
331	US-Tw1	2018 TS_5	-0.32	75.09	331.40	7.31	9.459	230	16.77
332	US-Tw4	2015 TS_1	-0.02	15.93	327.22	10.04	11.56	199.4	21.6
333	US-Tw4	2015 TS_3	-0.08	20.21	329.78	10.48	10.96	202.3	21.44
334	US-Tw4	2015 TS_4	-0.16	23.88	332.52	10.86	10.42	205.7	21.28
335	US-Tw4	2015 TS_5	-0.32	29.16	338.59	11.49	9.449	212.4	20.94
336	US-Tw4	2016 TS_1	-0.02	9.56	358.75	8.16	11.29	201.7	19.45
337	US-Tw4	2016 TS_3	-0.08	13.17	360.06	8.67	10.58	205.7	19.25
338	US-Tw4	2016 TS_4	-0.16	15.94	362.56	9.11	9.991	209.2	19.11
339	US-Tw4	2016 TS_5	-0.32	21.05	367.55	9.91	8.876	216.2	18.78
340	US-Tw4	2017 TS_1	-0.02	38.35	347.31	8.07	11.52	211.9	19.59
341	US-Tw4	2017 TS_3	-0.08	42.12	351.81	8.45	10.91	215.3	19.36
342	US-Tw4	2017 TS_4	-0.16	46.03	354.70	8.83	10.35	218.6	19.18
343	US-Tw4	2017 TS_5	-0.32	53.54	361.37	9.52	9.275	224.9	18.79
344	US-Tw4	2018 TS_1	-0.02	58.11	344.87	8.00	10.93	218	18.93
345	US-Tw4	2018 TS_3	-0.08	63.91	349.15	8.38	10.41	222	18.79
346	US-Tw4	2018 TS_4	-0.16	67.95	352.10	8.71	9.862	225	18.57
347	US-Tw4	2018 TS_5	-0.32	75.31	357.88	9.33	8.8	231	18.13
348	US-Tw5	2018 TS_1	-0.02	NaN	414.83	0.00	8.894	222.2	18.37
349	US-Tw5	2018 TS_2	-0.1	NaN	401.00	0.00	12.32	204.4	22.24
350	US-Tw5	2018 TS_3	-0.02	NaN	414.83	0.00	8.894	222.2	18.37
351	US-Tw5	2018 TS_4	-0.08	NaN	423.43	0.00	7.898	227.3	18.14
352	US-Tw5	2018 TS_5	-0.16	NaN	430.15	0.00	7.531	230	17.94
353	US-Uaf	2011 TS_1	-0.09	86.20	372.46	-12.29	21.95	199.6	9.667
354	US-Uaf	2012 TS_1	-0.09	73.77	338.53	-11.83	20.86	202.4	9.028
355	US-Uaf	2013 TS_1	-0.09	109.63	395.51	-10.08	20.52	200.4	10.44
356	US-Uaf	2014 TS_1	-0.09	76.07	365.40	-10.94	19.94	206	8.999
357	US-Uaf	2015 TS_1	-0.09	80.99	423.19	-9.77	19.76	190	9.998
358	US-Uaf	2016 TS_1	-0.09	77.38	315.75	-7.74	19.13	198	11.39
359	US-Uaf	2017 TS_1	-0.09	84.88	380.17	-7.39	19.08	196	11.69
360	US-Uaf	2018 TS_1	-0.09	96.04	333.33	-5.60	17.72	199	12.11
361	US-WPT	2011 TS_1	-0.1	80.95	342.17	5.27	19.27	202.6	24.54
362	US-WPT	2011 TS_2	-0.3	NaN	347.04	6.38	16.62	209.7	23.01
363	US-WPT	2012 TS_1	-0.1	40.29	345.57	3.70	21.6	197.4	25.3
364	US-WPT	2012 TS_2	-0.3	44.91	354.96	4.52	19.21	203.8	23.72
365	US-WPT	2013 TS_1	-0.1	74.61	340.47	3.73	18.23	207.2	21.96
366	US-WPT	2013 TS_2	-0.3	77.62	352.35	4.32	16.69	211.7	21.01

Column Descriptions

SITE_ID	Site identification code as assigned by regional flux data
Year	Data year
Probe_name	Temperature probe name as given in data files

Soil_temp_depth_m	Depth of soil temperature probe (m), with negative values
Start_TS_(DOY)	Season start for elevated TS (DOY), point "f" in Figure 1
End_TS_(DOY)	Season end for elevated TS (DOY), point "h" in Figure 1
Base_value_TS_(C)	Baseline TS during non-elevated season (C), average of points
Ampl_TS_(C)	Amplitude of TS during elevated temperature season (C), difference between point "e" in Figure 1 and Base_value_TS
Peak_TS_(DOY)	Day of maximum elevated TS (DOY), point "g" in Figure 1
Peak_value_TS_(C)	Maximum value of TS (C) point "e" in Figure 1

Table B7 - Soil temperature probe depths (m)

	SITE_ID	Year	Probe name	Soil_temp_depth_m	Additional_notes
1	AT-Neu		TS_1	-0.05	
2	AT-Neu		TS_2	-0.1	
3	AT-Neu		TS_3	-0.2	
4	BR-Npw		TS_1		
5	BR-Npw		TS_2		
6	BW-Gum		no data		
7	BW-Nxr		no data		
8	CA-SCB		TS_1	0	
9	CA-SCB		TS_2	-0.02	
10	CA-SCB		TS_3	-0.04	
11	CA-SCB		TS_4	-0.08	
12	CA-SCB		TS_5	-0.16	
13	CA-SCB		TS_6	-0.32	
14	CA-SCB		TS_7	-0.64	
15	CA-SCB		TS_8	-1.28	
16	CA-SCC		TS_1	-0.1	
17	CA-SCC		TS_2	-0.15	
18	CA-SCC		TS_3	-0.2	
19	CA-SCC		TS_4	-0.25	
20	CA-SCC		TS_5	-0.3	
21	CA-SCC		TS_6	-0.5	
22	CA-SCC		TS_7	-0.6	
23	CA-SCC		TS_8	-0.7	
24	CH-Cha		TS_1	-0.01	
25	CH-Cha		TS_2	-0.02	
26	CH-Cha		TS_3	-0.04	
27	CH-Cha		TS_4	-0.07	
28	CH-Cha		TS_5	-0.1	
29	CH-Cha		TS_6	-0.15	
30	CH-Cha		TS_7	-0.25	
31	CH-Cha		TS_8	-0.4	
32	CH-Dav		TS_9	-0.95	
33	CH-Dav		TS_1	-0.05	
34	CH-Dav		TS_2	-0.15	
35	CH-Dav		TS_3	-0.5	
36	CH-Dav		TS_4	-	
37	CH-Dav		TS_5	-	
38	CH-Dav		TS_6	-	
39	CH-Oe2		TS_1	-0.05	
40	CH-Oe2		TS_2	-0.1	
41	CH-Oe2		TS_3	-0.15	
42	CH-Oe2		TS_4	-	
43	CH-Oe2		TS_5	-0.3	
44	CH-Oe2		TS_6	-0.5	

45	CH-Oe2	TS_7	-	
46	CN-Hgu	TS		
47	DE-Dgw	no data		
48	DE-Hte	TS_1	0	
49	DE-Hte	TS_2	-0.1	
50	DE-Hte	TS_3	-0.2	
51	DE-SfN	TS_1	-0.02	
52	DE-SfN	TS_3	-0.1	
53	DE-SfN	TS_4	-0.2	
54	DE-SfN	TS_5	-0.5	
55	DE-Zrk	TS_1	-0.05	
56	DE-Zrk	TS_2	-0.1	
57	DE-Zrk	TS_3	-0.2	
58	DE-Zrk	TS_4	-0.3	
59	DE-Zrk	TS_5	-0.5	
60	FI-Hyy	TS_1	-0.02	
61	FI-Hyy	TS_2	-0.04	
62	FI-Hyy	TS_3	-0.12	
63	FI-Hyy	TS_4	-0.25	
64	FI-Hyy	TS_5	-0.5	
65	FI-Lom	TS_1	-0.07	
66	FI-Lom	TS_2	-0.3	
67	FI-Lom	TS_3	-0.5	
68	FI-Si2	TS_1	-0.05	
69	FI-Si2	TS_2	-0.2	
70	FI-Si2	TS_3	-0.35	
71	FI-Si2	TS_4	-0.5	
72	FI-Sii	pre 2016	TS_1	-0.05
73	FI-Sii	pre 2016	TS_2	-0.2
74	FI-Sii	pre 2016	TS_3	-0.35
75	FI-Sii	pre 2016	TS_4	-0.5
76	FI-Sii	after 2017	TS_1	0
77	FI-Sii	after 2017	TS_2	-0.5
78	FI-Sii	after 2017	TS_3	-0.1
79	FI-Sii	after 2017	TS_4	-0.15
80	FI-Sii	after 2017	TS_5	-0.25
81	FI-Sii	after 2017	TS_6	-0.45
82	FI-Sii	after 2017	TS_7	-0.95
83	FR-LGt		TS_1	-0.02
84	FR-LGt		TS_2	-0.05
85	FR-LGt		TS_3	-0.1
86	FR-LGt		TS_4	-0.2
87	FR-LGt		TS_5	-0.4
88	HK-MPM		TS_1	
89	HK-MPM		TS_2	
90	HK-MPM		TS_3	
91	ID-Pag		TS_1	-0.05

92	IT-BCi	TS_1	-0.05
93	IT-BCi	TS_2	-0.1
94	IT-BCi	TS_3	-0.3
95	IT-BCi	TS_4	-0.5
96	IT-BCi	TS_5	-1
97	IT-Cas	TS_1	-0.035
98	IT-Cas	TS_2	-0.075
99	IT-Cas	TS_3	-0.15
100	JP-BBY	TS_1	-0.183
101	JP-BBY	TS_2	-0.233
102	JP-BBY	TS_3	-0.283
103	JP-BBY	TS_4	-0.383
104	JP-BBY	TS_5	-0.483
105	JP-Mse	TS_1	-0.01
106	JP-Mse	TS_2	-0.025
107	JP-Mse	TS_3	-0.05
108	JP-Mse	TS_4	-0.1
109	JP-Mse	TS_5	-0.2
110	JP-Mse	TS_6	-0.4
111	JP-SwL	no data	
112	KR-CRK	TS_1	-0.05
113	KR-CRK	TS_2	-0.15
114	MY-MLM	TS_1	-0.05
115	NL-Hor	TS_1	-0.01
116	NL-Hor	TS_2	-0.02
117	NL-Hor	TS_3	-0.04
118	NL-Hor	TS_4	-0.05
119	NL-Hor	TS_5	-0.1
120	NL-Hor	TS_6	-0.15
121	NL-Hor	TS_7	-0.25
122	NL-Hor	TS_8	-0.4
123	NL-Hor	TS_9	-0.6
124	NZ-Kop	TS_1	-0.5
125	NZ-Kop	TS_2	-0.1
126	NZ-Kop	TS_3	-0.2
127	PH-RiF	TS_1	
128	RU-Ch2	TS_1	-0.04
129	RU-Ch2	TS_2	-0.08
130	RU-Ch2	TS_3	-0.16
131	RU-Che	TS_1	-0.04
132	RU-Che	TS_2	-0.08
133	RU-Che	TS_3	-0.16
134	RU-Cok	no data	
135	RU-Fy2	TS_1	
136	RU-Fy2	TS_2	
137	RU-Fy2	TS_3	
138	RU-Fy2	TS_4	

139	RU-Fy2	TS_5	
140	SE-Deg	TS_1	-0.02
141	SE-Deg	TS_2	-0.05
142	SE-Deg	TS_3	-0.1
143	SE-Deg	TS_4	-0.15
144	SE-Deg	TS_5	-0.3
145	SE-Deg	TS_6	-0.5
146	UK-LBT	no data	
147	US-A03	TS_1	-0.025
148	US-A03	TS_2	-0.1
149	US-A03	TS_3	-0.3
150	US-A10	TS_1	-0.025
151	US-A10	TS_2	-0.1
152	US-A10	TS_3	-0.3
153	US-Atq	TS_1	
154	US-Atq	TS_2	
155	US-Atq	TS_3	
156	US-Beo	TS_1	
157	US-Beo	TS_2	
158	US-Beo	TS_3	
159	US-Bes	TS_1	
160	US-Bes	TS_2	
161	US-Bes	TS_3	
162	US-Bi1	TS_1	-0.02
163	US-Bi1	TS_2	-0.04
164	US-Bi1	TS_3	-0.08
165	US-Bi1	TS_4	-0.16
166	US-Bi1	TS_5	-0.32
167	US-Bi2	TS_1	-0.02
168	US-Bi2	TS_2	-0.04
169	US-Bi2	TS_3	-0.08
170	US-Bi2	TS_4	-0.16
171	US-Bi2	TS_5	-0.32
172	US-BZB	TS_1	-0.075
173	US-BZB	TS_2	-0.05
174	US-BZF	TS_1	-0.075
175	US-BZF	TS_2	-0.05
176	US-BZS	TS_1	
177	US-BZS	TS_2	
178	US-BZS	TS_3	
179	US-CRT	TS_1	
180	US-DPW	no data	
181	US-EDN	TS_1	-0.25
182	US-EDN	TS_2	-0.15
183	US-EDN	TS_3	-0.05
184	US-EDN	TS_4	0
185	US-EDN	TS_5	0.05

186	US-EDN	TS_6	0.1
187	US-EDN	TS_7	0.2
188	US-EDN	TS_8	0.3
189	US-EML	TS_1	-0.05
190	US-EML	TS_2	-0.1
191	US-EML	TS_3	-0.2
192	US-EML	TS_4	-0.4
193	US-Ho1	TS_1	-0.05
194	US-Ho1	TS_2	-0.1
195	US-HRA	no data	-0.02
196	US-HRC	no data	-0.02
197	US-ICs	TS_1	-0.075
198	US-ICs	TS_2	-0.05
199	US-Ivo	TS_1	-0.05
200	US-Ivo	TS_2	-0.1
201	US-Ivo	TS_3	-0.15
202	US-Ivo	TS_4	-0.3
203	US-Ivo	TS_5	-0.4
204	US-LA1	TS	-0.1
205	US-LA2	TS	-0.1
206	US-Los	TS_1	0
207	US-Los	TS_2	-0.05
208	US-Los	TS_3	-0.1
209	US-Los	TS_4	-0.2
210	US-Los	TS_5	-0.5
211	US-MRM	TS_1	
212	US-MRM	TS_2	
213	US-Myb	TS_1	-0.02
214	US-Myb	TS_2	-0.04
215	US-Myb	TS_3	-0.08
216	US-Myb	TS_4	-0.16
217	US-Myb	TS_5	-0.32
218	US-NC4	TS_1	-0.05
219	US-NC4	TS_2	-0.2
220	US-NGB	no data	
221	US-NGC	no data	
222	US-ORv	TS_1	-0.08
223	US-OWC	TS_1	-0.05
224	US-OWC	TS_2	-0.3
225	US-PFa		
226	US-Snd	TS_1	-0.08
227	US-Snd	TS_2	-0.16
228	US-Snd	TS_3	
229	US-Snd	TS_4	
230	US-Snd	TS_5	
231	US-Snd	TS_6	
232	US-Sne	TS_1	-0.01

233	US-Sne	TS_2	-0.02
234	US-Sne	TS_3	-0.08
235	US-Sne	TS_4	-0.16
236	US-Sne	TS_5	-0.32
237	US-Srr	TS_1	
238	US-Srr	TS_2	
239	US-Srr	TS_3	
240	US-Srr	TS_4	
241	US-Srr	TS_5	
242	US-StJ	TS_2	-0.05
243	US-StJ	TS_3	-0.1
244	US-Tw1	TS_1	-0.02
245	US-Tw1	TS_2	-0.04
246	US-Tw1	TS_3	-0.08
247	US-Tw1	TS_4	-0.16
248	US-Tw1	TS_5	-0.32
249	US-Tw3	TS_1	-0.02
250	US-Tw3	TS_2	-0.04
251	US-Tw3	TS_3	-0.08
252	US-Tw3	TS_4	-0.16
253	US-Tw3	TS_5	-0.32
254	US-Tw4	TS_1	-0.02
255	US-Tw4	TS_2	-0.04
256	US-Tw4	TS_3	-0.08
257	US-Tw4	TS_4	-0.16
258	US-Tw4	TS_5	-0.32
259	US-Tw5	TS_1	-0.02
260	US-Tw5	TS_2	-0.1
261	US-Tw5	TS_3	-0.02
262	US-Tw5	TS_4	-0.08
263	US-Tw5	TS_5	-0.16
264	US-Twt	TS_1	-0.02
265	US-Twt	TS_2	-0.04
266	US-Twt	TS_3	-0.08
267	US-Twt	TS_4	-0.16
268	US-Twt	TS_5	-0.32
269	US-Uaf	TS_1	-0.09 average of 3 depths: -0.15, -0.02, -0.1
270	US-Uaf	TS_2	-0.183333 average of 3 depths: -0.3, -0.05, -0.2
271	US-Uaf	TS_3	-0.283333 average of 3 depths: -0.45, -0.1, -0.3
272	US-Uaf	TS_4	-0.366667 average of 3 depths: -0.5, -0.2, -0.4
273	US-Uaf	TS_5	-0.5 average of 2 depths: -0.7, -0.3
274	US-Uaf	TS_6	-0.6 average of 2 depths: -0.8, -0.4
275	US-Uaf	TS_7	-0.75 average of 2 depths: -1, -0.5
276	US-Uaf	TS_8	-0.925 average of 2 depths: -1.25, 0.6,
277	US-Uaf	TS_9	-1
278	US-WPT	TS_1	-0.1
279	US-WPT	TS_2	-0.3

Column Descriptions

SITE_ID	Site identification code as assigned by regional flux data network
Year	When relevant, information about time-span of probe location. If
Probe_name	Temperature probe name as given in data files
Soil_temp_depth_m	Depth of soil temperature probe (m), with negative values being under
Additional_notes	When relevant, additional information about site